MICROMECHANICAL ASPECTS OF FAILURE

IN

UNIDIRECTIONAL FIBER REINFORCED COMPOSITES

Thesis by

Kenji Oguni

In Partial Fulfillment of the Requirements

for the Degree of

Doctor of Philosophy

California Institute of Technology

Pasadena, California

2000

(Submitted March 10, 2000)

Acknowledgements

It has been a pleasure and privilege to work under the guidance of my adviser, Professor G. Ravichandran. Discussions with him have always given me clear vision and encouragement for the next step. I would like to thank Professor Ravichandran for his patience and constant support during my stay in Caltech.

I would like to acknowledge the counseling committee members for my Ph.D. study, Professor K. Bhattacharya and Professor A. J. Rosakis for their timely, helpful advice. I am grateful to the other members of my thesis committee, Professor M. Ortiz and Professor E. Üstündag , for taking the time to review the dissertation.

The research presented in this dissertation was supported by the Office of Naval Research (Dr. Y. D. S. Rajapakse, Scientific Officer) and is gratefully acknowledged. I am also grateful to Professor A. M. Waas, University of Michigan, for providing the composite specimens used in the experimental investigations in this dissertation.

Conversations (mainly nonacademic) with members in our group, Eric Burcsu, Jun Lu, Shiming Zhuang and Dr. Sangwook Lee, made my experiences at Caltech fun. I would like to thank them.

Finally, I want to thank my wife, Asako, for her encouragement, patience and cheerful personality.

Abstract

Micromechanical aspects of failure in unidirectional fiber reinforced composites are investigated using combined experimental and analytical methods. Results from an experimental investigation on mechanical behavior of a unidirectional fiber reinforced polymer composite (E-glass/vinylester) with 50% fiber volume fraction under quasi-static uniaxial and proportional multiaxial compression are presented. Detailed examination of the specimen during and after the test reveals the failure mode transition from axial splitting to kink band formation as the loading condition changes from uniaxial to multiaxial compression.

Motivated by the experimental observations, an energy-based model is developed to provide an analytical estimate of the critical stress for axial splitting observed in unidirectional fiber reinforced composites under uniaxial compression in the fiber direction (also with weak lateral confinement). The analytic estimate for the compressive strength is used to illustrate its dependence on material properties, surface energy, fiber volume fraction, fiber diameter and lateral confining pressure.

To understand the effect of flaws on the strength of unidirectional fiber reinforced composites, a fracture mechanics based model for failure is developed. Based on this model, failure envelope, dominant initial flaw orientation and failure mode for the composites under a wide range of stress states are predicted. Parametric study provides quantitative evaluation of the effect of various mechanical and physical properties on failure behavior and identifies their influence on strength.

Finally, results from an experimental investigation on the dynamic mechanical behavior of unidirectional E-glass/vinylester composites with 30%, 50% fiber volume fraction under uniaxial compression are presented. Limited experimental results are also presented for the 50% fiber volume fraction composite under dynamic proportional lateral confinement. Specimens are loaded in the fiber direction using a modified Kolsky (split Hopkinson) pressure bar. The results indicate that the compressive strength of the composite increases with increasing strain rate and confinement. Post-test scanning electron microscopy reveals that axial splitting is the dominant failure mechanism in the composites under uniaxial compression in the entire range of strain rates. Based on the experimental results and observations, the energy-based analytic model is extended to predict the compressive strength of these composites under dynamic uniaxial loading conditions.

Table of contents

Chapter III A micromechanical failure model for unidirectional fiber reinforced composites

Introductory remark

This doctoral dissertation consists of four complementary Chapters, each containing its own abstract, introduction and conclusion. The common objective of these Chapters is to shed light on failure behavior of unidirectional fiber reinforced composites from a micromechanical point of view. Chapter 1 presents results from an experimental investigation on the mechanical behavior of a unidirectional fiber reinforced polymer composite (E-glass/vinylester) with 50% fiber volume fraction under quasi-static uniaxial and proportional multiaxial compression. The stress-strain curves and the acoustic emission records together with the post-mortem observations on the specimen show that the failure mode transitions from axial splitting to kink band formation as the loading condition changes from uniaxial to proportional multiaxial compression.

The experimental observations in Chapter 1 motivated the development of an energy-based model presented in Chapter 2 that provides an analytical estimate of the critical stress for axial splitting observed in unidirectional fiber reinforced composites under uniaxial compression in fiber direction (also with weak lateral confinement). This model is based on the principle of minimum potential energy and the evaluation of effective properties. The analytic estimate for the compressive strength is used to illustrate its dependence on material properties, surface energy, fiber volume fraction, fiber diameter and lateral confining pressure.

In Chapter 3, results from a fracture mechanics-based model for failure in unidirectional fiber reinforced composites under a wide range of stress states is presented. The model is based on (i) analysis of branch crack initiation from the tip of an initial

microcrack embedded in an anisotropic material, which serves as a model for the fiber reinforced composite and (ii) evaluation of anisotropy in homogenized elastic material properties and fracture toughness. Based on this model, failure envelope, dominant initial flaw orientation and failure mode for unidirectional fiber reinforced composites under a wide range of stress states are predicted. Parametric study provides quantitative evaluation of the effect of various mechanical and physical properties on failure behavior and their influence on strength is identified.

In Chapter 4, results from an experimental investigation on the mechanical behavior of unidirectional fiber reinforced polymer composites (E-glass/vinylester) with 30%, 50% fiber volume fraction under dynamic uniaxial compression are presented. Limited experimental results are presented for the 50% fiber volume fraction composite under proportional lateral confinement. Specimens are loaded in the fiber direction using a servo-hydraulic material testing system for low strain rates and a modified Kolsky (split Hopkinson) pressure bar for high strain rates, up to 3000/s. The results indicate that the compressive strength of the composite increases with increasing strain rate and confinement. Post-test scanning electron microscopy revealed that axial splitting is the dominant failure mechanism in the composites under uniaxial compression in the entire range of strain rates. Based on the experimental results and observations, an energy-based analytic model for studying axial splitting phenomenon in unidirectional fiber reinforced composites presented in Chapter 2 is extended to predict the compressive strength of these composites under dynamic uniaxial loading condition.

Chapter I Failure mode transition in unidirectional E-glass/vinylester composites under multiaxial compression

Abstract

Results from an experimental investigation on the mechanical behavior of a unidirectional fiber reinforced composite with 50% volume fraction E-glass/vinylester and the vinylester matrix under uniaxial and proportional multiaxial compression are presented. The stress-strain curve and the acoustic emission records together with the post-mortem observations on the specimen show the failure mode transition from axial splitting to kink band formation as the loading condition changes from uniaxial to proportional multiaxial compression. Axial splitting and 'splitting induced' kink formation were observed in the uniaxially loaded specimen and the multiaxially loaded specimen showed conjugate kink bands and no axial splitting.

I-1 Introduction

Composites are found to be more efficient and attractive materials for high performance structural members because of their high specific modulus (E/ρ) and high specific strength (σ_{ult}/ρ) in the direction of reinforcement than monolithic materials (Kaw, 1997). In order to take advantage of their directional properties, composite materials are used in the laminate form. However, the failure modes in such laminates are complex and the measurement of the local physical quantities in experiments is a very difficult task (Shuart, 1989; Schultheisz and Waas, 1996; Waas and Schultheisz, 1996).

On the other hand, unidirectional fiber reinforced composites serve as excellent model materials to investigate the associated strength and failure issues in analysis and experiment. The compressive strength of unidirectional fiber reinforced composites in fiber direction is generally much lower than their tensile strength and is a limiting factor in the design of composite structures. The compressive strength of most fiber-reinforced composites in fiber direction is roughly one-half of their tensile strength. Therefore, the prediction of the compressive strength is a critical issue in designing composite materials and structures. However, the mechanisms of compressive failure in composites are not fully understood.

For unidirectionally fiber reinforced composites, experimentally determined compressive strength has been consistently and considerably lower than theoretical predictions. Extensive experimental studies have been carried out on unidirectional fiber reinforced composites under uniaxial compression (Schultheisz and Waas, 1996; Waas and Schultheisz, 1996). In these studies, two distinct compressive failure modes have been widely observed, namely, longitudinal splitting (Bazhenov and Kozey, 1991; Madhukar and Drzal, 1992; Waas and Schultheisz, 1996) and formation of kink bands (Soutis, 1991; Waas and Schultheisz, 1996; Fleck, 1997). Under uniaxial compression, the failure modes are influenced by factors such as material properties of fibers and matrix, fiber volume fraction, fiber diameter and interfacial properties (strength, toughness) (Oguni and Ravichandran, 2000). The effect of lateral confinement on the choice of failure modes can not be evaluated through uniaxial compression tests. In general, the loading in many applications such as pressure vessels and submersibles is multiaxial. The stress state in a laminate is multi-dimensional even under uniaxial loading

due to inter-laminar shear coupling. However, as mentioned before, most experiments have been performed under uniaxial compression and relatively less is known regarding the multiaxial behavior of fiber reinforced composites (Weaver and Williams, 1975; Parry and Wronski, 1982; Sigley et al., 1992; Rhee and Pae, 1995; Lankford, 1997). In these limited experimental observations, two failure modes, longitudinal splitting and kink band formation, were observed under multiaxial compression. Also, failure mode transition from longitudinal splitting to formation of kink band with increasing confining pressure was observed. These experiments concerning behavior of composites under multiaxial compression have been performed under hydrostatic pressure. In many applications involving composites, e.g., laminates, the loading path is proportional, i.e., stress components change in proportion to one another.

Motivated by the above discussion, this chapter presents a simple and effective experimental technique for studying the mechanical behavior of fiber reinforced composites under compression with proportional confinement. The mechanical behavior of a unidirectionally reinforced 50% volume fraction E-glass/vinylester polymeric composite under quasi-static proportional multiaxial compression has been investigated. The deformation and failure response of the composite under uniaxial compression and under compression with proportional lateral confinement are investigated and compared. Stress-strain behavior together with post-mortem observation of the specimen using optical and scanning electron microscopy were used in order to identify the failure modes in E-glass/vinylester composites. The results show the failure mode transition from longitudinal splitting to formation of kink band as the loading condition changes from uniaxial to multiaxial compression.

I-2 Experimental procedure

I-2-1 Specimen

Experiments were performed on unidirectional fiber reinforced composites with 50% volume fraction E-glass/vinylester. This material is finding increasing structural applications because of the relatively low cost in manufacturing using techniques such as vacuum assisted resin transfer molding (VARTM).

Continuous E-glass (Certainteed R099-625) fibers of 24.1 μ m in diameter are aligned in a glass tube and are impregnated with vinylester resin (Dow Derakane 411-C50). Following curing, specimens of desired length (12.7 mm) are sectioned using a low speed diamond saw and are sized to desired diameter (6.35 mm) using low speed machining. The ends of the specimen are made parallel and polished using diamond paste. The lateral surface of the specimens used in the multiaxial compression tests is carefully machined to maintain sliding/running fit with confining sleeve. Experiments were also performed on the pure matrix material, vinylester resin (Dow Derakane 411-C50). The materials were processed in the Composite Structures Laboratory at the University of Michigan. The details of the material and specimen preparation can be found elsewhere (Waas et al., 1997). The relevant properties and geometry of the fiber, the matrix and the composite are given in Table 1.

I-2-2 Compression fixture

Figure 1 shows the compression fixture used in the quasi-static compression tests. It ensured that the two loading sleeves were perfectly aligned with each other so that any unwanted shear forces on the specimen are minimized. The specimen was sandwiched in

between the loading rods and the compression is applied by a servo hydraulic materials testing system (MTS). The quasi-static compression tests in fiber direction were performed with and without lateral confining sleeve to investigate the behavior of the specimens under the compression with proportional confinement and uniaxial compression, respectively. The loading rods are made of high strength maraging steel (C-350, Rockwell hardness, R_c=60) and the loading sleeves are made of heat treated drill rod (AISI/SAE Grade W1, Rockwell hardness, R_c=65~68).

I-2-3 Lateral confinement

The confining sleeve shown in Fig. 2 is a hollow cylinder, which resists the lateral expansion of the specimen during the axial compression. And thus, lateral confinement, which is proportional to axial compression, is applied on the specimen. The experimental set-up for the experiment with confinement consists of a cylindrical specimen placed in a hollow cylinder with a sliding/running fit and the specimen is axially compressed using loading sleeves. The confining sleeve and the loading rods/sleeves are made of high strength alloys and designed to remain elastic during the experiments. Proper choice of the material properties and the geometry (inner and outer radii, *a* and *b*, respectively) of the confining sleeve gives the desired ratio of confinement to applied stress σ_c/σ. In the elastic regime of the specimen, the relationship between the axial compressive stress σ and the lateral confinement σ_c is expressed in terms of the geometry and the elastic properties of the composite specimen and the confining sleeve as follows:

$$\sigma_c = \frac{\sigma}{\left[\frac{(1-\nu_s)E_2 a^2}{\nu_{21}E_s(b^2-a^2)}\left\{1+\frac{(1+\nu_s)b^2}{(1-\nu_s)a^2}\right\}+\frac{(1+\nu_{23})}{\nu_{21}}\right]} \tag{1}$$

where E_s and ν_s are the Young's modulus and the Poisson's ratio of the confining sleeve and E_2, ν_{21} and ν_{23} are the elastic properties of the specimen (see Appendix). Equation (1) shows that even if the material properties of the specimen are not given, lateral confinement σ_c is always proportional to the axial compression σ as long as the confining sleeve remains elastic. Since the material properties of the specimen are not known a priori all the way up to failure, the confining stress applied on the specimen is monitored using a strain gauge (Micro-measurements CEA-06-062UW-350) mounted on the external surface of the confining sleeve. Most of the cross section of the confining sleeve can be approximated to be a hollow cylinder subject to the internal pressure σ_c under plane stress loading condition. Therefore, the relationship between the hoop strain (ε_θ) of the external surface of the confining sleeve measured through the strain gauge and the lateral confining pressure σ_c applied on the specimen can be obtained

$$\sigma_c = \frac{E_s\left(b^2-a^2\right)}{2\,a^2}\varepsilon_\theta . \tag{2}$$

The confining sleeve is typically made of a high strength aluminum alloy (Al 7075-T651, $\sigma_Y = 505\text{MPa}$). The inner diameter is carefully machined to provide smooth sliding fit on the specimen as well as the loading sleeves. The typical inner and outer

radii of the confining sleeve used in the experiments are a=3.28 mm and b=17.3 mm, respectively. A similar technique has been used in investigating the behavior of polymers under multiaxial compression (Ma and Ravi-chandar, 2000).

I-2-4 Acoustic emission

Acoustic emission (AE) is due to the stress waves generated by the nucleation and/or propagation of defects such as cracks and voids in materials, which undergo deformation. In composites, the cracking of matrix, debonding and fiber breakage generates acoustic emission. Acoustic emission from the confined specimen during compression was used to identify the onset of failure events. A 1/4-inch diameter piezo-electric AE transducer (Physical Acoustics Corp., Micro-30) was mounted on the outer surface of the confining sleeve and the signal was recorded using an analogue/digital (A/D) converter (Motorola DSP56ADC16) (Tan, 1997).

I-3 Results and discussion

Experiments on the unidirectional fiber reinforced 50% volume fraction E-Glass/vinylester composite material described above were performed at quasi-static strain rate, $\dot{\varepsilon}$=0.001/s under displacement control using a servo hydraulic materials testing system (MTS). The stress states used in these tests are uniaxial compression and multiaxial compression with proportional lateral confinement. In all the experiments, load-displacement response of the specimen was measured. After the experiment, post-mortem observations of the specimen using optical and scanning electron microscopy

were used to identify the failure modes in material. For the tests with confinement, besides the stress-strain response of the specimen, the acoustic emission counts from the specimen during the test was measured to identify the incidence of failure in the material. Experiments were also performed on the pure matrix material, vinylester resin (Dow Derakane 411-C50) to examine the stress-strain characteristics of the matrix material.

I-3-1 Stress-strain response

A typical stress-strain curve obtained from experiments for the unconfined composite specimens loaded in the fiber direction is shown in Fig. 3. The stress-strain curve is linear (E = 33.7 GPa) up to the maximum stress followed by the catastrophic load drop. After this sudden drop, the specimen continues to deform at a lower level of stress. The peak stress achieved during the test is 470 MPa (at axial strain $\varepsilon \approx 0.018$) and when the stress reached to the maximum, the specimen split in the fiber direction with an audible 'ping' sound. All the specimens in this uniaxial experiments failed in the same manner, i.e., longitudinal (axial) splitting. After the sudden drop of the load, specimen bulged out in lateral direction as additional axial displacement was applied. The lower plateau stress observed in the stress-strain curve corresponds to the strength of the specimen following axial splitting.

A typical stress-strain curve in axial direction obtained from experiments for the proportionally confined composite specimens loaded in the fiber direction together with the lateral confining stress is shown in Fig. 4. In this experiment, the confining sleeve is designed in such a way that the stress ratio σ_c/σ applied on the specimen in the elastic regime should be approximately 0.3 following (1). Indeed, the stress ratio obtained

through the data from the strain gauge mounted on the outer surface of the confining sleeve is almost of the desired value. The material exhibited a linear response up to 500 MPa followed by a small load drop and degradation of modulus. Although this stress is close to the maximum stress observed in the unconfined experiments (470 MPa), the stress drop is much less and not catastrophic. The initial slope of the stress-strain relationship is 40 GPa. Based on the linear elasticity theory, the stress-strain relationship of the confined specimen under consideration is given as follows:

$$\varepsilon_{11} = \frac{1}{E_1}\{\sigma - (\nu_{12} + \nu_{13})\,\sigma_c\} \tag{3}$$

where compressive stress and strain are given positive signs. Because of the transversely isotropic distribution of the fibers, Poisson's ratios ν_{12} and ν_{13} are assumed to have the same value and for the composite under consideration, $\nu_{12} = \nu_{13} = 0.28$ based on the analytic estimate of the effective properties (Hashin and Rosen, 1964). Also from the experiment, $\sigma/\varepsilon_{11} = 40.0$ GPa and $\sigma_c/\sigma \approx 0.3$. Substituting these values into (3), the Young's modulus E_1 of confined specimen obtained from experimental data is 33.3 GPa, which is close to the value obtained from unconfined experiment. After a small load drop at the stress level of 500 MPa, the specimen continued to deform with subsequent drops in load and the stress was nearly saturating at a maximum value of approximately 650 MPa in the strain regime, $\varepsilon = 0.033$ to 0.065.

Figure 5 shows the acoustic emission (AE) data in the form of event counts as a function of time together with axial stress for the confined composite specimen (Fig. 4).

Large AE counts are observed corresponding to the stress drops. This indicates that the fibers have possibly broken at each stress drop and that fiber breakage doesn't occur in the entire diameter of the specimen, instead, successive fiber breakage is confined to small regions.

The stress-strain curves of compression test on pure matrix material, vinylester resin (Dow Derakane 411-C50) without lateral confinement and with proportional lateral confinement ($\sigma_c/\sigma \approx 0.4$) are shown in Figs. 6 and 7, respectively. Without confinement, the stress-strain relationship is highly nonlinear with the initial slope of 3.69 GPa, and when the axial strain reaches to $\varepsilon \approx 0.03$, the material flows at 52 MPa. On the other hand, with proportional confinement, stress-strain relationship is linear with slope of 5.90 GPa and doesn't yield even at 600 MPa. This slope for the confined vinylester corresponds to the Young's modulus of 4.11GPa following the same argument for the confined composite material, using Poisson's ratio of the matrix, $\nu_m = 0.38$ and $\sigma_c/\sigma \approx 0.4$. These results indicate i) matrix material is highly ductile with no confinement and ii) yielding of the matrix material is highly pressure sensitive.

I-3-2 Failure modes

The failure surfaces of the specimen from the uniaxial experiments and the surfaces of the specimen from the multiaxial experiments sectioned using a low speed diamond saw (to minimize damage) were examined using optical and scanning electron microscopy (SEM). Figure 8(a) is the SEM micrograph of the failure surface of the specimen from a uniaxial compression test on the composite. Figure 8(b) shows a magnified view around the region marked **X** in Fig. 8(a). From Fig. 8(a), it is seen that

the compressive failure mode for the case without confinement is the longitudinal splitting. Figure 8(b) shows that the splitting occurs either in the matrix or at the interface of fiber and matrix. In another part of the same specimen from the uniaxial compression experiment revealed 'longitudinal splitting induced' kink band formation (Fig. 9(a)). In Fig. 9(b), which shows a higher magnification of Fig. 9(a), one can observe that the split failure surface is bent by the kink band. This indicates that the kink band was formed after the longitudinal splitting. Hence, the kink band observed in the unconfined experiments is called 'longitudinal splitting induced' and thus, the dominant compressive failure mechanism of the specimen in the case without confinement for the composites is identified as longitudinal splitting. The longitudinal splitting is manifested as a catastrophic drop in the stress as seen from the stress-strain response of the composite (Fig. 3). The post failure modes of the kink band formation results in sustaining a lower level of resistance observed in the stress-strain curve and the large lateral expansion of the specimen.

A SEM micrograph of the sectioned surface of the specimen recovered from compression test with proportional confinement is shown in Fig. 10(a). In this micrograph, no longitudinal splitting is visible and two distinct kink bands can be easily observed; one is from **F** to **A** (kink band **F-A**) and the other is from **B** through **C** to **D** (kink band **B-C-D**). The boundary of these kink bands is clearly visible by the fiber failure due to bending at both top and bottom ends. The absence of the axial splitting and the existence of kink bands confirm that the dominant compressive failure mechanism of the specimen with proportional lateral confinement is the kink band formation. Also, two kink bands mentioned above are conjugate to each other. As the kink band **F-A** reaches

the lateral boundary of the specimen (at the right-hand end of the micrograph), the kink band **B-C-D** is formed to accommodate further axial compressive deformation, or vice versa. In this sense, these two kink bands are conjugate. Under this context, the kink band formation can be regarded as the process in which the axial loading is transferred to the transverse direction due to the change of geometry. A higher magnification of Fig. 10(a) around points **A** and **B** (Fig. 10(b)) shows the region of conjugate kink band formation. Under this higher magnification, multiple kink formation due to the reflection at the specimen boundary is visible. The multiple load drops observed in the stress-strain curve are related to the formation of these local conjugate kink bands. Fiber failure due to bending of these conjugate kink bands can be regarded as the source of the strong acoustic emission (AE) activities accompanying the stress drops observed in the experiments as seen in Fig. 5. The plateau observed in the strength of the confined specimen (Fig. 4) can be viewed as a direct consequence of the inability to accommodate further kink band formation in the specimen.

As an overall summary of observation of failure modes, the following is concluded: with increasing confinement, the axial splitting mode of the failure in the unidirectional E-glass fiber reinforced vinylester composite is suppressed and transitions to kink band formation. The observed failure modes and their transition are functions of the mechanical properties of fiber and matrix and their interface, volume fraction and geometry of fiber and the applied stress state.

I-4 Conclusion

The mechanical behavior of a unidirectional fiber reinforced composite with 50% volume fraction E-glass/vinylester at low strain rates has been investigated. The loading conditions were uniaxial and proportional multiaxial compression with quasi-static strain rate. The proportional lateral confinement has been achieved by using a specially designed confining sleeve. Results from proportional loading multiaxial compression experiments on the composite showed an increase in compressive strength in comparison to its unconfined compressive strength. The failure mode transition from axial splitting to kink band formation as the loading condition changed from uniaxial to proportional multiaxial compression was confirmed by the observations from the post-mortem micrographs of the specimen. The longitudinal splitting and the 'splitting induced' kink formation were observed in the uniaxially loaded specimen. On the other hand, observations from the multiaxially loaded specimen showed conjugate kink bands and no longitudinal splitting.

The experiments on the pure matrix material, vinylester resin, revealed pressure dependent flow behavior of the matrix material. Lateral confinement increases the axial stress required for the yielding of the matrix. In laterally confined fiber reinforced composite, matrix is subjected to the same lateral confining pressure as the fibers. Under this condition, the matrix material, vinylester no longer can yield except in regions of stress concentration such as the tip of a micro-crack.

Acknowledgements

The research reported in this chapter is supported by the Office of Naval Research (Dr. Y. D. S. Rajapakse, Scientific Officer) through a grant to the California Institute of Technology and is gratefully acknowledged. We thank Professor A. M. Waas, University of Michigan, for providing the composite specimens used in this study.

Appendix

The confining sleeve (Fig. 2) with inner and outer radii a and b respectively can be regarded as a hollow cylinder under plane stress condition subject to the internal pressure, σ_c. The Airy stress function (Φ), radial stress component (σ_{rr}) and radial displacement (u_r) in polar coordinate system can be expressed as a function of radial coordinate (r),

$$\Phi = A\log r + Cr^2, \qquad \sigma_{rr} = \frac{A}{r^2} + 2C, \qquad u_r = \frac{1+\nu_s}{E_s}\left\{C(\kappa-1)r - A\frac{1}{r}\right\}$$

where $k = (3-\nu_s)/(1+\nu_s)$ (plane stress), A and C are constants determined by boundary conditions. Substituting boundary conditions $\sigma_{rr}|_{r=a} = -\sigma_c$ and $\sigma_{rr}|_{r=b} = 0$, constants A and C are given as follows:

$$A = -\frac{a^2b^2}{b^2-a^2}\sigma_c, \qquad C = \frac{a^2}{2\left(b^2-a^2\right)}\sigma_c.$$

Using the expression for A, C and k, the radial displacement of the inner surface of the confining sleeve is

$$u_r|_{r=a} = \frac{a^2\,\sigma_c}{E_s\left(b^2-a^2\right)}\left\{(1-\nu_s)\,a + (1+\nu_s)\frac{b^2}{a}\right\}. \qquad \text{(A1)}$$

Specimen can be regarded as solid cylinder of anisotropic material. Letting x_1

direction of the cartesian coordinate system be the fiber direction, boundary conditions are $\sigma_{11} = -\sigma$, $\sigma_{22} = \sigma_{33} = -\sigma_c$. Hence,

$$\varepsilon_{22} = \frac{1}{E_2}\{\nu_{21}\sigma - (1-\nu_{23})\sigma_c\},$$

$$u_r\big|_{r=a} = \int_0^a \varepsilon_{22}\,dr = \frac{a}{E_2}\{\nu_{21}\sigma - (1-\nu_{23})\sigma_c\}. \tag{A2}$$

To satisfy the compatibility condition at $r = a$,

$$\left(u_r\big|_{r=a}\right)_{\text{specimen}} = \left(u_r\big|_{r=a}\right)_{\text{confinement}}. \tag{A3}$$

Solving (A3) for σ_c by using (A1) and (A2), relationship between confining pressure, σ_c and axial compressive stress, σ is given as follows:

$$\sigma_c = \frac{\sigma}{\left[\dfrac{(1-\nu_s)E_2a^2}{\nu_{21}E_s(b^2-a^2)}\left\{1+\dfrac{(1+\nu_s)b^2}{(1-\nu_s)a^2}\right\}+\dfrac{(1+\nu_{23})}{\nu_{21}}\right]}. \tag{A4}$$

References

Bazhenov, S. L. and Kozey, V. V., 1991, "Compression fracture of unidirectional GFRP," *Journal of Materials Science*, Vol. 26, pp. 201-208.

Fleck, N. A., 1997, "Compressive failure of fiber reinforced composites," *Advances in Applied Mechanics*, Vol. 33, pp. 43-117.

Hashin, Z. and Rosen, B. W., 1964, "The elastic moduli of fiber-reinforced materials," *Journal of Applied Mechanics*, Vol. 31, pp. 223-232.

Kaw, A. K., 1997, Mechanics of Composite Materials, CRC Press LLC.

Lankford, J., 1997, "Shear versus dilatational damage mechanisms in the compressive failure of fibre-reinforced composites," *Composites*, Vol. 28A, pp. 215-222

Madhukar, M. S. and Drzal, L. T., 1992, "Fiber-matrix adhesion and its effect on composite mechanical properties. III. Longitudinal (0°) compressive properties of graphite/epoxy composites," *Journal of Composite Materials*, Vol. 26, pp. 310-333.

Oguni, K. and Ravichandran, G., 2000, "An energy-based model of longitudinal splitting in unidirectional fiber reinforced composites," to appear in *Journal of Applied Mechanics*.

Parry, T. V. and Wronski, A. S., 1982, "Kinking and compressive failure in uniaxially aligned carbon fibre composite tested under superposed hydrostatic pressure," *Journal of Materials Science*, Vol. 17, pp. 893-900.

Ma, Z. and Ravi-chandar, K., 2000, "Confined compression: A stable homogeneous deformation for constitutive characterization," *Experimental Mechanics*, Vol. 40, pp. 38-45.

Rhee, K. Y and Pae, K. D., 1995, "Effects of hydrostatic-pressure on the compressive

properties of laminated, 0-degrees unidirectional, graphite fiber epoxy matrix thick-composite," *Journal of Composite Materials*, Vol. 29, pp. 1295-1307.

Schultheisz, C. R. and Waas, A. M., 1996, "Compressive failure of composites, Part I: Testing and micromechanical theories," *Progress in Aerospace Sciences*, Vol. 32, pp. 1-42.

Shuart, M. J., 1989, "Failure of compression-loaded multidirectional composite laminates," *AIAA Journal*, Vol. 27, pp. 1274-1279.

Sigley, R. H., Wronski, A. S. and Parry, T. V., 1992, "Axial compressive failure of glass-fibre polyester composites under superposed hydrostatic pressure: influence of fibre bundle size," *Composites Science and Technology*, Vol. 43, pp. 171-183.

Soutis, C., 1991, "Measurement of the static compressive strength of carbon-fiber epoxy laminates," *Composites Science and Technology*, Vol. 42, pp. 373-392.

Tan, C. Y., 1997, "The effect of lateral confinement on compressive strength and failure mechanism of glass fibre reinforced (GFRP) composites," *M.Eng. Thesis*, Imperial College of Science, Medicine and Technology, London.

Waas, A. M. and Schultheisz, C. R., 1996, "Compressive failure of composites, Part II: Experimental studies," *Progress in Aerospace Science*, Vol. 32, pp. 43-78.

Waas, A. M., Takeda, N., Yuan, J. and Lee, S. H., 1997, "Static and dynamic compressive behaviour of glass fibre reinforced unidirectional composites," *Proceedings of the American Society for Composites, Twelfth Technical Conference*: pp. 552-561, Dearborn, Michigan.

Weaver, C. W. and Williams, J. G., 1975, "Deformation of a carbon-epoxy composite under hydrostatic pressure," *Journal of Materials Science*, Vol. 10, pp. 1323-1333.

List of tables

List of figures

Table 1 Material constants of fiber, matrix and geometry of fiber

Fiber				Matrix	
Young's Modulus E_f (GPa)	Poisson's Ratio ν_f	Volume Fraction v_f	Fiber Radius a (μm)	Young's Modulus E_m (GPa)	Poisson's Ratio ν_m
72.4	0.2	0.5	12.1	3.69	0.38

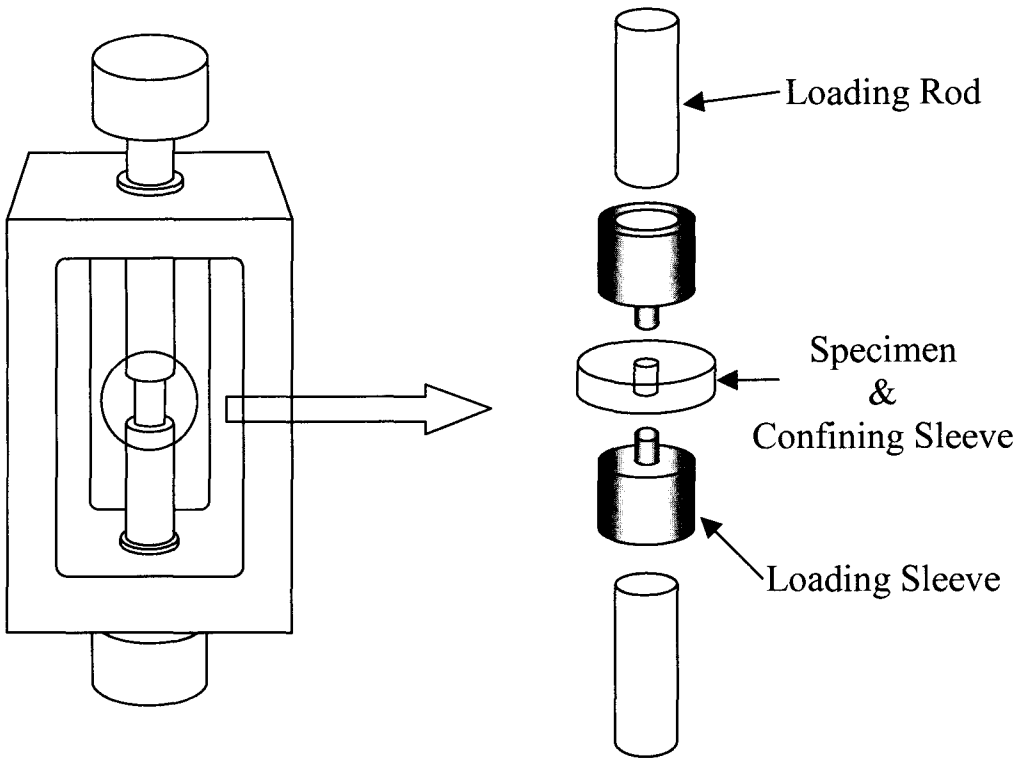

Figure 1 Compression fixture and sleeve for imposing proportional confinement on composites

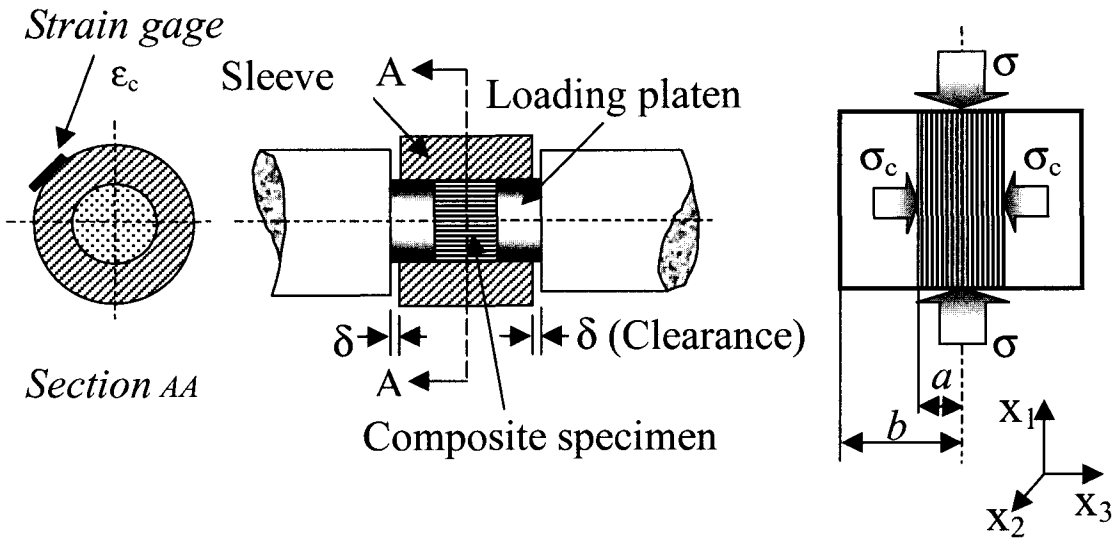

Figure 2 Schematics of a composite specimen surrounded by the confining sleeve

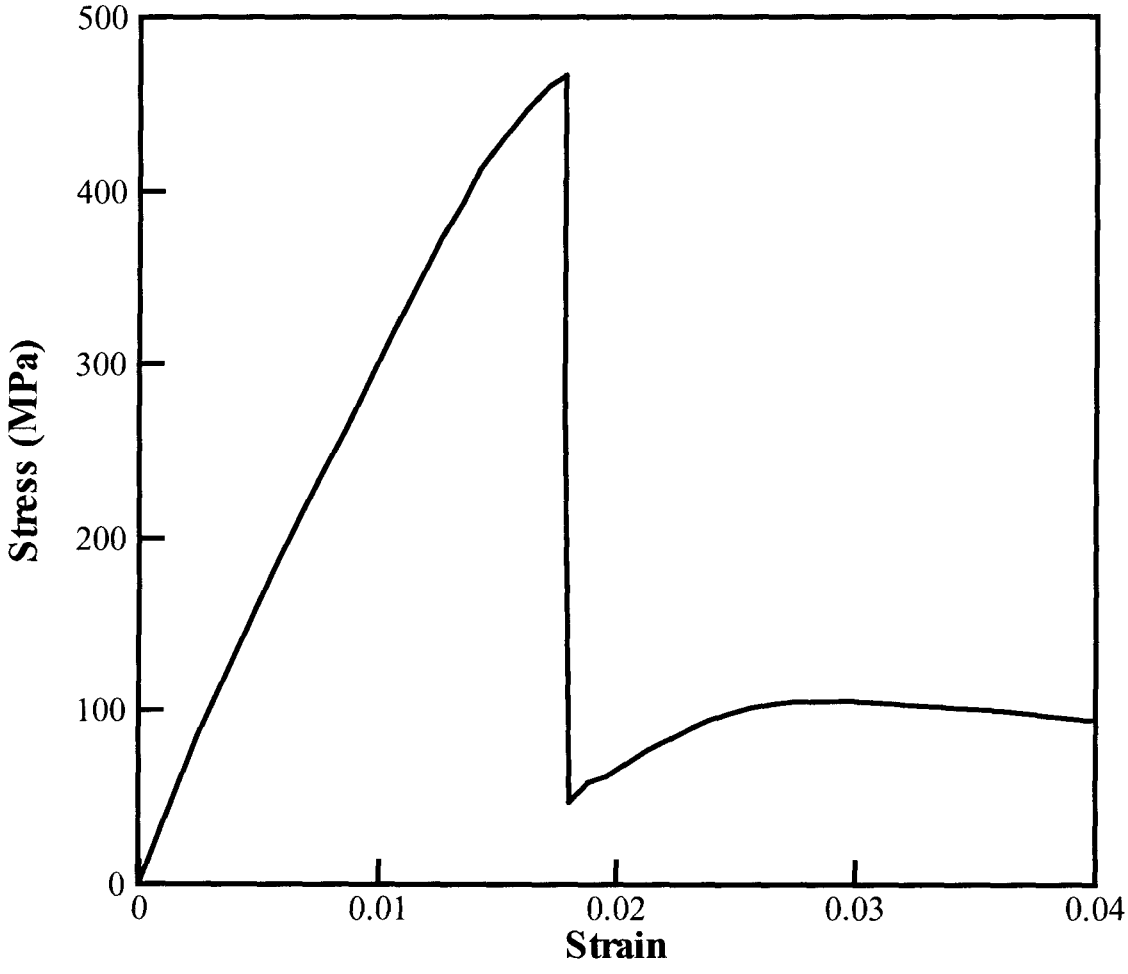

Figure 3 A typical stress-strain curve for unconfined 50% E-Glass/vinylester composite

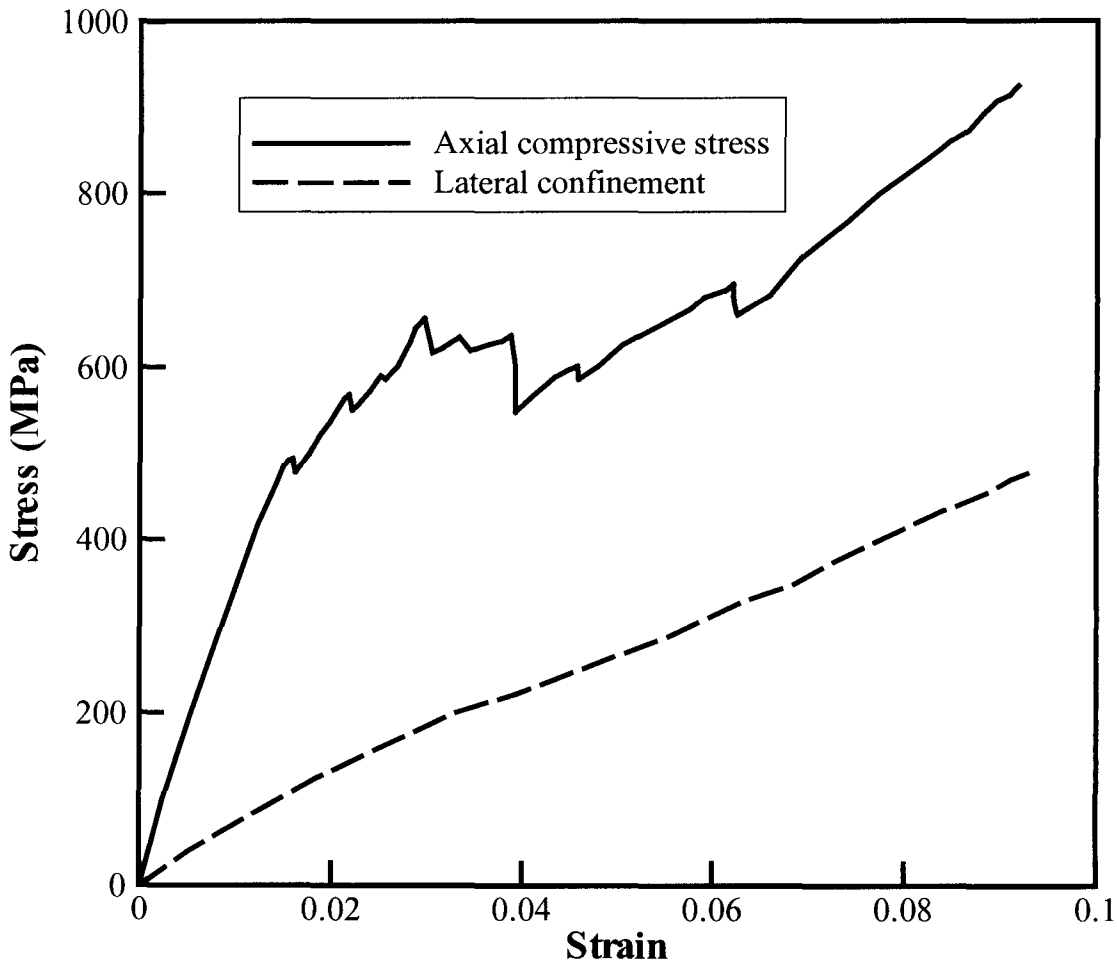

Figure 4 A typical stress-strain curve for laterally confined 50% E-Glass/vinylester composite

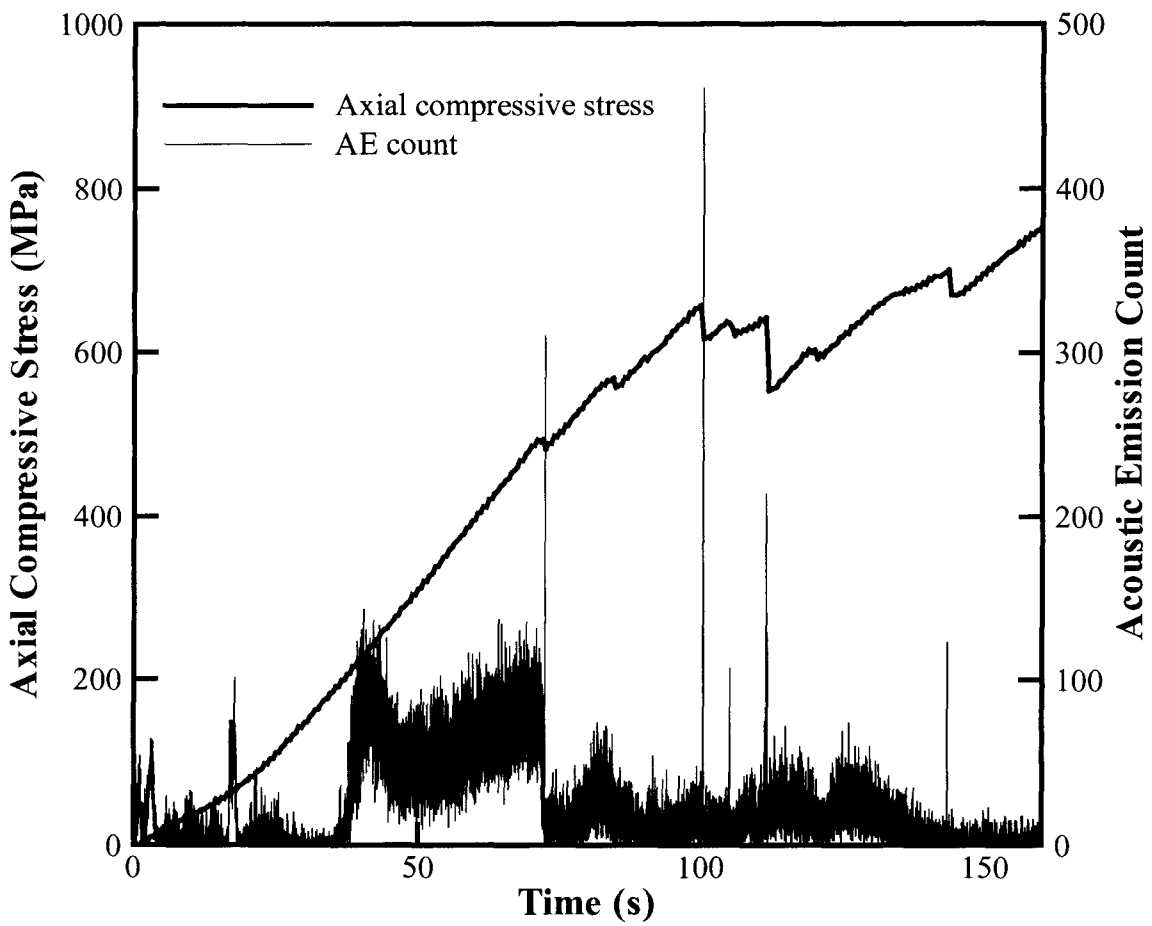

Figure 5 Stress and acoustic emission (AE) count as a function of time for laterally confined 50% E-Glass/vinylester composite

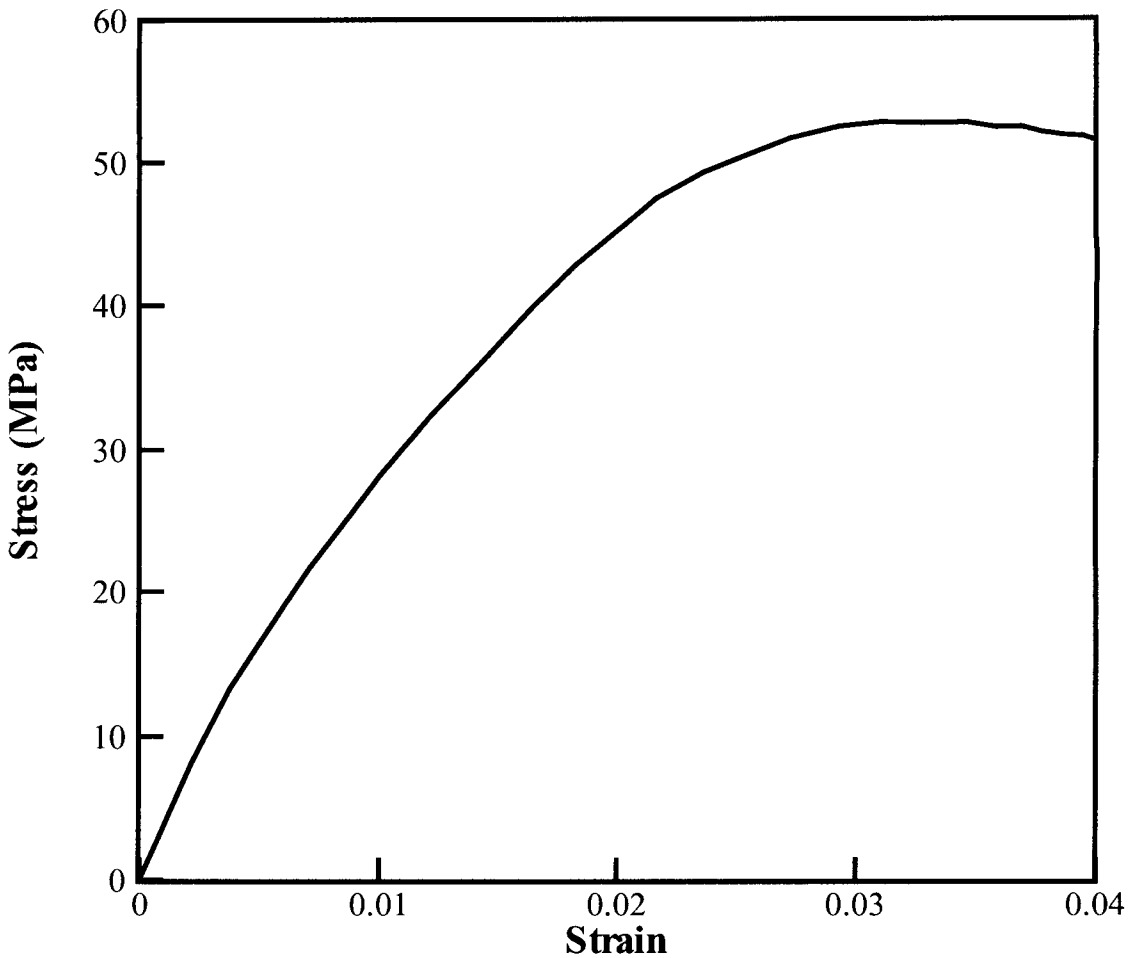

Figure 6 Stress-strain curve for unconfined vinylester (Dow Derakane 411-C50)

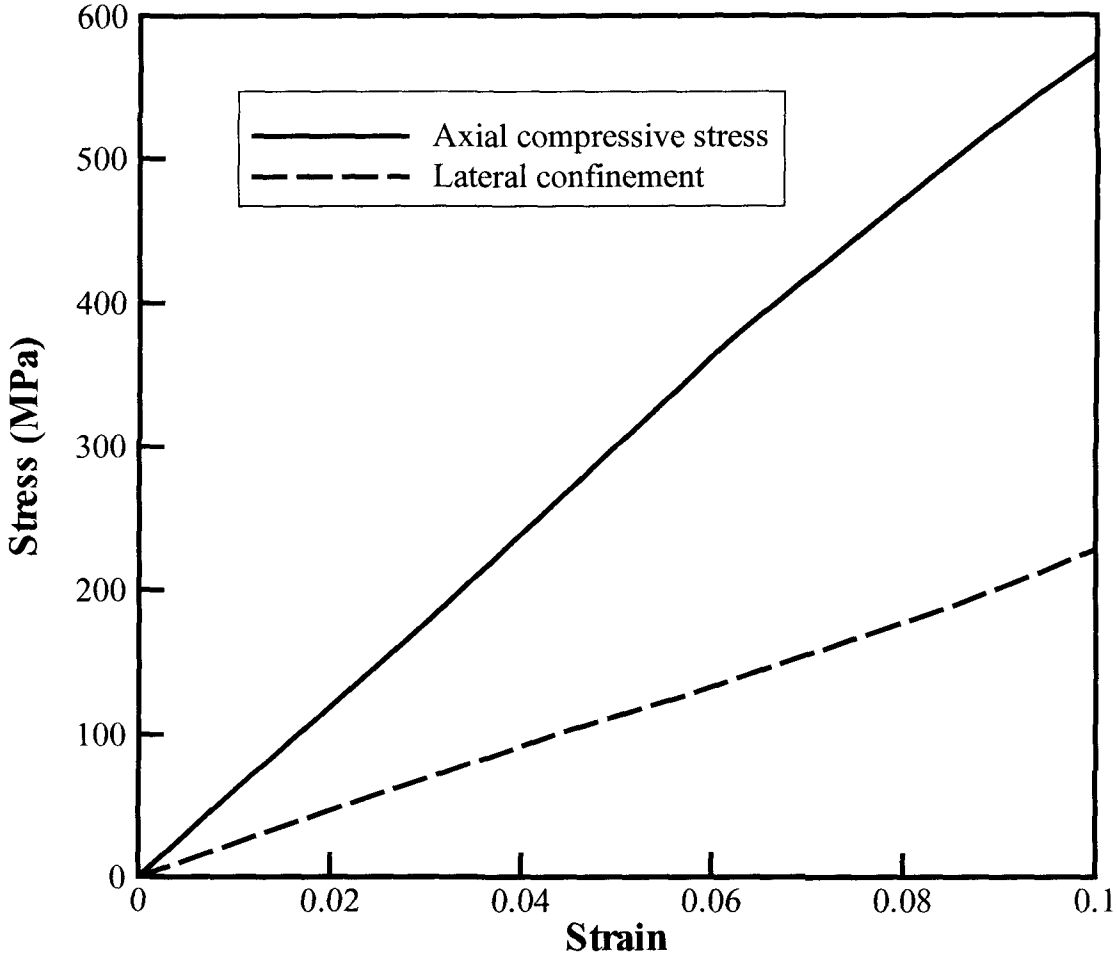

Figure 7 Stress-strain curve for laterally confined vinylester (Dow Derakane 411-C50)

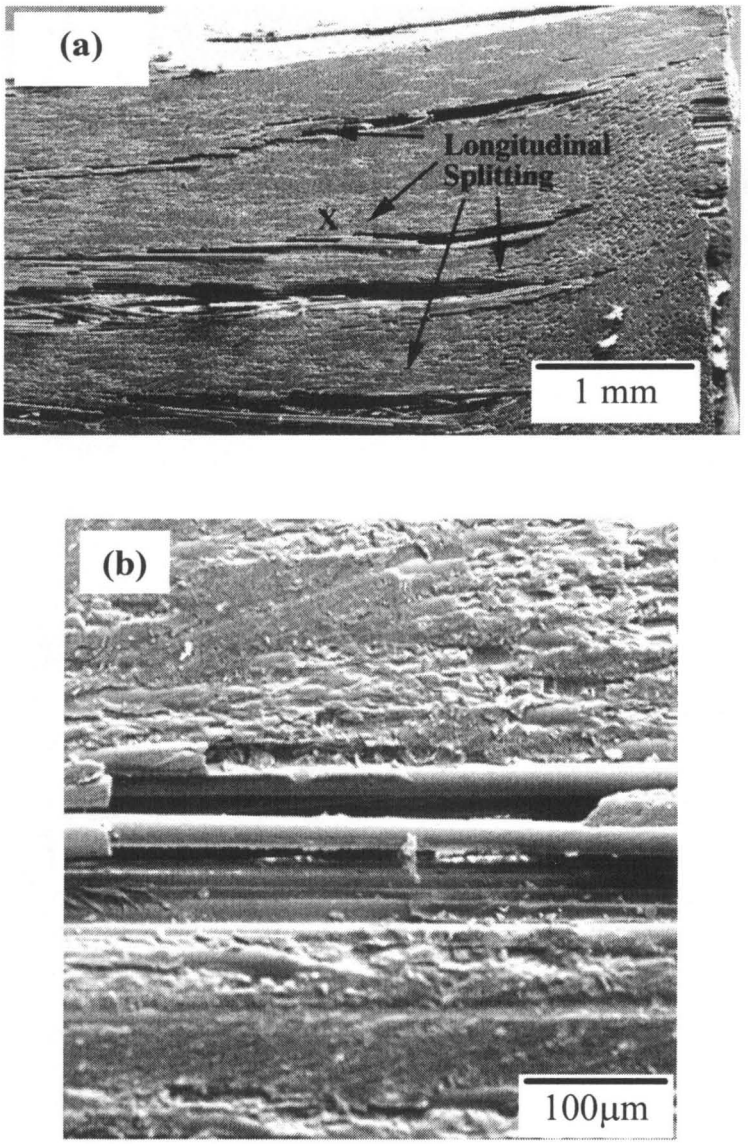

Figure 8 Longitudinal cross-section of a failed composite specimen with no lateral confinement

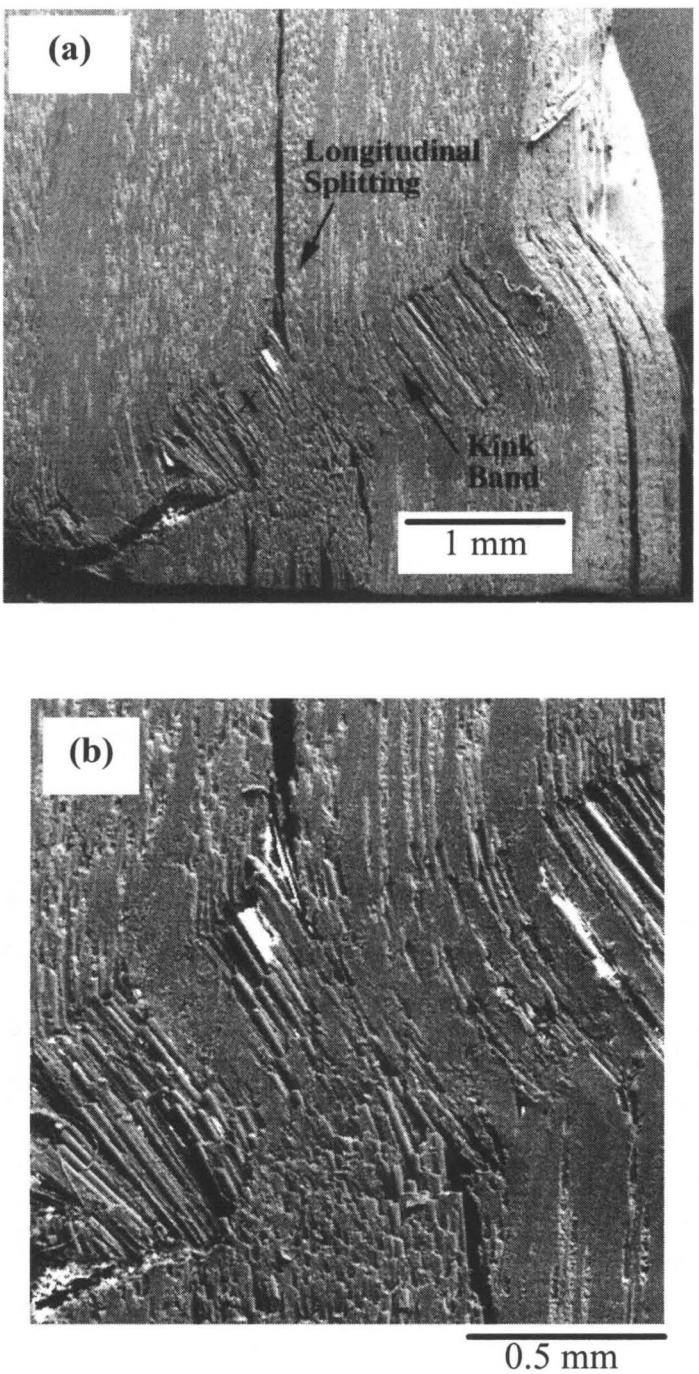

Figure 9 Longitudinal cross-section of a failed composite specimen with no lateral confinement showing 'longitudinal splitting induced' kink band formation

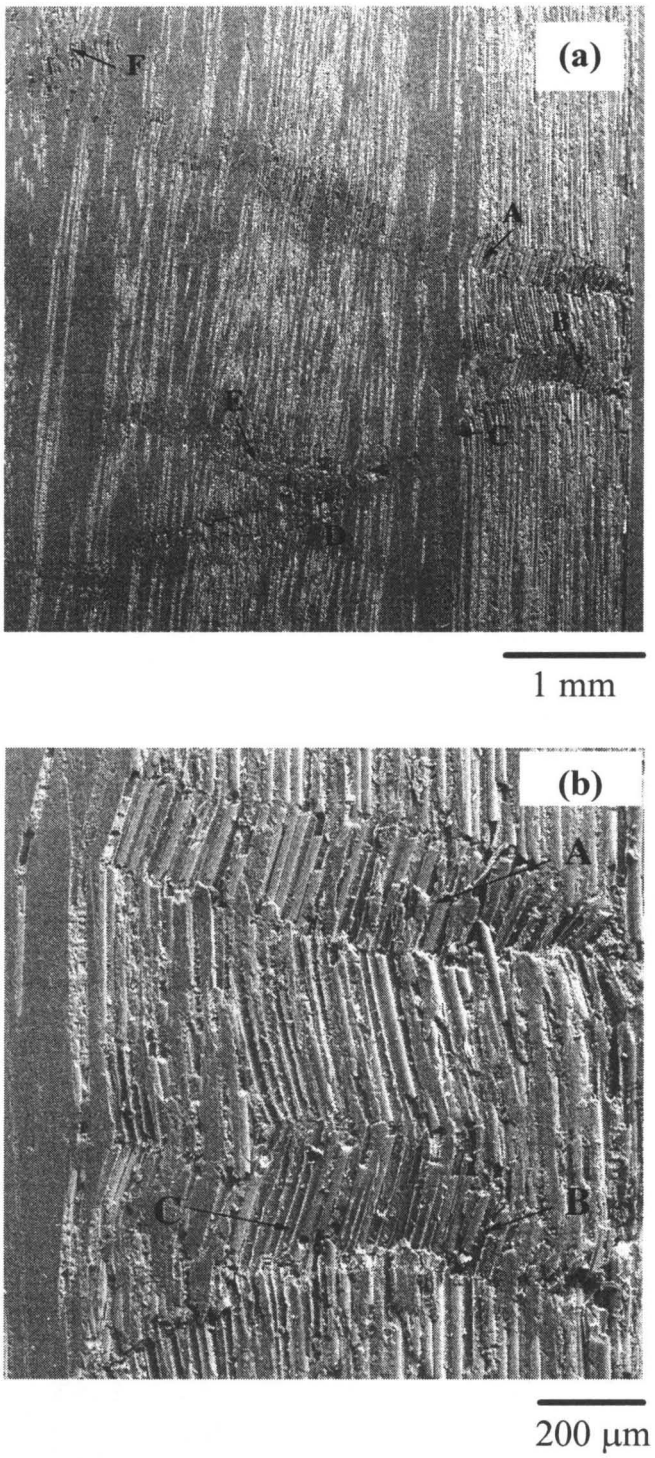

Figure 10 Longitudinal cross-section of a failed composite specimen with proportional lateral confinement showing conjugate kink band formation

Chapter II An energy-based model of longitudinal splitting in unidirectional fiber reinforced composites

Abstract

Unidirectional fiber reinforced composites are often observed to fail in a longitudinal splitting mode in the fiber direction under far-field compressive loading with weak lateral confinement. An energy-based model is developed based on the principle of minimum potential energy and the evaluation of effective properties to obtain an analytical approximation to the critical stress for longitudinal splitting. The analytic estimate for the compressive strength is used to illustrate its dependence on material properties, surface energy, fiber volume fraction, fiber diameter and lateral confining pressure. The predictions of the model show good agreement with available experimental data.

II-1 Introduction

Fiber reinforced composite materials are used in the form of laminates in numerous structural applications by taking advantage of their directional properties. Such applications are often limited by the compressive strength of the composite materials that are used. Failure modes in composite laminates are complex and are not always easily understood (e.g., Shuart, 1989; Waas and Schultheisz, 1996). On the other hand, unidirectional fiber reinforced composites serve as excellent model materials for investigating the associated strength and failure issues. Unidirectional fiber reinforced

composites also have much lower compressive strength than their tensile strength for loading in the fiber direction. Therefore, the prediction of the compressive strength is a critical issue in designing composite materials and composite structures. Commonly observed failure modes in unidirectional composites under compression in the fiber direction include (i) longitudinal or axial splitting due to transverse cracking; (ii) fiber kinking (initiation and propagation of kink bands or microbuckles) and (iii) longitudinal splitting followed by fiber kinking; see, e.g., Waas and Schultheiz (1996) and Fleck (1997). These failure modes are also observed under axial compression in the presence of lateral confinement. However, the mechanisms, which govern these failure modes in composites, are not completely understood. The effect of lateral confinement on compressive strength is an outstanding issue because of its relevance in developing and validating existing phenomenological failure models for composites (e.g., Tsai and Wu, 1971; Christensen, 1997). Also, in composite laminates, even under uniaxial compression, the stress-state is multi-axial, and hence there is a need for models that can reliably predict their strength under multiaxial stress states. For the kinking mode of failure, a wide range of experimental, analytical, computational efforts have been undertaken (e.g., Budiansky and Fleck, 1993; Kyriakides et al., 1995; Schultheisz and Waas, 1996; Waas and Schultheisz, 1996; Fleck, 1997; Lee and Waas, 1999). On the other hand, relatively little is known about longitudinal splitting due to transverse cracking. A number of researchers have observed an increase in the compressive strength with increasing lateral confinement (e.g., Weaver and Williams, 1975; Parry and Wronski, 1982; Sigley et al., 1992). Further, from a materials design point of view, it is

desirable to have models that can predict the strength of the composites in terms of the properties of fiber, matrix and their interface. Motivated by these experimental observations and the current lack of satisfactory models for longitudinal (axial) splitting in composites (with an exception in the work by Lee and Waas, 1999), a new energy based approach for predicting compressive strength of unidirectional fiber reinforced composites has been developed and is presented here.

One way to investigate the longitudinal splitting under compression is to compute the energy release rate and track the evolution of dominant micro-cracks in the composites. However, the stress field and the evolution law for a crack embedded in a highly heterogeneous material such as fiber reinforced composites is extremely complicated and hence a satisfactory analytic approach appears not to be plausible in this case. In this chapter, an energetic approach similar to the one that has been used for studying axial splitting in isotropic brittle solids such as ceramics (Bhattacharya et al., 1998) is employed to gain insights into longitudinal splitting phenomena in fiber reinforced composites. By combining the principle of minimum potential energy and the effective properties of the composite, an energy-based criterion for longitudinal splitting of unidirectional fiber reinforced composite is established. Hashin (1996) has used a similar approach in determining the energy release rate for fracture in laminated composites.

Due to the heterogeneity and anisotropy of the fiber reinforced composite, excessive elastic energy is stored in the composite under compression. Longitudinal splitting can be regarded as a process in which the excessive elastic energy is released through the formation of new surfaces. Therefore, when the reduction of the stored elastic energy by

splitting compensates the surface energy, the specimen splits. This energy-based failure criterion combined with the effective properties of the composite based on the elastic properties of the matrix and the fiber provides an analytical expression for the critical stress (compressive strength) for longitudinal splitting. This expression illustrates the effect of material properties, surface energy, fiber volume fraction, fiber diameter, and lateral confining pressure on the critical axial compressive stress for longitudinal splitting. The model predictions are compared with available experimental results in the literature (Weaver and Williams, 1975; Parry and Wronski, 1982; Waas et al., 1997) and show good agreement. The predictions break down for large confining pressures due to failure mode transition to kinking which is not accounted for in the present model.

II-2 Energy-based model for longitudinal splitting

II-2-1 Problem formulation

Consider a cylindrical specimen of an ideal[1] unidirectional fiber reinforced composite under lateral confining stress, σ_c, and axial compressive stress, σ, shown schematically in Fig. 1(a). Under this setting, compare two configurations shown in Fig. 1: (a) one is unsplit, and (b) the other is totally split in the fiber direction. Let the total potential energy density of unsplit and split specimen be Π_u and Π_s, respectively. Comparison between Π_u and Π_s provides the critical axial stress for splitting under given lateral

[1] The fibers of the same diameter are aligned and homogeneously distributed in the plane (x_2-x_3) perpendicular (transverse) to the fiber direction (x_1).

confining stress, σ_c. The criterion for longitudinal splitting is the minimization of the total potential energy density of the specimen. In other words, when Π_u exceeds Π_s, the specimen splits (Bhattacharya et al., 1998).

The total potential energy is computed in terms of the effective material properties as a function of the properties of fiber and matrix using the concept of Representative Volume Element (RVE). Instead of considering the entire problem, an auxilliary problem is set up focusing on an element (RVE) which consists of a fiber surrounded by the matrix according to the volume fraction under the same strain or stress boundary condition as that of the original problem. If the specimen is macroscopically homogeneous, the average strain and stress over the RVE are the same as that of the entire specimen. In the problem under consideration, because of the random in-plane distribution of the fibers, the RVE reduces to a circular cylinder which consists of a single straight fiber of the specimen length surrounded with matrix according to the fiber volume fraction. The issues related to establishing RVEs in fiber reinforced composites are well established (e.g., Hashin and Rosen, 1964; Hill, 1964; Nemat-Nasser and Hori, 1993).

II-2-2 Energy criterion for longitudinal splitting

Total potential energy of unsplit specimen

The total potential energy density of the unsplit specimen, Π_u, is the same as the elastic energy density. Hence, under stress (traction) boundary condition, Π_u is given as follows:

$$\Pi_u = \frac{1}{V}\int_V \left\{\frac{1}{2}\boldsymbol{\varepsilon}(x):\boldsymbol{C}(x):\boldsymbol{\varepsilon}(x) - \boldsymbol{\sigma}(x):\boldsymbol{\varepsilon}(x)\right\}dx$$
$$= \frac{1}{V}\int_V \left\{-\frac{1}{2}\boldsymbol{\sigma}(x):\boldsymbol{S}(x):\boldsymbol{\sigma}(x)\right\}dx = -\frac{1}{2}\bar{\boldsymbol{\sigma}}:\boldsymbol{S}_*:\bar{\boldsymbol{\sigma}} \qquad (1)$$

where V is the volume of the RVE, $\boldsymbol{C}(x)$ and $\boldsymbol{S}(x)$ are the fourth-order elasticity and compliance tensors at point $\boldsymbol{x}$, respectively, $\boldsymbol{\varepsilon}(x)$ is the strain field, $\boldsymbol{\sigma}(x)$ is the stress field, and $\bar{\boldsymbol{\sigma}}$ is the volumetric average stress tensor over V which corresponds to the prescribed stress on the boundary of the specimen. $\boldsymbol{S}_*$ is the effective compliance tensor of the unsplit specimen.

Because of the unidirectional reinforcement of the fibers, the specimen is transversely isotropic. Besides, the cartesian coordinates, x_1, x_2, and x_3 directions are also the principal directions. Therefore, to evaluate Π_u, we need only four independent effective moduli, namely, the longitudinal Young's modulus, E_1^*, Poisson ratio, ν_{21}^*, the plane strain bulk modulus, K_{23}^* and the shear modulus, G_{23}^*. Using the cylindrical RVE introduced before, effective elastic moduli of the unidirectional composite for random in-plane distribution of fibers, $E_1^*, \nu_{21}^*, K_{23}^*$, and the upper and lower bounds for G_{23}^* have been obtained by Hashin and Rosen (1964). Since the lower bound corresponds to the macro stress prescribed problem, the lower bound for G_{23}^* is used here. The expressions for the moduli tensor and related elasticity constants are shown in Appendix in terms of the elastic constants of the fiber and the matrix as well as their volume fractions.

The average stress–strain relation for the RVE is given as follows[2]:

$$\begin{aligned}
\bar{\sigma}_{11} &= C_{11}^{*}\bar{\varepsilon}_{11} + C_{12}^{*}\bar{\varepsilon}_{22} + C_{12}^{*}\bar{\varepsilon}_{33} \\
\bar{\sigma}_{22} &= C_{12}^{*}\bar{\varepsilon}_{11} + C_{22}^{*}\bar{\varepsilon}_{22} + C_{23}^{*}\bar{\varepsilon}_{33} \\
\bar{\sigma}_{33} &= C_{12}^{*}\bar{\varepsilon}_{11} + C_{23}^{*}\bar{\varepsilon}_{22} + C_{22}^{*}\bar{\varepsilon}_{33}
\end{aligned} \qquad (2)$$

The prescribed stress boundary conditions are

$$\bar{\sigma}_{11} = -\sigma \qquad \bar{\sigma}_{22} = \bar{\sigma}_{33} = -\sigma_c \qquad \bar{\sigma}_{12} = \bar{\sigma}_{13} = \bar{\sigma}_{23} = 0 \qquad (3)$$

where σ and σ_c are the magnitudes of the axial stress and the lateral confinement. Compressive stress components are assumed to be negative. The total potential energy density for the unsplit specimen, Π_u, is a quadratic form of the compressive stress, σ

$$\begin{aligned}
\Pi_u &= -\frac{1}{2}\begin{bmatrix} -\sigma \\ -\sigma_c \\ -\sigma_c \end{bmatrix}^T \cdot \begin{bmatrix} C_{11}^{*} & C_{12}^{*} & C_{12}^{*} \\ C_{12}^{*} & C_{22}^{*} & C_{23}^{*} \\ C_{12}^{*} & C_{23}^{*} & C_{22}^{*} \end{bmatrix}^{-1} \begin{bmatrix} -\sigma \\ -\sigma_c \\ -\sigma_c \end{bmatrix} \\
&= \frac{\left(C_{22}^{*} + C_{23}^{*}\right)\sigma^2 - 4C_{12}^{*}\sigma_c\sigma + 2C_{11}^{*}\sigma_c^{\,2}}{4C_{12}^{*\,2} - 2C_{11}^{*}\left(C_{22}^{*} + C_{23}^{*}\right)} \\
&= -\frac{1}{2}\left\{ \frac{\sigma^2}{E_1^{*}} + \frac{4\nu_{21}^{*}\sigma_c\sigma}{E_1^{*}} + \left(\frac{1}{K_{23}^{*}} + \frac{4\nu_{21}^{*\,2}}{E_1^{*}} \right)\sigma_c^{\,2} \right\}.
\end{aligned} \qquad (4)$$

[2]Expressions for $C_{11}^{*}, C_{12}^{*}, C_{22}^{*}, C_{23}^{*}$ are shown in the Appendix.

Total potential energy of split specimen

Under the same boundary condition as that of the unsplit specimen (3) and assuming that *each* RVE splits at the boundary of the matrix and the fiber, i.e., the split is caused by an interfacial crack (delamination), the split RVE can be regarded as two columns, consisting of either the fiber or the matrix. Such a simplifying assumption enables gaining insights into the strength of composites. The elastic energy density of the RVE after splitting, E_s, is given by

$$\begin{aligned} E_s &= \frac{1}{V}\int_V \left\{-\frac{1}{2}\sigma(x) : S(x) : \sigma(x)\right\} dx = -\frac{1}{2}\bar{\sigma} : S^* : \bar{\sigma} \\ &= -\frac{1}{2}\bar{\sigma} : \left(v_f S_f + v_m S_m\right) : \bar{\sigma} \end{aligned} \tag{5}$$

where S^* is the effective compliance tensor of the split specimen, v_f and v_m are volume fractions of fiber and matrix, respectively. The matrix volume fraction v_m is assumed throughout to be $(1 - v_f)$.

The fiber and the matrix are assumed to be isotropic and the compliance tensor of fiber and matrix, S_f, S_m can be expressed in terms of their respective Young's moduli (E_f, E_m) and Poisson's ratios (ν_f, ν_m). Therefore, the elastic energy density for the split specimen, E_s, is given as a quadratic form of the axial compressive stress, σ

$$E_s = -\frac{1}{2}\bar{\sigma} : \left(v_f \boldsymbol{S}_f + v_m \boldsymbol{S}_m\right) : \bar{\sigma}$$
$$= -\frac{1}{2}\left[\frac{v_f}{E_f}\left\{\sigma^2 - 4\nu_f \sigma\sigma_c + 2\left(1-\nu_f\right)\sigma_c^2\right\} + \frac{\left(1-v_f\right)}{E_m}\left\{\sigma^2 - 4\nu_m \sigma\sigma_c + 2\left(1-\nu_m\right)\sigma_c^2\right\}\right]. \tag{6}$$

The surface energy per unit volume, Γ, of the RVE due to splitting can be obtained by introducing a surface energy per unit area, γ

$$\Gamma = \frac{2\gamma A}{V} = \frac{2\gamma\left(2\pi a h\right)}{\pi R^2 h} = \frac{4\gamma v_f}{a} \tag{7}$$

where A is the lateral surface area of a fiber in the RVE, a is the radius of the fiber and R is the radius of the RVE. Note that Γ in (7) is independent of the height of the RVE, h, the height of the specimen. The surface energy γ can be interpreted as the energy release rate (G_c=2γ) for interfacial crack initiation along the fiber-matrix interface or delamination (Liu et al., 1997) and the failure is assumed to proceed catastrophically following initiation (Lambros and Rosakis, 1997). The relationship between the energy release rate G, and the local stress intensity factors K_I and K_{II} and the phase angle can be found in Liu et al. (1997).

In the present analysis, the surface energy per unit area, γ, is assumed to be a constant (i.e., γ is independent of σ and σ_c). In reality, as confining pressure, σ_c increases, the resistance to longitudinal (axial) splitting or delamination failure increases considerably

and hence, the fracture energy, G_c or γ . Even though this appears to be consistent with what one might expect, nothing is known at present concerning the effect of pressure on fracture toughness of composite materials.

The total potential energy density of the split specimen, Π_s , is the sum of the elastic energy density, E_s , and the surface energy density, Γ

$$\Pi_s = E_s + \Gamma . \qquad (8)$$

II-2-3 Criterion for longitudinal splitting

From the principle of minimum potential energy, the criterion for axial splitting can be expressed as

$$\begin{aligned} \Pi_u - \Pi_s < 0 &\Rightarrow \text{Unsplit} \\ \Pi_u - \Pi_s = 0 &\Rightarrow \text{Neutral} \\ \Pi_u - \Pi_s > 0 &\Rightarrow \text{Split} \end{aligned} \qquad (9\text{ a, b, c})$$

Assuming that Γ is independent of stress state, the equi-potential line $\Pi_u - E_s = \Gamma$, i.e., $\Pi_u - \Pi_s = 0$ provides the stress state for the neutral condition (9b). Examining the quadratic form $\Pi_u - E_s$, it can be shown that $\Pi_u - E_s$ is a monotonically increasing function of σ for $\sigma_c = constant$ provided $\sigma > \sigma_c$. Therefore, the critical condition is

given by the equality,

$$\Pi_u - \Pi_s = 0. \tag{10}$$

The criterion for longitudinal splitting (10) could be interpreted in terms of the surface energy of the newly created surfaces (G_c=2γ) which cause the reduction in the elastic energy of the intact (unsplit) material.

II-3 Results

II-3-1 Compressive strength

Substituting for Π_u and Π_s from (4) to (8), the critical stress for longitudinal splitting can be obtained by solving (10). Since the form of the total potential energy is a quadratic of σ , there are two roots σ_1 and σ_2

$$\sigma_{1,2} = \frac{p_2\sigma_c \pm \sqrt{p_2{}^2\sigma_c{}^2 - p_1\left(p_3\sigma_c{}^2 - \Gamma\right)}}{p_1} \tag{11}$$

where p_1, p_2 and p_3 are expressed in terms of the elastic constants of the materials

$$p_1 = \frac{1}{2}\left(\frac{\nu_f}{E_f} + \frac{\nu_m}{E_m} - \frac{1}{E_1^*}\right), \quad p_2 = \frac{\nu_f\nu_f}{E_f} + \frac{\nu_m\nu_m}{E_m} - \frac{\nu_{21}^*}{E_1^*},$$

$$p_3 = \frac{v_f(1-\nu_f)}{E_f} + \frac{v_m(1-\nu_m)}{E_m} - \frac{1}{2}\left(\frac{1}{K_{23}^*} + \frac{4\nu_{21}^{*2}}{E_1^*}\right).$$

For a given confining pressure σ_c and surface energy density γ, $\sigma_1 \geq \sigma_2$, hence, σ_1 is taken as the critical stress, σ^*. Letting $\sigma_c = 0$ in (11), the critical stress without confinement, i.e., the unconfined longitudinal compressive strength for the composite can be obtained,

$$\sigma^*|_{\sigma_c=0} = 2\left(\frac{2\gamma\, v_f}{a}\right)^{\frac{1}{2}}\left(\frac{v_f}{E_f} + \frac{v_m}{E_m} - \frac{1}{E_1^*}\right)^{-\frac{1}{2}}. \qquad (12)$$

Equation (12) shows that unconfined strength is proportional to the square root of surface energy and inversely proportional to the square root of fiber diameter. This result indicates that for a given volume fraction, all other things remaining unchanged, composites with larger fiber diameter are more susceptible to axial splitting than smaller diameter fibers. Since $E_f >> E_m$ in usual fiber reinforced composites, $v_m/E_m >> v_f/E_f$ and $E_1^* \cong v_f E_f$ hold. Based on these evaluations, (12) can be simplified as follows:

$$\sigma^*|_{\sigma_c=0} = 2\left(\frac{2\gamma\, v_f}{a}\right)^{\frac{1}{2}}\left(\frac{1-v_f}{E_m} - \frac{1}{v_f E_f}\right)^{-\frac{1}{2}}. \qquad (13)$$

Examining the quadratic form of the energy surface, $\Phi(\sigma,\sigma_c)=\Pi_u-\Pi_s$ for a constant surface energy density γ, and assumimg that the longitudinal (fiber direction) compliance is smaller than the lateral (transverse) compliance in the composite (typical for most fiber reinforced composites), the following inequality holds:

$$\frac{d\sigma^*}{d\sigma_c}\leq 1 \qquad (14)$$

subject to the constraints

$$\sigma>\sigma_c \text{ and } d\Phi=\frac{\partial\Phi}{\partial\sigma}d\sigma+\frac{\partial\Phi}{\partial\sigma_c}d\sigma_c=0 \qquad (15\text{ a,b})$$

The first constraint (15a) corresponds to axial compression and the second constraint (15b) corresponds to the equi-potential line. From (14), one can conclude that if the splitting failure is governed by the principle of minimum total potential energy and the surface energy density γ is a constant, the slope of the relationship between compressive strength and confining pressure, i.e., σ^* vs. σ_c, can not exceed unity. Even if the surface energy density γ is an increasing function of confining pressure σ_c, the inequality (14) holds at least for small σ_c. The effect of lateral confinement and material properties on the compressive strength of composites can be investigated by using (11).

II-3-2 Model predictions

Examining the functional form shown in (11) and (12), important parameters for longitudinal splitting can be identified as γ/a, v_f and σ_c. To investigate the dependence of compressive strength on each of these parameters and compare the effect of each parameter, parametric studies have been performed. In the present parametric study, two different types of commonly used fiber reinforced composite are investigated to illustrate the dependence of compressive strength on material properties. These materials are a unidirectional E-glass/vinylester composite (indicated as "G/VE" in the figures) and a unidirectional carbon/epoxy composite (indicated as "C/ER" in the figures). Experimental data and material properties for these materials are available in the literature (Parry and Wronski, 1982; Waas et al., 1997). The relevant material properties including those of the fiber and the matrix as well as the radius of the fibers for these composites are shown in Table 1. Surface energy density γ 's shown in Table 1 are obtained by calibration to the corresponding experimental data for unconfined compressive strength.

Figure 2 shows the compressive strength of two types of composite for different γ/a and σ_c (0 and 100 MPa) with fixed fiber volume fraction $v_f = 60\%$. One can observe a strong dependence of compressive strength on γ/a (proportional to $\sqrt{\gamma/a}$) and relatively weak dependence on σ_c. Also, the compressive strength seems to be almost insensitive to the choice of the material for a given value of γ/a. Small values of γ/a correspond to low interfacial energy (weak interface) and/or large diameter fibers where

large values of γ/a correspond to large interfacial energy (tough interface) and/or small diameter fibers. The unconfined compressive strengths of E-glass/vinylester composite and carbon/epoxy composite with $v_f = 60\%$ are 667 MPa (Waas et al., 1997) and 1.5 GPa (Parry and Wronski, 1982), respectively. Based on these experimental observations, if the v_f is identical, the carbon/epoxy composite appears to be stronger than the E-glass/vinylester composite. However, the strong dependence on γ/a plays a significant role here. Suppose γ is of the same order for both composites, fiber radii a for E-glass/vinylester composite and carbon/epoxy composite are 12.1 μm and 3.4 μm, respectively (see Table 1). This results in γ/a for the carbon/epoxy composite to be approximately four times as that of the E-glass/vinylester composite.

Figure 3 shows unconfined compressive strength (i.e., $\sigma_c = 0$) as a function of γ/a and v_f. For a given γ/a, effect of v_f on compressive strength is much stronger than that of the material properties. This observation together with the insensitivity of the strength to the choice of the material observed in Fig. 2 has the following implication. The compressive strength of the unidirectional fiber reinforced composite is relatively insensitive to the magnitude of the material properties of each constituent, i.e., fiber and matrix. Instead, the degree of anisotropy introduced by combining the materials with different material properties is an important factor in the determination of compressive strength. Longitudinal splitting can be considered to be the process in which excessive stored elastic energy due to the heterogeneity and anisotropy can be released through the formation of new surfaces. The importance of anisotropy has been evidenced in this

parametric study.

Compressive strength for different v_f and σ_c with fixed γ/a is shown in Fig. 4. Based on experimental observations, $\gamma/a = 1.32\times10^7\ \mathrm{J/m^3}$ and $\gamma/a = 4.17\times10^7\ \mathrm{J/m^3}$ are used for E-glass/vinylester and carbon/epoxy respectively as the best fitting values for the model prediction of their unconfined compressive strength (Parry and Wronski, 1982; Waas et al., 1997). It is again seen that if the same values for γ/a were used, the compressive strength for both materials are close to each other as expected from previously shown parametric studies (Fig. 2, Fig.3). In this case, the difference between the results for two different levels of confinement $\sigma_c = 0\ \mathrm{MPa}$ $\sigma_c = 100\ \mathrm{MPa}$ is small and nearly constant for all values of v_f shown here. This shows that the effect of σ_c on compressive strength is much weaker than that of v_f and is relatively insensitive for a given v_f.

II-3-3 Comparison with experiments

To verify the validity of the energy-based model for longitudinal splitting, the compressive strengths predicted by the present model are compared with the experimental results obtained for E-glass/vinylester and carbon/epoxy composites. Uniaxial compression tests on unidirectional fiber reinforced E-glass/vinylester composite with different fiber volume fraction ranging from 0% to 60% were performed by Waas et al. (1997). For carbon/epoxy composites, compression tests on unidirectional fiber reinforced composites under superposed hydrostatic confinement have been

performed by Weaver and Williams (1975) and Parry and Wronski (1982). The input parameters for the model prediction including material properties, fiber radius and surface energy of the material used in their experiments have been shown in Table 1.

Comparison between the model prediction and experimental results by Waas et al. (1997) provides the measure of the validity of the present model with respect to changing v_f. Experimental results for the unconfined copressive strength from Waas et al. (1997) are shown in Fig. 5. Examining the trend in compressive strength, one can observe a dip between $v_f = 30\%$ and $v_f = 40\%$. Based on this observation, analysis is performed for two groups of data sets. One is for low v_f, i.e., $v_f \leq 30\%$, the other is for high v_f, i.e., $v_f \geq 40\%$. Only the difference in these analyses is the input parameter for the surface energy γ. The values of the surface energy which enable the model predictions to show good agreement with experimental results are $\gamma = 210\ \mathrm{J/m^2}$ for the low v_f data set and $\gamma = 110\ \mathrm{J/m^2}$ for the high v_f data set. In the present model, γ has been assumed to be the surface energy associated with delamination between the fiber and the matrix. The surface energy associated with the creation of new surfaces in the matrix has been neglected. In the case of high v_f, surface energy associated with matrix failure is negligible since the average distance between fibers is small and the area of the surface created by matrix failure is much smaller than the one created by interface (fiber-matrix) debonding. On the other hand, as the fiber volume fraction decreases, the average distance between fibers increases and the surface energy associated with matrix failure becomes no longer negligible, which results in the increase of total surface energy. Also,

the non-linearity of the matrix for vinylester (Waas et al., 1997) which is important at low volume fractions of the fiber has been neglected in the present analysis. The increase in surface energy associated with matrix failure is consistent with the requirement for larger surface energy γ for lower v_f. Further work towards quantification of fracture energies as a function of volume fraction in fiber reinforced composites is needed. The model predictions for matrix dominated region and fiber interface dominated region can be regarded respectively as upper and lower bound for compressive strength of the composite.

The experimental result shows considerable scatter for $v_f \geq 40\%$. In general, the interfacial toughness is highly dependent on local conditions such as size/orientation of initial imperfection, mode mixity and bonding (interface strength and toughness). As a result, the interface properties vary more than the material properties of each constituent of composite, i.e., fiber and matrix. The fracture energy of fiber reinforced composites (G_c) depends strongly on the local mode mixity (Liu et al., 1997). Therefore, for the case of low v_f, the scatter in compressive strength is relatively small since the matrix plays a signifiant role in determining the surface energy associated with splitting. On the other hand, since the surface energy associated with fiber/matrix debonding is dominant for high v_f, the local interfacial conditions play a significant role in determining the compressive strength. This results in a large scatter of the compressive strength for composites with high v_f as seen from the experimental results in Fig. 5.

Comparison between the model prediction and experimental results by Weaver and

Williams (1975) (WW) and Parry and Wronski (1982) (PW) provides a measure of the validity of the present model with respect to the confining pressure, σ_c. To the best knowledge of the authors, WW and PW are the most widely accepted reliable experimental data regarding compressive failure of unidirectional fiber reinforced composites under superposed hydrostatic confinement including detailed discussion on failure modes. Although some specimen geometry dependence of failure mode is reported in PW and short specimens used in WW show end effect, their experiments are convincing enough to regard longitudinal splitting as the dominant failure mode under weak lateral confinement. The critical stress σ^* is plotted against the confining pressure σ_c in Fig. 6 (WW for $0 \le \sigma_c \le 150\,\text{MPa}$) and in Fig. 7 (PW for $0 \le \sigma_c \le 300\,\text{MPa}$). In the experiments by PW, for higher confining pressure ($\sigma_c > 150\,\text{MPa}$), the slope of σ_c vs. σ^* graph is steeper than those for lower confining pressure as seen in Fig. 7. This increase of the slope is also observed in the experiments by WW. Besides, both observed failure mode transition from longitudinal splitting to kink banding around $\sigma_c = 150\,\text{MPa}$. Therefore, the comparisons are restricted to low levels of confinement, i.e., $0 \le \sigma_c \le 150\,\text{MPa}$. Surface energy per unit area, γ used here is assumed to be the same for both the cases and is shown in Table 1. The model predictions show significant agreement with the experimental results, especially with those obtained by PW (Fig. 7). The theoretical predictions agree with the experimental results given by WW (Fig. 6) for confining pressures $0 \le \sigma_c \le 50\,\text{MPa}$. However, in the range of $50 \le \sigma_c \le 150\,\text{MPa}$, the agreement is not good. The experimental results show considerable scatter for confining

pressures $50 \le \sigma_c \le 150$ MPa although the samples A, B and C are made of the same material. It is believed that due to low fiber volume fraction (36%), a host of failure modes might have occurred under the confining pressure $50 \le \sigma_c \le 150$ MPa in the experiments by WW, and this could explain the scatter in experimental results. Also, $v_f = 36\%$ happens to be in the range of transition zone from matrix dominated region to interface dominated region for longitudinal (axial) splitting of E-glass/vinylester composite discussed above. Although the material is different, the geometrical interpretation about the increase of the area of the matrix failure still holds in this case. Therefore, the large scatter in compressive strength might be a result of the characteristic of the transition zone between low and high volume fraction of fibers.

In the present model, the only adjustable parameter is surface energy per unit area, γ, which is not readily available for the composites considered here from experimantal measurements. However, the values γ used in the model predictions appear to be consitent with data available for similar compsoite materials (Daniel and Ishai, 1994) by assuming $G_c=2\gamma$.

II-4 Conclusions and discussion

An energy-based model has been developed for predicting the compressive strength of unidirectional fiber reinforced composites which fail by longitudinal (axial) splitting. The following conclusions are based on the analytic results (11) and (12):

(i) The critical stress for longitudinal splitting is proportional to $\sqrt{\gamma/a}$ and this parameter is the most dominant term in the determination of the compressive strength of fiber reinforced composites. According to the present model, composites with larger fracture energy and small fiber diameters would result in higher strength;

(ii) the degree of the anisotropy plays a significant role and the effect of fiber volume fraction appears only in this context in influencing the compressive strength;

(iii) the effect of confining pressure on compressive strength is relatively weak.

The model prediction has been compared with the experimental results and showed good agreement. This agreement supports the validity of the present method for the analysis of longitudinal splitting (delamination failure) in unidirectional fiber reinforced composites.

The assumption of a constant γ would predict longitudinal splitting at all levels of confinement and with markedly lower strength than experimentally observed ones at high confining pressures. Beyond certain confining pressure, longitudinal splitting is completely suppressed and the failure mode translates to kink banding (Weaver and Williams, 1975; Parry and Wronski, 1982; Sigley et al., 1992). In order to illustrate the effect of increasing fracture surface energy, γ with increasing pressure, γ is assumed to depend on σ_c as follows:

$$\gamma = \gamma_0 \left\{ 1 + \alpha_n \left(\frac{\sigma_c}{\sigma_0^*} \right)^n \right\} \qquad (16)$$

where γ_0 is surface energy for $\sigma_c = 0$, σ_0^* is the unconfined compressive strength, n is the confining pressure hardening exponent and α_n is a positive dimensionless parameter corresponding to the exponent n. For $n \neq 0$ in (16), γ increases as σ_c increases and this results in nonlinear dependence of model prediction of compressive strength on σ_c. In this case, the inequality (14) for the slope of σ^* vs. σ_c being less than unity holds at least for small σ_c. The dependence of γ on σ_c (16) can be viewed to reflect the increase in the energy release rate G_c as the local mode mixity for interface cracking changes from mostly mode-I to mode-II (Liu et al., 1997) with increasing confinement.

The model predictions of compressive strength for the carbon/epoxy composite used by Parry and Wronski (1982) for the cases n=2 and n=4 in (16) are shown in Fig. 7. Input parameters for the model predictions are $\gamma_0 = 140$ J/m^2, $\sigma_0^* = 1.5$ GPa, $\alpha_2 = 15.58$ and $\alpha_4 = 823.6$. Comparison between the cases of n=2 and n=4 shows that as the exponent n increases, the curvature of the failure envelope can be increased and as a result, the model prediction for longitudinal splitting stays close to experimental result in wider range of confinement than the prediction based on smaller n and exceeds the experimental value at high confining pressures where formation of kink bands, instead of longitudinal splitting, is observed in experiments. This observation implies that if γ increases as a function of σ_c and its dependence on σ_c is strong, i.e., exponent n is large, longitudinal or axial splitting can be observed up to certain levels of confinement and is suppressed at high levels of confinement where other failure modes such as kink band formation should be considered.

Acknowledgements

This work was supported by the Office of Naval Research (Dr. Y. D. S. Rajapakse, Scientific Officer) through a grant to the California Institute of Technology.

Appendix

Following Hashin & Rosen (1964), the expression for the effective moduli of the unidirectional fiber composite (x_1 – fiber direction) E_1^*, ν_{21}^*, K_{23}^* and G_{23}^* are given below:

$$E_1^* = \left(\nu_f E_f + \nu_m E_m\right)\frac{E_m\left(D_1 - D_3F_1\right) + E_f\left(D_2 - D_4F_2\right)}{E_m\left(D_1 - D_3\right) + E_f\left(D_2 - D_4\right)}; \qquad \nu_{21}^* = \frac{\nu_f E_f L_1 + \nu_m E_m L_2 \nu_m}{\nu_f E_f L_3 + \nu_m E_m L_2}$$

$$K_{23}^* = K_m \frac{K_f\left(1 + 2\nu_m \nu_f\right) + 2K_m \nu_m \nu_m}{K_f \nu_m + K_m\left(\nu_f + 2\nu_m\right)}; \quad G_{23}^* = G_m \Big/ \left[1 + \frac{2\left(1-\nu_m\right)}{1-2\nu_m}\nu_f A_4\right] \qquad \text{(lower bound)}$$

where $D_1 = 1 - \nu_f$, $D_2 = \dfrac{1+\nu_f}{\nu_m} + \nu_m$, $D_3 = 2\nu_f^{\,2}$, $D_4 = 2\nu_m^{\,2}\dfrac{\nu_f}{\nu_m}$,

$$F_1 = \frac{\nu_m \nu_f E_f + \nu_f \nu_m E_m}{\nu_f \nu_f E_f + \nu_m \nu_m E_m}, \quad F_2 = \frac{\nu_f}{\nu_m} F_1,$$

$$L_1 = 2\nu_f\left(1-\nu_m^{\,2}\right)\nu_f + \nu_m\left(1+\nu_m\right)\nu_m, \quad L_2 = \nu_f\left(1-\nu_f-2\nu_f^{\,2}\right), \quad L_3 = 2\left(1-\nu_m^{\,2}\right)\nu_f + \left(1+\nu_m\right)\nu_m,$$

$$\begin{aligned} A_4 = {} & 2\left(G_f - G_m\right)\left(2\nu_m - 1\right)\left[G_m\left(4\nu_f - 3\right)\left(\nu_f^{\,3} - 1\right) - G_f\left\{\left(4\nu_m - 3\right)\nu_f^{\,3} - 1\right\}\right] / \\ & \left[G_m^{\,2}\left(4\nu_f - 3\right)\left(\nu_f - 1\right)^4 - 2G_f G_m\left\{-5 + 6\nu_m - 4\nu_f + 6\nu_f^{\,2} - 4\nu_m \nu_f^{\,3} + \left(3 - 2\nu_m\right)\nu_f^{\,4}\right.\right. \\ & \left.\left. + 2\nu_f\left(3 - 4\nu_m + 4\nu_m - 6\nu_f^{\,2} + 4\nu_m \nu_f^{\,3} - \nu_f^{\,4}\right)\right\} \\ & + G_f^{\,2}\left\{3 + 4\nu_f - 6\nu_f^{\,2} + 4\nu_f^{\,3}\left(3 - 6\nu_m + 4\nu_m^{\,2}\right) + \left(3 - 4\nu_m\right)\nu_f^{\,4} - \nu_m\right\}\Big] \end{aligned}$$

E_f, ν_f, v_f and E_m, ν_m, v_m are the Young's moduli, Poisson's ratios and the volume fractions of the fiber and the matrix, respectively.

The elastic moduli $C_{11}^*, C_{12}^*, C_{22}^*, C_{23}^*$ are expressed using E_1^*, ν_{21}^*, K_{23}^* and G_{23}^* given above,

$$C_{11}^{*} = E_1^{*} + 4\nu_{21}^{*\,2} K_{23}^{*}$$
$$C_{12}^{*} = 2\nu_{21}^{*} K_{23}^{*}$$
$$C_{22}^{*} = K_{23}^{*} + G_{23}^{*}$$
$$C_{23}^{*} = K_{23}^{*} - G_{23}^{*} .$$

References

Bhattacharya, K., Ortiz, M. and Ravichandran G., 1998, "Energy-based model of compressive splitting in heterogeneous brittle solids," *J. Mech. Phys. Solids*, Vol. 46, pp. 2171-2181.

Budiansky, B. and Fleck, N. A., 1993, "Compressive failure of composites," *J. Mech. Phys. Solids*, Vol. 41, pp. 183-211.

Christensen, R. M., 1997, "Stress based yield/failure criteria for fiber composites," *Int. J. Solids Structures*, Vol. 34, pp. 529-543.

Daniel, I. M. and Ishai, O., 1994, Engineering Mechanics of Composite Materials, Oxford University Press.

Fleck, N. A., 1997, "Compressive failure of fiber reinforced composites," *Advances in Applied Mechanics*, Vol. 33, pp. 43-117.

Hashin, Z. and Rosen, B. W., 1964, "The elastic moduli of fiber-reinforced materials," *J. Appl. Mech.*, Vol. 31, pp. 223-232.

Hashin, Z., 1996, "Finite thermoelastic fracture criterion with application to laminate cracking analysis," *J. Mech. Phys. Solids*, Vol. 44, pp. 1129-1145.

Hill, R., 1964, "Theory of mechanical properties of fibre-strengthened materials: I. Elastic behaviour," *J. Mech. Phys. Solids*, Vol. 12, pp. 199-212.

Kyriakides, S., Arseculeratne, R., Perry, E. J. and Liechti, K. M., 1995, "On the compressive failure of fiber reinforced composites," *Int. J. Solids Structures*, Vol. 32, pp. 689-738.

Lambros, J. and Rosakis, A. J., 1997, "Dynamic crack initiation and growth in thick

unidirectional graphite/epoxy plates," *Composites Science And Technology*, Vol. 57, pp. 55-65.

Lee, S. H. and Waas, A. M., 1999, "Compressive response and failure of fiber reinforced unidirectional composites," *Int. J. Fracture*, to appear.

Liu, C., Huang, Y., Lovato, M. L. and Stout, M. G., 1997, "Measurement of the fracture toughness of a fiber-reinforced composite using the Brazilian disk geometry," *Int. J. Fracture*, Vol. 87, pp. 241-263.

Nemat-Nasser, S. and Hori, M., 1993, Micromechanics: Overall Properties of Heterogeneous Materials, Elsevier, New York.

Parry, T. V. and Wronski, A. S., 1982, "Kinking and compressive failure in uniaxially aligned carbon fibre composite tested under superposed hydrostatic pressure," *J. Mater. Sci.*, Vol. 17, pp. 893-900.

Schultheisz, C. R. and Waas, A. M., 1996, "Compressive failure of composites, Part I: Testing and micromechanical theories," *Prog. Aerospace Sci.*, Vol. 32, pp. 1-42.

Shuart, M. J., 1989, "Failure of compression-loaded multidirectional composite laminates," *AIAA Journal*, Vol. 27, pp. 1274-1279.

Sigley, R. H., Wronski, A. S. and Parry, T. V., 1992, "Axial compressive failure of glass-fibre polyester composites under superposed hydrostatic pressure: influence of fibre bundle size," *Compos. Sci. Tech.* Vol. 43, pp. 171-183.

Tsai, S. W. and Wu, E. M., "A general theory of strength for anisotropic materials," *J. Composite Materials*, Vol. 5, pp. 58-80.

Waas, A. M. and Schultheisz, C. R., 1996, "Compressive failure of composites, Part

II: Experimental studies," *Prog. Aerospace Sci.*, Vol. 32, pp. 43-78.

Waas, A. M., Takeda, N., Yuan, J. and Lee, S. H., 1997, "Static and dynamic compressive behavior of glass fiber reinforced unidirectional composites," *Proceedings of the American Society for Composites, Twelfth Technical Conference,* pp. 552-561, Dearborn, Michigan.

Weaver, C. W. and Williams, J. G., 1975, "Deformation of a carbon-epoxy composite under hydrostatic pressure," *J. Mater. Sci.*, Vol. 10, pp. 1323-1333.

List of tables

List of figures

Table 1 Material properties of fiber and matrix and geometry of fiber

	Fiber				Matrix		Interface
	E_f (GPa)	ν_f [(d)]	ν_f	a (μm)	E_m (GPa)	ν_m	γ [(d)] (J/m^2)
E-Glass/ Vinylester	72.4[(a)]	0.2	0.1 – 0.6[(a)]	12.1[(a)]	3.69[(a)]	0.38[(d)]	110, 210
Carbon/Epoxy	260[(b)]	0.2	0.36[(b)]	3.4[(b)]	1.63[(b)]	0.34[(b)]	140
Carbon/Epoxy	234[(c)]	0.2	0.6[(c)]	3.4[(d)]	4.28[(c)]	0.34[(d)]	140

[(a)] Waas et al. (1997); [(b)] Weaver and Williams (1975); [(c)] Parry and Wronski (1982);

[(d)] assumed

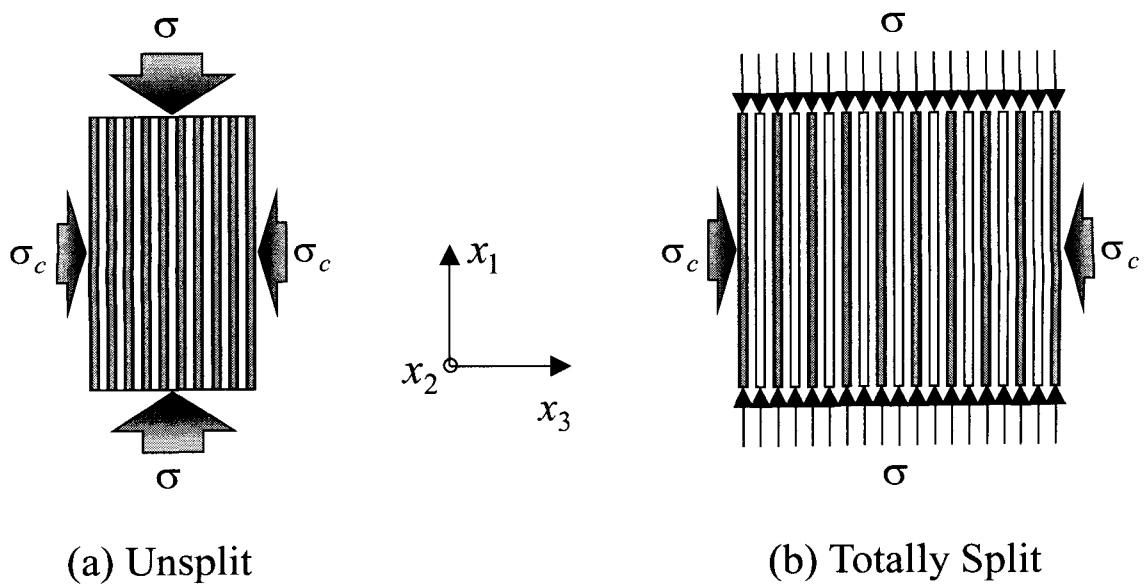

Figure 1 Schematics of unsplit and longitudinally split configurations for a unidirectional fiber composite

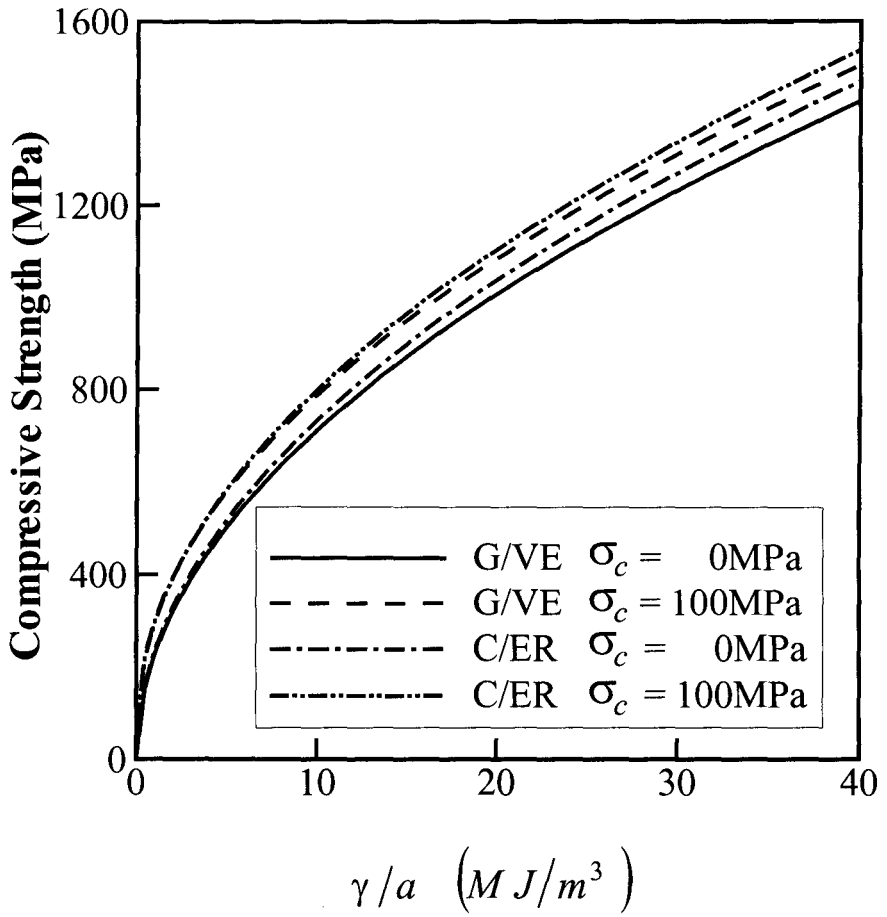

Figure 2 Effect of surface energy and lateral confinement on compressive strength (G/VE stands for E-Glass/vinylester and C/ER stands for carbon/epoxy)

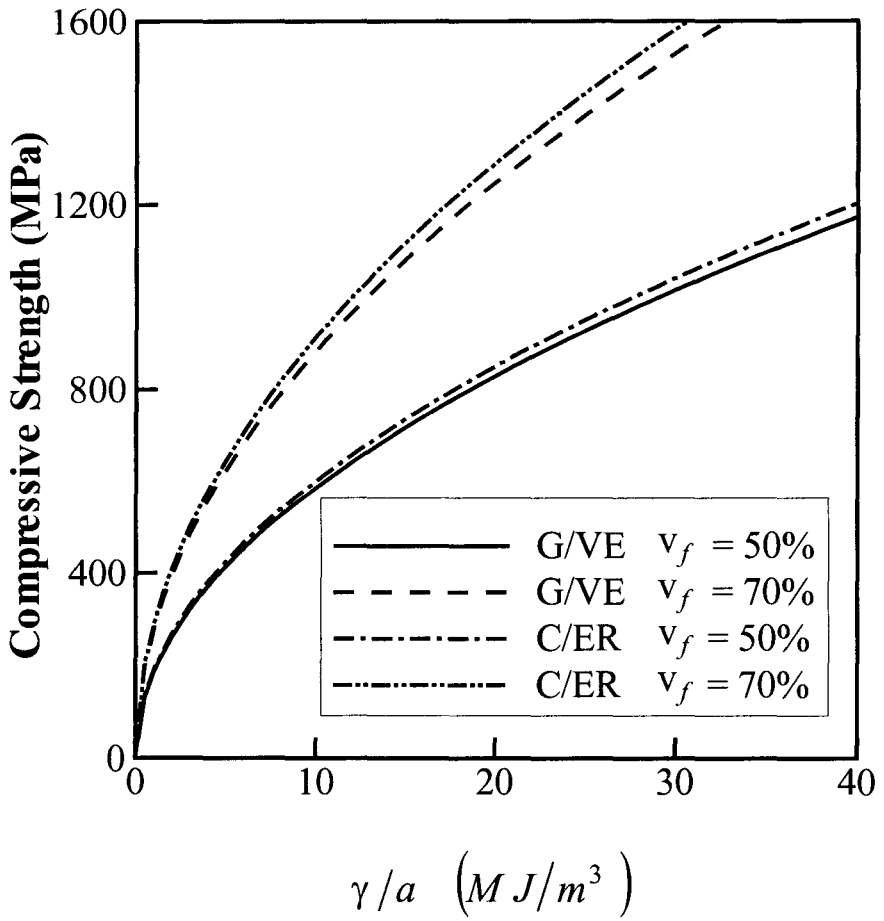

Figure 3 Effect of surface energy and fiber volume fraction on unconfined compressive strength ($\sigma_c = 0$) (G/VE stands for E-Glass/vinylester and C/ER stands for carbon/epoxy)

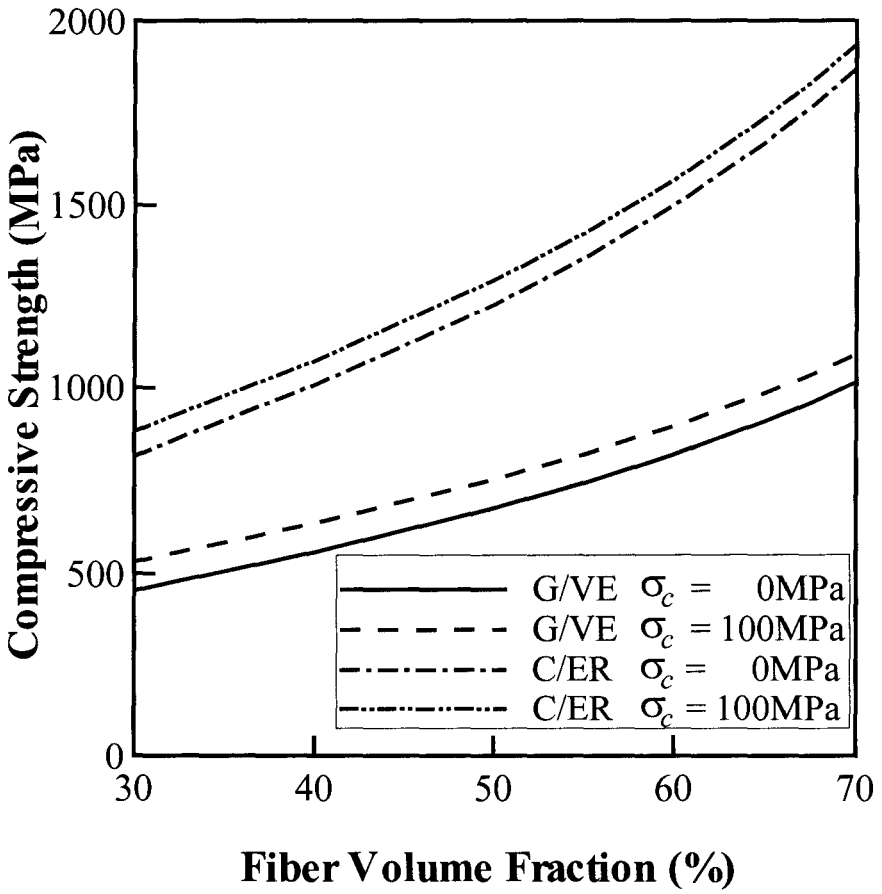

Figure 4 Effect of fiber volume fraction and lateral confinement on compressive strength

(G/VE stands for E-Glass/vinylester and C/ER stands for carbon/epoxy)

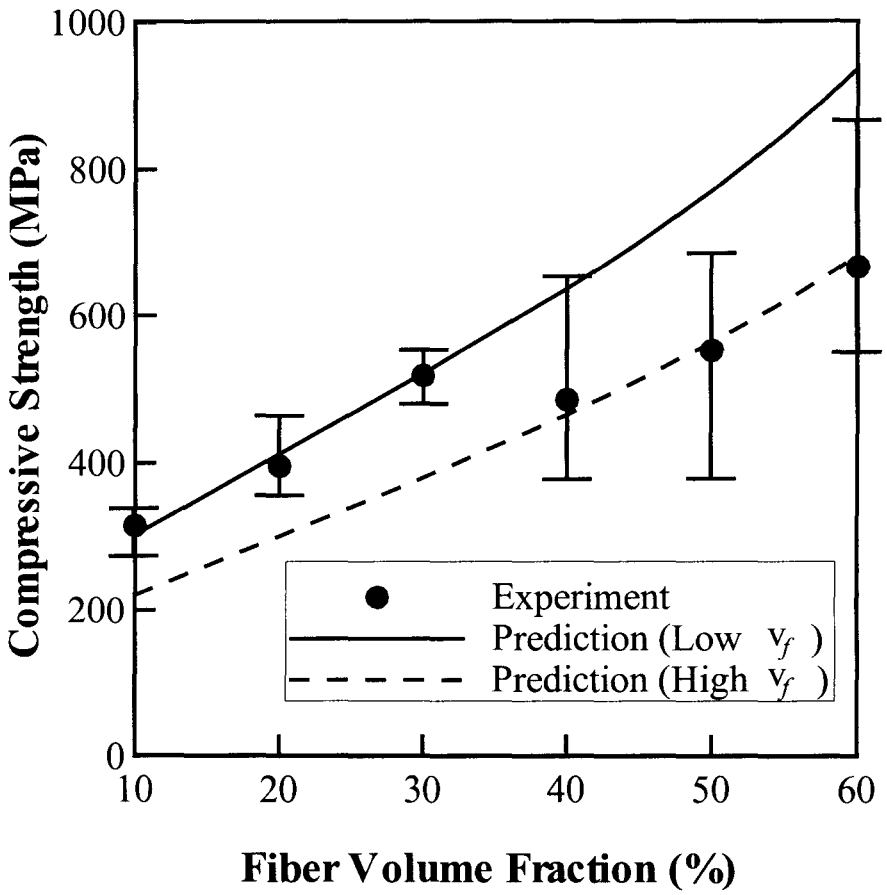

Figure 5 Comparison between experimental results (Waas et al., 1997) and model predictions for E-Glass/vinylester composite

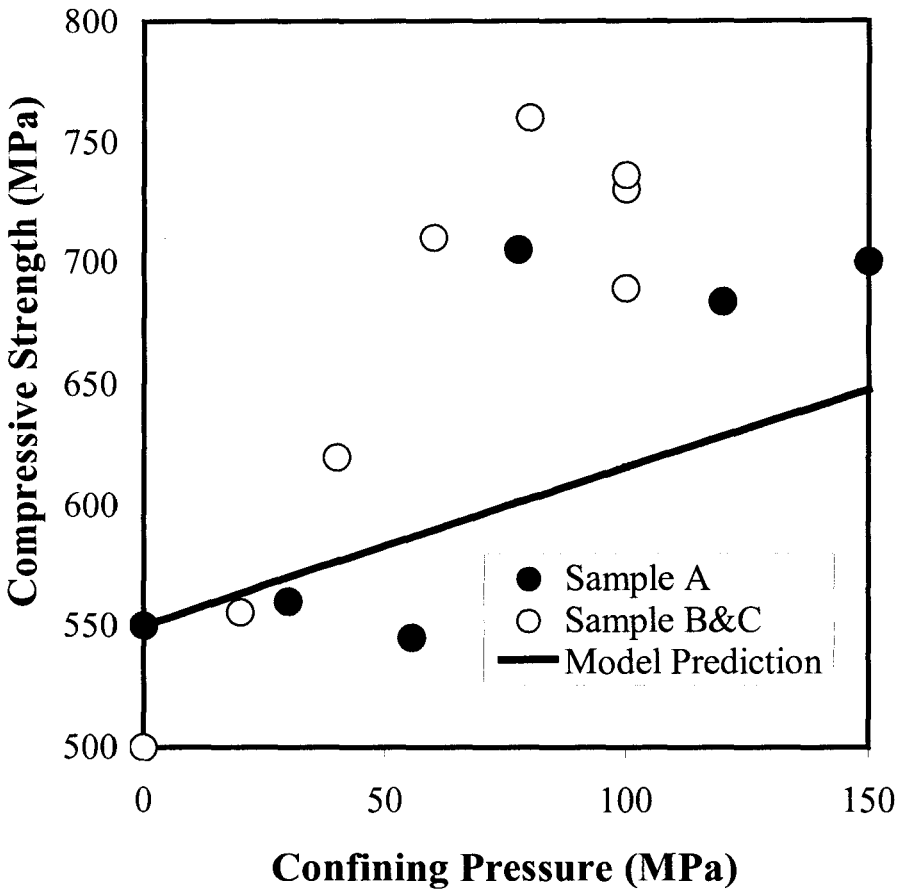

Figure 6 Comparison between experimental results (Weaver and Williams, 1975) and model prediction for carbon/epoxy composite, $v_f = 36\%$

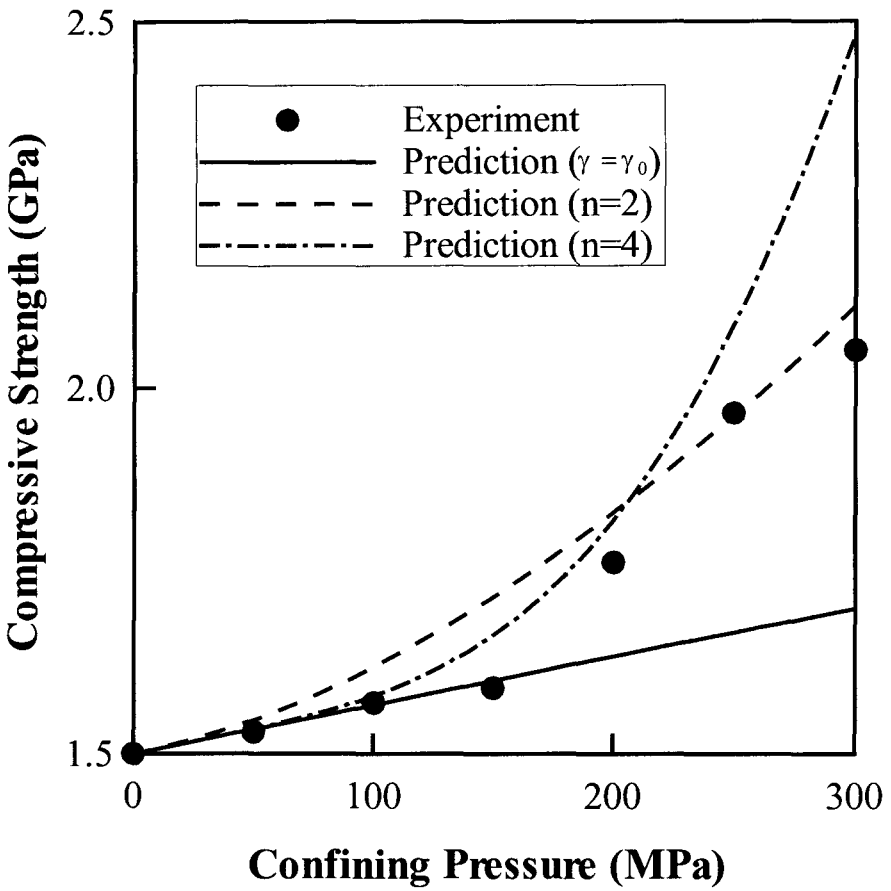

Figure 7 Comparison between experimental results (Parry and Wronski, 1982) and model predictions with the effect of increasing surface energy for carbon/epoxy composite, v_f = 60%

Chapter III A micromechanical failure model for unidirectional fiber reinforced composites

Abstract

Results from a newly developed model for failure in unidirectional fiber reinforced composites based on fracture mechanics are presented. The model is based on (i) analysis of branch crack initiation from the tip of an initial microcrack embedded in an anisotropic material, which serves as a model for the fiber reinforced composite and (ii) evaluation of anisotropy in homogenized elastic material properties and fracture toughness. Based on this model, failure envelope, dominant initial flaw orientation and failure mode for unidirectional fiber reinforced composites under a wide range of stress states are predicted. Parametric study provides quantitative evaluation of the effect of various mechanical and physical properties on the failure behavior, and their influence on strength is identified. Results from the current model are compared with those of existing phenomenological models, which show reasonable agreement.

III-1 Introduction

Failure of fiber reinforced composites is an important issue in engineering applications, especially in design and analysis of composite structures. Composites are widely used in the form of laminates to take advantage of their directional properties. The failure modes in laminates are complex and not always easily understood because of the interaction between different layers (e.g., Shuart, 1989; Waas and Schultheisz, 1996).

Hence, unidirectional fiber reinforced composites are often used as model materials in analysis and experiment to develop a better understanding of laminate failure. However, in spite of its simplicity in structure, failure of unidirectional fiber reinforced composites is still a complex phenomenon. Also, in these materials, critical stress state and failure modes vary according to the stress state.

Failure of unidirectional fiber reinforced composites are commonly analyzed using phenomenological or micromechanics based models. In the analysis based on phenomenological models, a yield function, which satisfies the invariant requirements of coordinate transformation, is usually postulated. The most widely accepted phenomenological model is that of Tsai and Wu (1971). One of the more recently developed models of this type is that of Christensen (1997). Various phenomenological models for predicting failure of composite laminates have been compared in a recent reviews by Echaabi et al. (1996) and Soden et al. (1998). In general, these models are applied in failure analysis for wide range of loading conditions and the postulated failure (yield) functions are polynomials of stress components. This assumption provides operationally simple models that can be used in analysis and design. However, these models are not based on the underlying mechanism of failure that governs the strength of composites. The validity of such models needs to be examined by critical comparison with experiments. In other words, such models provide analytical/numerical description of failure envelopes for composites but can not explain what governs the shape of failure envelopes or the associated strength. Also, prediction of failure modes in composites is out of the scope for most phenomenological models. On the other hand, micromechanical models are based on a physical mechanism of deformation/failure and is generally based

on rigorous theoretical framework, e.g., effective properties, fracture mechanics.

The proposed model is based on well-established analysis of a crack embedded in the composite under consideration and the strength of the material under specified stress state is deduced. In most micromechanics based models, loading condition, crack configuration and crack growth orientation (i.e., failure mode) are specified. For example, in the analysis on strength of fiber reinforced composites under uniaxial tension in fiber direction, initial microcrack and the crack growth orientation are specified to be normal to the fibers (e.g., Budiansky et al., 1986; Marshall and Cox, 1987; Budiansky and Amazigo, 1989). The failure phenomena are then individually analyzed for different loading conditions. Only narrow range of all possible stress states can be covered by one such micromechanics-based model. As a result, in order to capture the overall picture of failure phenomena of fiber reinforced composites under complex stress states with randomly distributed initial flaws and unknown crack growth orientation, a unified theory, which is applicable to arbitrary loading conditions is required.

A new model for failure of unidirectional fiber reinforced composites based on fracture mechanics is presented in this chapter. It is based on rigorous theoretical framework and is applicable to a wide range of loading conditions, i.e., stress states. The present model consists of (i) analysis of branch crack initiation from the tip of an initial microcrack embedded in an anisotropic material which serves as a homogenized model for the fiber reinforced composite and (ii) evaluation of elastic material properties and fracture toughness as a function of anisotropy. This model provides predictions of failure envelopes for a wide range of macroscopic stress states, corresponding dominant initial flaw orientation and branch crack growth orientation. Parametric study performed in this

chapter provides quantitative evaluation of the effect of physical and mechanical properties on the failure behavior of unidirectional fiber reinforced composites. Also, the parameters that are needed for the model predictions from experiments are pointed out. The model prediction is compared with the predictions by phenomenological models (Tsai-Wu model and Christensen's model) and experimental data available in the literature. The present model shows reasonable agreement with these phenomenological models.

III-2 Fracture mechanics based model

Failure of unidirectional composites is influenced by a number of parameters including the constituent properties of the material, fiber, matrix and their interface. In the present modeling, failure of unidirectional fiber reinforced composites is assumed to be determined by attaining a critical state at the tip of a favorably oriented microcrack in the material. Hence, the present model is applicable only to brittle failure modes (e.g., longitudinal (axial) splitting) and not to failure dominated by mechanisms such as shear yielding or kink band formation. In addition, the composites are assumed to have a strong interface between the fiber and the matrix.

III-2-1 Problem formulation

Consider an isolated microcrack embedded in a unidirectional fiber reinforced composite under uniform far-field normal stress σ_{11} and $\sigma_{22} = \sigma_{33}$ (hydrostatic lateral confinement), shown schematically in Fig. 1(a). Fixed rectangular Cartesian coordinate

system, x_1, x_2 and x_3 is used where the fibers are aligned to the x_1-axis and are randomly distributed in x_2-x_3 plane so that the material properties are transversely isotropic. The problem stated above (Fig. 1(a)) can be approximated by an isolated microcrack embedded in an infinite, anisotropic, homogeneous, linearly elastic solid in plane strain subjected to far-field stress boundary condition, shown schematically in Fig. 1(b). Assumptions corresponding to this approximate analytical model are the following:

i) the crack surface is parallel to the x_3-axis and far from the boundary (plane strain condition);

ii) the crack length is large compared to the scale of heterogeneity in the composite such as fiber diameter (homogenization);

The validity of the second (homogenization) assumption might be limited. For very small microcrack with dimensions on the order of a single fiber diameter, this assumption does not hold. However, the largest flaws in the material dominate failure of composites, which in general satisfy (ii) above as will be discussed later.

Under these assumptions, condition for branch crack initiation from the tip of the embedded microcrack is analyzed. It is further assumed that once the branch crack initiates, it grows in an unstable manner and thus loosing the load carrying ability. Hence, the macroscopic stress state at which the branch crack initiates is assumed to correspond to the failure strength of the composite. The coordinate system and loading condition for analysis on branch crack initiation are also shown in Fig. 1(b). β is the angle between fiber direction, x_1 and direction of initial microcrack surface, x, where clockwise direction is taken to be positive and $0 \leq \beta \leq \pi/2$. ψ is the angle between initial crack surface and branch crack surface where counter-clockwise direction is taken to be

positive and $|\psi| < \pi$. Θ is the orientation of the branch crack with respect to the fiber direction. $\Theta = 0, \pm\pi$ means that the branch crack orientation is parallel to the fiber direction where clockwise direction is taken to be positive and $|\Theta| \leq \pi$. Also, the polar coordinate system (r, θ) is introduced at the right-hand tip of the initial crack.

In the analysis, stress component at the tip of the embedded microcrack is computed based on fracture mechanics of anisotropic solid (Sih and Chen, 1981; Suo, et al. 1991) and attainment of orientation dependent critical hoop stress is used as the criterion for branch crack initiation. Based on this analysis, failure envelopes for unidirectional fiber reinforced composite are constructed using the stress states corresponding to the initiation of branch crack. Also, the orientations of initial microcrack and branch crack corresponding to the critical states are obtained. These orientations provide the information about possible failure modes as a function of macroscopic stress state.

III-2-2 Crack tip stress field

For the geometry and loading condition shown in Fig. 1(b), since the loading condition is self-equilibrated, the stress intensity factors at the tips of the initial microcrack are the same as those for a crack in an isotropic material (Sih, et al. 1965) and expressed as follows:

$$K_I = \begin{cases} \sigma_N \sqrt{\pi a} & (\sigma_N \geq 0) \\ 0 & (\sigma_N < 0) \end{cases} \tag{1a}$$

$$K_{II} = \begin{cases} \tau\sqrt{\pi a} & (\sigma_N \geq 0) \\ (\tau - \mu|\sigma_N|)\sqrt{\pi a} & (|\tau| > \mu|\sigma_N|, \sigma_N < 0) \\ 0 & (|\tau| \leq \mu|\sigma_N|, \sigma_N < 0) \end{cases} \tag{1b}$$

where σ_N and τ are the resolved normal and shear stress on the surface of the microcrack, $\sigma_N = \sigma_{11}\sin^2\beta + \sigma_{22}\cos^2\beta$, $\tau = (\sigma_{11} - \sigma_{22})\sin\beta\cos\beta$; $\mu \geq 0$ is the friction coefficient of the crack surface (Fig. 1(c)). Using these stress intensity factors, crack tip stress tensor field $\boldsymbol{\sigma}$ can be expressed as follows:

$$\boldsymbol{\sigma} = \frac{K_I}{\sqrt{2\pi r}} \boldsymbol{f}_I(\theta, \boldsymbol{C}) + \frac{K_{II}}{\sqrt{2\pi r}} \boldsymbol{f}_{II}(\theta, \boldsymbol{C}) \tag{2}$$

where $\boldsymbol{f}_I$ and $\boldsymbol{f}_{II}$ are purely functions of the angle θ and $\boldsymbol{C}$, the effective elastic moduli of the fiber reinforced composite. Equation (2) implies that the effect of loading and geometry of the crack is contained in the stress intensity factors and the effect of the material properties is confined in the orientation dependence of stress components. Detailed expressions for the stress components are given in Appendix.

III-2-3 Failure criterion and critical stress intensity factor

In the present analysis, branch crack initiation from the tip of an embedded microcrack is considered to be the failure of the composite material. When the hoop stress in the local orientation, Θ, reaches the strength of the material in that direction, the branch crack is initiated. This criterion can be written equivalently in terms of an orientation dependent critical stress intensity factor, $K_{Ic}(\Theta)$.

$$\lim_{r\to 0}\sigma_{\theta\theta}\sqrt{2\pi r} = K_{Ic}(\Theta). \tag{3}$$

Stress component $\sigma_{\theta\theta}$ (tangential component of the stress), which is relevant to the present failure criterion, can be expressed as follows:

$$\begin{aligned}\sigma_{\theta\theta} = \frac{K_I}{\sqrt{2\pi\, r}}\mathrm{Re}\left[\frac{s_1 s_2}{2(s_1 - s_2)}\left\{\frac{1+s_2^{\,2}+(1-s_2^{\,2})\cos 2\theta + 2s_2\sin 2\theta}{s_2\sqrt{\cos\theta + s_2\sin\theta}}\right.\right. \\ \left.\left. - \frac{1+s_1^{\,2}+(1-s_1^{\,2})\cos 2\theta + 2s_1\sin 2\theta}{s_1\sqrt{\cos\theta + s_1\sin\theta}}\right\}\right] \\ + \frac{K_{II}}{\sqrt{2\pi\, r}}\mathrm{Re}\left[\frac{1}{s_1 - s_2}\left\{(\cos\theta + s_2\sin\theta)^{3/2} - (\cos\theta + s_1\sin\theta)^{3/2}\right\}\right] + O(r^0).\end{aligned} \tag{4}$$

In (3), fracture toughness K_{Ic} is assumed to depend only on local orientation of the prospective fracture plane, Θ, i.e., $K_{Ic} = K_{Ic}(\Theta)$. In fiber reinforced composite, fracture toughness K_{Ic} might depend on position of the crack tip and local orientation of the crack surface. Assumption $K_{Ic} = K_{Ic}(\Theta)$ corresponds to the homogenization of K_{Ic}.

The functional dependence of K_{Ic} on Θ and on mechanical properties of constituents and fiber volume fraction is not readily available in literature at this time. From the definition of Θ and the material symmetry of fiber reinforced composites, $K_{Ic}(\Theta)$ is a periodic even function with period π and symmetric with respect to $\Theta = \pi/2$. This statement is the best one can currently say about $K_{Ic}(\Theta)$. Under this circumstance, i.e., in lack of detailed experimental data, analytic estimates for $K_{Ic}(0, \pm\pi)$ and $K_{Ic}(\pm\pi/2)$

have been employed in the present analysis. Analytic estimates for these two values are obtained through energy consideration on growth of a straight crack in fiber direction and transverse direction, respectively. This method was originally developed by Hutchinson and Suo (1992) for the analysis on failure modes of brittle adhesive joints and sandwich layers. The method presented here is a modified version of the one proposed by Hutchinson and Suo (1992) applied to an orthotropic solid.

The macroscopic plane strain energy release rate at the tip of a mode-I crack embedded in an orthotropic material (homogenized model for fiber reinforced composite) with crack face aligned with the axis of material symmetry is (Tada et al., 1985)

$$G = gK_I^2 \tag{5}$$

where $g = \sqrt{\frac{b_{11}b_{22}}{2}}\left[\sqrt{\frac{b_{22}}{b_{11}}} + \frac{2b_{12}+b_{66}}{2b_{11}}\right]^{\frac{1}{2}}$ with b_{ij} defined in (A3). For unidirectional fiber reinforced composites, b_{ij} can be obtained from the effective elasticity tensor, $\boldsymbol{C}$. Examining the same phenomena locally, the microscopic (local) plane strain energy release rate required for crack initiation in unidirectional fiber reinforced composite is

$$G_m = \frac{\left(1-\nu_m^2\right)}{E_m} K_{Ic}^{m\,2} \tag{6}$$

where K_{Ic}^m is the critical stress intensity factor (fracture toughness) for matrix material. It is assumed that the crack tip is located in the matrix material. When the macroscopic

energy release rate reaches the critical energy release rate of the matrix material, matrix crack initiation takes place. Therefore, the criterion for matrix crack initiation is given as follows:

$$G=G_m \tag{7}$$

Substitution of (5) and (6) into (7) yields the expression for *apparent critical stress intensity factor*, K_{Ic}, as follows:

$$K_{Ic} = K_{Ic}^m \sqrt{\frac{(1-\nu_m{}^2)}{g\,E_m}} \tag{8}$$

Expressions for $K_{Ic}(\pm\pi/2)$ and $K_{Ic}(0,\pm\pi)$ can be obtained by substituting g into (8) with normal vector to crack surface (y-direction) aligned to fiber direction (x_1 direction) and transverse direction (x_2 direction), respectively. $K_{Ic}(\pm\pi/2)$ and $K_{Ic}(0,\pm\pi)$ normalized by K_{Ic}^m are plotted against fiber volume fraction, ν_f for carbon/epoxy composite in Fig. 2. Using this method, Budiansky and Cui (1994) obtained the following expression for $K_{Ic}(\pm\pi/2)$.

$$K_{Ic}(\pm\pi/2) = K_{Ic}^m \sqrt{\frac{(1-\nu_m{}^2)}{g\,E_m}(1-\nu_f)} \tag{9}$$

The factor of $(1-\nu_f)$ in the right-hand side of (9) reflects the reduction of the area of the

matrix crack surface due to the presence of unbroken fibers. According to (9), $K_{Ic}(\pm\pi/2)$ is a convex function of v_f maximized at $v_f \cong 0.5$ as shown in Fig. 2. However, as long as tough fibers are introduced, matrix crack growth should be suppressed as v_f increases within the practical range of its value, i.e., $v_f < 0.7$. Therefore, physical considerations indicate that $K_{Ic}(\pm\pi/2)$ should be an increasing function of v_f. In the derivation of (9), instead of (7), $G=(1-v_f)G_m$ has been used as the criterion for matrix crack initiation in the direction perpendicular to the direction of fibers. Physically, $G=(1-v_f)G_m$ is interpreted as the criterion for matrix crack *growth* since the critical energy release rate is averaged over the whole event of matrix crack growth leaving the fibers unbroken. On the other hand, (7) can be regarded as the criterion for matrix crack *initiation* since neglecting the factor $(1-v_f)$ results in the assumption of infinitesimal crack growth only in matrix material. In the present analysis, the main focus is on the initiation of a branch crack. Hence, critical stress intensity factor obtained from (8) has been employed.

As mentioned before, no reliable data for the functional dependence of K_{Ic} on Θ is available in literature. Besides, the energy-based estimate for K_{Ic} discussed above is not applicable for the off axis crack because of the mode mixity caused by the anisotropy. However, based on the commonly known properties of fiber reinforced composites, some restrictions can be imposed on the functional form of $K_{Ic}(\Theta)$. In most commonly encountered fiber reinforced composites, the toughening effect of the fibers is maximized in the direction of fibers. Therefore, $\Theta = \pi/2$ and $\Theta = 0$ are the toughest and the weakest directions, respectively. Hence, $K_{Ic}(0) \le K_{Ic}(\Theta) \le K_{Ic}(\pi/2)$ holds for all Θ. The effect

of interpolation of $K_{Ic}(\Theta)$ on critical stress state is evaluated by performing parametric study in the following section. Although analytic estimation of $K_{Ic}(\Theta)$ is employed and the effect of interpolation will be investigated through parametric study in the present analysis, it should be emphasized that systematic experimental evaluation of this physical parameter is essential to apply and/or validate the present model to actual fiber reinforced composites.

III-2-4 Construction of failure envelope

Failure envelope for a unidirectional fiber reinforced composite is obtained through the following procedure:

i) material properties, elasticity tensor $\boldsymbol{C}$ is computed for given volume fractions and elastic properties of fiber and matrix, and lateral stress σ_{22} is specified;

ii) for a given $\boldsymbol{C}$ and specified value of σ_{22}, minimum $|\sigma_{11}|$ ($\sigma_{11} > 0$ and $\sigma_{11} < 0$ correspond to tensile and compressive critical stress, respectively) for branch crack initiation, corresponding initial microcrack orientation β and branch crack orientation ψ are computed;

iii) for different values of σ_{22}, ii) is repeated.

In the present analysis, the initiation of branch crack is regarded as the failure of composite. As long as the governing equation for the stable growth of branch crack is concerned, this is not always true. According to the governing equation, when the branch crack is initiated in the direction perpendicular to compression axis, branch crack is closed and never grows. However, in experiments, unstable growth of cracks

perpendicular to the compression axis is observed (e.g., unstable growth of longitudinal splitting in unidirectional fiber reinforced composite under weak lateral confinement). This experimental observation (e.g., Waas and Schultheisz, 1996; Oguni et al., 1999) implies that after the onset of branch crack, governing equation for the stable crack growth is no longer valid, instead, dynamic crack growth should be considered. Based on this, the initiation of branch crack is regarded as the failure of composite in the present analysis. However, under highly compressive stress, no unstable growth of open crack is observed in experiment, instead, ductile failure (e.g., formation of kink band, shear yielding) is observed. Since the failure criterion used in this analysis is based on maximum hoop stress, failure of fiber reinforced composite under highly compressive states of stress is out of the scope of the present analysis.

In step ii), initial microcrack orientation and branch angle corresponding to the critical stress state are obtained. These quantities provide the direction of failure plane $\Theta = \beta - \psi$, which indicates the failure mode for the corresponding stress state.

III-3 Results and discussion

III-3-1 Failure envelope

A typical failure envelope for a unidirectional fiber reinforced composite constructed using the present model is shown in Fig. 3. Stress components are normalized using a reference initial microcrack length, a_0, and the critical stress intensity factor for matrix material, K_{Ic}^m, as follows:

$$\alpha_1 = \frac{\sigma_{11}\sqrt{\pi a_0}}{K_{Ic}^m}, \quad \alpha_2 = \frac{\sigma_{22}\sqrt{\pi a_0}}{K_{Ic}^m}. \tag{10}$$

The composite modeled here is a carbon/epoxy composite with fiber volume fraction $v_f = 60\%$. Constituents of this composite are the same as those used in the experiment by Parry and Wronski (1982). Relevant material properties and geometry of fiber and matrix are shown in Table 1. Other parameters used in the construction of this failure envelope are shown in the caption of Fig. 3. Explanations on the physical meaning of 'reference crack length, a_0', 'aspect ratio, p' and 'interpolating function, ϕ' are discussed in the following sections. Ellipses and solid lines shown around the envelope indicate the dominant initial microcrack orientation, β, and direction of branch crack initiation, ψ, corresponding to the critical stress states. The crack size shown is not representative of the initial flaw size. At $(\alpha_1, \alpha_2) = (0, 0.2)$, the dominant initial microcrack is aligned with the fibers and the branch crack is also aligned with the fibers. This implies that when a unidirectional fiber reinforced composite is subjected to tension in the direction

transverse to the direction of the fibers, failure occurs in a direction perpendicular to the loading direction, i.e., delamination failure. At $(\alpha_1,\alpha_2)=(-4.5, 0)$, branch crack aligned to the fibers with inclined dominant initial microcrack ($\beta \cong 48°$) is predicted. This corresponds to the longitudinal (axial) splitting under uniaxial compression in fiber direction, which is often observed in experiments (e.g., Parry and Wronski, 1982; Lee and Waas, 1999; Oguni et al., 1999).

Since the failure criterion is the tensile hoop stress criterion, the present model is applicable only when the matrix material remains elastic and fails in brittle manner. For commonly used polymer and ceramic composites, this condition is satisfied as long as $\sigma_{22} \geq 0$ even if $\sigma_{11} < 0$. Because the fibers are much stiffer than matrix material in most fiber reinforced composites of interest, stress in fiber direction, i.e., x_1-direction, is mostly carried by fibers. Therefore, yielding is confined in a negligibly small region at the tip of initial microcrack and the matrix material fails in brittle manner. On the other hand, if $\sigma_{22} < 0$, matrix material tends to yield at some stress level since the matrix has to carry the same order of stress as fibers do in transverse direction. Hence, under large negative σ_{22} (compression), failure behavior might change from brittle to ductile. As a result, the validity of the present model is limited to the regions $\sigma_{22} \geq 0$ and small negative $\sigma_{22} < 0$. Also, from an experimental point of view, for compression tests with high lateral confinement, i.e., $\sigma_{11} < 0$ and large compressive σ_{22}, the model prediction of axial splitting is not valid. Under high lateral confining pressure, not axial splitting but kink band formation is observed in experiments. When the failure mode changes from axial splitting to kink band formation, the slope of the failure envelope is much higher in experiments. Hence, the model prediction is not valid for the region of high lateral

confinement and this region is out of the scope of the present brittle failure based analysis. However, even if the matrix material ceases to be brittle and the present failure criterion becomes no longer applicable, qualitative discussion can be made for highly confined region. As long as fracture is the main mechanism that governs the failure of fiber reinforced composites, the failure envelope need not be a closed surface in stress space. The failure envelope never crosses the line of $\sigma_{11} = \sigma_{22} = \sigma_{33} < 0$ (hydrostatic pressure) since no crack can be opened or sheared under hydrostatic pressure. With the foregoing discussion in mind, in the following sections, failure envelopes are presented only for $\alpha_2 \geq -2$.

The present model predicts lower tensile strength than compressive strength in the direction of fibers as shown in Fig. 3 which is not in accordance with experimental data (e.g., Daniel and Ishai, 1994). In the present model, the initiation of branch crack, i.e., onset of the material degradation is regarded as the failure of the composite. On the other hand, in experiments, fiber breakage is considered to be the uniaxial tensile failure of composite. The definition of 'failure of composite' is 'nucleation of irreversible damage' in the present model and is 'ultimate strength' in experiments. These definitions give the same strength in the cases of catastrophic failure such as failure under uniaxial compression in fiber direction and uniaxial tension in transverse direction. However, in the case of uniaxial tension in fiber direction, failure consists of different steps, material cracking/debonding followed by fiber bridging and failure. This is the reason for predicting lower tensile strength in fiber direction. In order to predict the ultimate tensile strength in fiber direction using fracture mechanics-based model, $K_{Ic}(\Theta)$ should be refined including the effect of fiber bridging. Expression for $K_{Ic}(\pm\pi/2)$ including fiber

bridging effect has been obtained by Budiansky and Amazigo (1989). However, for Θ other than $\Theta = \pi/2$, no general trend in the form of $K_{Ic}(0) \le K_{Ic}(\Theta) \le K_{Ic}(\pi/2)$ can be expected. Without data from systematic and detailed experiments for $K_{Ic}(\Theta)$, ultimate strength can not be obtained using the present model. It should be noted that all the failure envelopes predicted by the present model provide a lower bound for 'strength' instead of 'ultimate strength' of unidirectional fiber reinforced composites.

III-3-2 Parametric study

In order to investigate the influence of physical and mechanical properties on failure behavior of fiber reinforced composites, a systematic parametric study is performed in this section. The important parameters under consideration are (i) orientation dependence of the maximum size of the initial microcrack, a, i.e., the functional form of $a = a(\beta)$, (ii) orientation dependence of K_{Ic}, i.e., $K_{Ic}(0, \pm\pi)$, $K_{Ic}(\pm\pi/2)$ and the form of the interpolation function $K_{Ic} = K_{Ic}(\Theta)$, (iii) elastic properties of the materials, (iv) fiber volume fraction, v_f and (v) friction coefficient of crack surface, μ. In the following sections, elastic properties of the constituents of unidirectional fiber reinforced composites that are used are the same as those shown in Table 1 unless mentioned otherwise.

Orientation dependence of the maximum size of the initial microcrack

Based on the microstructure of fiber reinforced composite, $a(\pi/2) \le a(\beta) \le a(0)$, for $0 \le \beta \le \pi/2$, could be the only restriction on the maximum size of the initial flaw or microcrack. As a choice for the function, $a(\beta)$, which satisfies the restriction above, an ellipsoidal distribution of the size for the initial microcrack is assumed,

$$a(\beta) = \frac{p\, a_0}{\sqrt{p^2 \sin^2 \beta + \cos^2 \beta}} \tag{11}$$

where p is the aspect ratio of the ellipse which envelopes the initial microcracks in all orientations and $a_0 = a(\pi/2)$ is taken to be the reference initial microcrack length. Figure 4 shows the failure envelopes of a carbon/epoxy composite with fiber volume fraction v_f = 60%. Material properties are shown in Table 1 and other parameters used are shown in the caption of Fig. 4. Since the stress components are given by $\sigma_{11} = \alpha_1 K_{Ic}^m / \sqrt{\pi a_0}$ and $\sigma_{22} = \alpha_2 K_{Ic}^m / \sqrt{\pi a_0}$, critical stress state is inversely proportional to the square root of the reference initial microcrack length. Changing the aspect ratio p has major effect on the tensile strength in the direction perpendicular to the direction of fibers. Significant effect of the aspect ratio can be observed only for small values of p ($p \cong 1$), otherwise virtually no effect of p on failure envelopes is observable. Failure envelopes for p=10 and p=100 are almost identical except for the region of transverse tensile failure. This is because the orientation of the dominant initial microcrack is far from the direction of fiber ($\beta = 0$) except in the case of unidirectional

tension normal to the fibers as shown in Fig. 4. Because of the assumption of elliptic distribution, for large p, $a(\beta)$ is insensitive to the change of the aspect ratio except for $\beta \cong 0$.

Carbon/epoxy composite with v_f = 60% used in Parry and Wronski (1982) has uniaxial compressive strength in fiber direction, $\sigma_{11}^c = 1.5\text{GPa}$. The present fracture mechanics-based model predicts $(\alpha_1, \alpha_2) = (-4.5, 0)$ as shown in Fig. 3. Based on this information together with typical fracture toughness of epoxy matrix, $K_{Ic}^m = 1 \sim 3\ \text{MPa}/\sqrt{m}$, typical physical dimension of the reference initial microcrack is $a_0 = 15 \sim 26\mu\text{m}$. Compared with the fiber diameter ($3.4\mu\text{m}$, see Table 1), initial microcrack size is large enough for the homogenization assumption in problem formulation.

Orientation dependence of K_{Ic}

Illustration of the choice of interpolation function in terms of $\phi=2\Theta/\pi$, $-\phi^2$, ϕ, ϕ^2 and $\cos\phi$ for $K_{Ic}(\Theta)$ can be seen from Fig. 5 in which normalized fracture toughness is plotted as a function of the crack surface direction. Figure 6 shows the failure envelopes for different interpolating functions for $K_{Ic}(\Theta)$. $K_{Ic}(0, \pm\pi)$ and $K_{Ic}(\pm\pi/2)$ are computed using (8). Not much difference is observed among the results for different interpolations. Figure 7 shows the failure envelopes for the same interpolations with different $K_{Ic}(0, \pm\pi)$ and $K_{Ic}(\pm\pi/2)$. In this case, fixed values $K_{Ic}(0, \pm\pi) = K_{Ic}^m$ and $K_{Ic}(\pm\pi/2) = 5K_{Ic}^m$ are used. Corresponding failure envelopes change according to the choice of interpolation functions. Comparison between Figs. 6 and 7 shows that as the

ratio $K_{Ic}(\pm\pi/2)/K_{Ic}(0,\pm\pi)$ increases, the effect of interpolation becomes significant. However, as long as the values obtained using (8) are used for the fracture toughness, $K_{Ic}(\pm\pi/2)/K_{Ic}(0,\pm\pi)$ is small enough and the effect of interpolation is not important (see Fig. 2). Although the effect of interpolation is not significant, use of the most reasonable interpolation function is preferable. Since the effect of fibers on fracture toughness might be significant, as soon as the crack direction deviates from the fiber direction, sudden increase in $K_{Ic}(\Theta)$ should be expected for small Θ. To account for this effect, negative quadratic interpolation $-\phi^2$ has been employed in constructing all the failure envelopes. The choice and validity of the interpolation function would clearly depend on experimental data for $K_{Ic}(\Theta)$.

Elastic properties of the constituent materials

Figure 8 shows failure envelopes for composites with different material properties. "60%" indicates the failure envelope for the 60% v_f carbon/epoxy composite. The relevant properties of the matrix and the fiber correspond to the values given by Parry and Wronski (1982) shown in Table 1. "0.1 E_f - K_{Ic} by Eq. (8)" is the failure envelope for the same composite as "60%" except for reduced fiber stiffness (10% of the value shown in Table 1). In this case, fracture toughness $K_{Ic}(0,\pm\pi)$ and $K_{Ic}(\pm\pi/2)$ are computed by (8) based on the material properties with reduced fiber stiffness. The failure envelope with legend "0.1 E_f - K_{Ic}" corresponds to composite with reduced fiber stiffness but using the same $K_{Ic}(0,\pm\pi)$ and $K_{Ic}(\pm\pi/2)$ as those for "60%". The net effect of the choice of material properties can be assessed by comparing the two failure envelopes "60%" and

"0.1 E_f - K_{Ic} by Eq. (8)." Based on this comparison, elastic properties of the materials appear to have a strong effect on failure behavior of composites. However, comparison between "60%" and "0.1 E_f - K_{Ic}," which contrasts the effect of the choice of material properties on failure behavior of composites provides a different perspective. These two failure envelopes are close enough to conclude that the effect of elastic properties of the materials on the failure behavior of composites is not due to the change in the effective elastic properties of the materials but rather due to the change in K_{Ic}. In other words, the effective elastic properties of the composite have relatively small effect in comparison to the one due to the change in fracture properties, namely $K_{Ic}(\Theta)$.

Fiber volume fraction

Based on the above observation of the effect of material properties, effect of volume fraction on failure phenomena is expected to be due to the change in fracture toughness (Fig. 2). Therefore, the results with fixed $K_{Ic}(0, \pm\pi)$ and $K_{Ic}(\pm\pi/2)$ are not shown for the sake of brevity. Results with $K_{Ic}(0, \pm\pi)$ and $K_{Ic}(\pm\pi/2)$ computed by (8) are shown in Fig. 9. As the fiber volume fraction increases, the failure envelope is enlarged, i.e., composite becomes stronger. Hence, one can conclude that the increase in fracture toughness due to the increase of v_f plays a significant role. However, other factors should be also taken into account such as the size of the initial microcrack, $a(\beta)$. Due to the microstructure of the unidirectional fiber reinforced composites, as the fiber volume fraction increases, mean free path for an initial microcrack perpendicular to the fibers decreases. For the initial microcrack parallel to the fibers, virtually no effect of the fibers should be observed. As a result, the increase in the aspect ratio of the distribution of the

size and the decrease in the reference size of the initial microcrack should be taken into account as the fiber volume fraction increases. As seen from Fig. 4, increase of the aspect ratio, p, results in increase of anisotropy in strength. Also, as seen from (10), increase in strength for all loading conditions for the same normalized stress can be expected as the reference size of the initial microcrack decreases. In conclusion, as the fiber volume fraction increases, strength in fiber direction increases mainly because of the reduction of reference size of the initial microcrack. On the other hand, transverse tensile strength increases due to toughening effect (Eq. (8)) in the transverse direction.

Friction coefficient of crack surface

Figure 10 shows the failure envelopes for different friction coefficients of the crack surface, μ. As one expects, the effect of this physical parameter is confined to the region where the initial crack surfaces are in contact (compression dominated stress states). In this region, as μ increases, the failure envelopes deviate away from the line of hydrostatic pressure ($\sigma_{11} = \sigma_{22} = \sigma_{33} < 0$). Also as expected, higher friction coefficient results in higher strength.

III-3-3 Comparison with existing phenomenological failure theories

In the analysis of failure of unidirectional fiber reinforced composites, phenomenological models have been accepted and widely used. These models are easy to apply and the predictions obtained from these models suffice for many practical applications. In most phenomenological models, a yield function, which consists of stress invariants, is postulated. This enables a model to satisfy the objectivity with respect to the

coordinate transformation. Using this yield function and some basic parameters such as unidirectional tensile/compressive strength in fiber/transverse direction, curve fitting is performed to construct a failure envelope. Since the distinction between failure modes is not included in the yield functions, it is impossible for most phenomenological models to predict failure modes. Various phenomenological models for predicting failure strength of composites have been reviewed by Echaabi et al. (1996) and Soden et al. (1998). The most widely accepted phenomenological model is Tsai-Wu model (Tsai and Wu, 1971) and one of the more recent one is the model by Christensen (1997). In this section, predictions based on the present fracture mechanics-based model are compared with these two phenomenological models.

The Tsai-Wu model is based on the total strain energy theory of Beltrami. The yield function postulated for unidirectional fiber reinforced composite under plane stress loading condition without shear loading is given as follows:

$$f_1\alpha_1 + f_2\alpha_2 + f_{11}\alpha_1^{\,2} + f_{22}\alpha_2^{\,2} + 2f_{12}\alpha_1\alpha_2 = 1 \tag{12}$$

where α_1 and α_2 are the normalized stresses defined in (10), F_{1t}, F_{1c} are the normalized absolute values of unidirectional tensile/compressive strength of composite in fiber direction, respectively, and F_{2t}, F_{2c} are the normalized absolute values of unidirectional tensile/compressive strength of composite in transverse direction, respectively. Coefficients of the yield function are given as follows:

$$f_1 = \frac{1}{F_{1t}} - \frac{1}{F_{1c}}, \qquad f_2 = \frac{1}{F_{2t}} - \frac{1}{F_{2c}}, \qquad f_{11} = \frac{1}{F_{1t}F_{1c}}, \qquad f_{22} = \frac{1}{F_{2t}F_{2c}},$$

$$f_{12} = -\frac{1}{2}\sqrt{\frac{1}{F_{1t}F_{1c}F_{2t}F_{2c}}}.$$

Failure envelopes obtained from (12) and prediction of the present fracture mechanics-based model are shown in Fig. 11. Strength parameters used in (12) are $F_{1t} = 3.16$, $F_{1c} = 4.22$ $F_{2t} = 0.18$ and $F_{2c} = 0.37$. Parameters used in the fracture mechanics-based model are shown in the caption of Fig. 11. Since F_{2t}/F_{1c} is very small in unidirectional fiber reinforced composites, failure envelope obtained by Tsai-Wu model becomes an extremely sharp ellipse with its major axis almost aligned to α_1 axis. As a result, large overshoot and extremely small slope of failure envelope are observed for negative values of α_1 and α_2. In the experiments on compressive failure of fiber reinforced composite with lateral confinement, $d\sigma^{cr}/d\sigma_c = 1 \sim 3$ (where σ^{cr} and σ_c are the magnitudes of compressive strength and lateral confinement, respectively) has been observed (Weaver and Williams, 1975; Parry and Wronski, 1982). Prediction by Tsai-Wu model provides $d\sigma^{cr}/d\sigma_c >> 3$ for small negative α_1. On the other hand, the present fracture mechanics-based model predicts $d\sigma^{cr}/d\sigma_c \cong 1$, which agrees with experimental results available in literature and the recent analytical prediction of Oguni and Ravichandran (2000) based on minimization of global energy. Also, sharp corners in failure envelope predicted in the present model are not predicted by Tsai-Wu model due to the ellipsoidal shape of the postulated yield function, which is the main cause of the difference in failure envelopes predicted by the two models.

The phenomenological model by Christensen (1997) postulates two different yield functions, namely, matrix dominated ('mode I') and fiber dominated ('mode II'). Both matrix and fibers play important roles in determining strength under all stress states. However, based on the structure of unidirectional fiber reinforced composites, one can expect that strength in transverse direction is dominantly governed by the strength of matrix and strength in fiber direction is controlled by the strength of fibers. The yield functions postulated for unidirectional fiber reinforced composite under hydrostatic lateral confinement ($\sigma_{22} = \sigma_{33}$) in transverse direction without shear loading are given as follows:

Mode I (Matrix Dominated)

$$\lambda_1 k_1 (\sigma_{22} + \sigma_{33}) + \frac{1}{4}(1 + 2\lambda_1)(\sigma_{22} - \sigma_{33})^2 = {k_1}^2 \tag{13}$$

Mode II (Fiber Dominated)

$$-\lambda_2 k_2 \sigma_{11} + \frac{1}{4}(1 + 2\lambda_2){\sigma_{11}}^2 - \frac{(1+\lambda_2)^2}{4}(\sigma_{22} + \sigma_{33})\sigma_{11} = {k_2}^2 \tag{14}$$

where $\lambda_1 = \frac{1}{2}\left(\frac{F_{2c}}{F_{2t}} - 1\right)$, $\lambda_2 = \frac{1}{2}\left(\frac{F_{1t}}{F_{1c}} - 1\right)$, $k_1 = \frac{F_{2c}}{2}$ and $k_2 = \frac{F_{1t}}{2}$. Failure envelopes obtained from Christensen's model and prediction of the present fracture mechanics-based model are shown in Fig. 12. Parameters used in (13) and (14) are the same as those used in Tsai-Wu model prediction. Parameters used in the fracture mechanics-based

model are shown in the caption of Fig. 12. Results show good agreement between the two models. In the present fracture mechanics-based model, sharp corners in failure envelope are produced based on the predicted change of failure modes. Although Christensen's model does not provide information about failure modes, different yield functions are employed based on the micromechanical consideration to capture the dominant character of failure under different loading conditions. This enables this model to produce sharp corners in failure envelope corresponding to the change in failure mechanism.

Although the comparison with Tsai-Wu model shows poor agreement, overall failure behavior of unidirectional fiber reinforced composite obtained from phenomenological models (see Soden et al. (1998)) are captured by the present fracture mechanics based failure model. The present model provides a rational means for critically evaluating phenomenological models. Besides, as a byproduct, predictions of failure modes and orientation of dominant initial microcrack can be obtained from the present model. However, the present model is not intended to be a substitute for phenomenological models. Phenomenological models are easy to use since the required parameters are readily obtained experimentally and the number of parameters is small. The present model is intended to provide insight into the possible underlying mechanics and parameters that govern the failure and strength of fiber reinforced composites.

III-4 Conclusions

A fracture mechanics-based model has been developed for predicting the failure behavior (failure envelope, orientation of dominant initial microcrack and failure mode) of unidirectional fiber reinforced composites. Based on the present study, the following conclusions are obtained:

(i) The critical stress state is controlled by the size of the dominant crack under given loading condition. The critical stress components are inversely proportional to $\sqrt{a}$, where, a is the half crack length of the dominant crack and is an expected direct consequence of linear elastic fracture mechanics employed here;

(ii) Fiber volume fraction, v_f, has a positive effect on strength of unidirectional fiber reinforced composites as long as the fibers are stiffer than matrix material. However, the strengthening mechanism is different for each direction. In fiber direction, strength increases mainly because of the reduction of reference size of the initial microcrack which is related to the increase of v_f. In transverse direction, strength increases mainly because of the increase of effective fracture toughness $K_{Ic}(0, \pm\pi)$ given by (8) as v_f increases;

(iii) Effect of anisotropy in elastic properties on failure behavior of unidirectional fiber reinforced composites is minor. Instead, anisotropy in fracture toughness plays a significant role;

(iv) Comparison between the results of the present model with those of phenomenological models shows reasonable agreement. Especially, good agreement is found with the result by Christensen's model (1997) which includes the micromechanical consideration of the structure of unidirectional fiber

reinforced composites.

Acknowledgements

We gratefully acknowledge support from the Office of Naval Research (Scientific Officer: Dr. Y. D. S. Rajapakse) through a grant (N0014-95-1-0453) to the California Institute of Technology.

Appendix

Stress components at the crack tip in an orthotropic solid

Following (Sih, et al. 1965), the expression for crack tip stress field σ in an orthtropic solid is given as follows:

$$\sigma = \frac{K_I}{\sqrt{2\pi r}} f_I(\theta, \boldsymbol{C}) + \frac{K_{II}}{\sqrt{2\pi r}} f_{II}(\theta, \boldsymbol{C}) \tag{A1}$$

where $\boldsymbol{C}$ is the elasticity tensor of fiber reinforced composite. Expression for $\boldsymbol{C}$ can be obtained in the form of effective elastic moduli based on the elastic properties of fiber and matrix (e.g., Hashin and Rosen, 1964).

The stress strain relations in *x-y* coordinate system, which is aligned to the crack orientation as shown in Fig. 1(b) using Voigt notation, can be written as

$$\varepsilon_i = a_{ij}\sigma_j \tag{A2}$$

where $\underline{\varepsilon} = \left[\varepsilon_{xx}, \varepsilon_{yy}, \varepsilon_{zz}, 2\varepsilon_{yz}, 2\varepsilon_{zx}, 2\varepsilon_{xy}\right]^T$, $\underline{\sigma} = \left[\sigma_{xx}, \sigma_{yy}, \sigma_{zz}, \sigma_{yz}, \sigma_{zx}, \sigma_{xy}\right]^T$ and $\boldsymbol{A} = \left[a_{ij}\right]$ is the effective compliance tensor of fiber reinforced composite. For plane strain problem with *x-y* plane being a plane of symmetry, (A2) reduces to

$$\begin{bmatrix} \varepsilon_{xx} \\ \varepsilon_{yy} \\ 2\varepsilon_{xy} \end{bmatrix} = \begin{bmatrix} b_{11} & b_{12} & b_{16} \\ b_{12} & b_{22} & b_{26} \\ b_{16} & b_{26} & b_{66} \end{bmatrix} \begin{bmatrix} \sigma_{xx} \\ \sigma_{yy} \\ \sigma_{xy} \end{bmatrix} \tag{A3}$$

where $b_{ij} = a_{ij} - \dfrac{a_{i3}a_{j3}}{a_{33}}$. (For plane stress problem with x-y plane being a plane of symmetry, the following argument holds for $b_{ij} = a_{ij}$.)

Functional dependence of $f_I(\theta, \boldsymbol{C})$ and $f_{II}(\theta, \boldsymbol{C})$ on material properties is expressed in terms of the roots of the characteristic equation

$$b_{11}s^4 - 2b_{16}s^3 + (2b_{12} + b_{66})s^2 - 2b_{26}s + b_{22} = 0 \tag{A4}$$

The roots of (A4) s_j are always complex or purely imaginary and will always occur in conjugate pairs, s_1, $\bar{s}_1$ and s_2, $\bar{s}_2$. Using these roots, stress components at the crack tip in x-y coordinate system are

$$\begin{aligned}\sigma_{xx} = {} & \frac{K_I}{\sqrt{2\pi r}}\mathrm{Re}\left\{\frac{s_1 s_2}{s_1 - s_2}\left(\frac{s_2}{\sqrt{\cos\theta + s_2\sin\theta}} - \frac{s_1}{\sqrt{\cos\theta + s_1\sin\theta}}\right)\right\} \\ & + \frac{K_{II}}{\sqrt{2\pi r}}\mathrm{Re}\left\{\frac{1}{s_1 - s_2}\left(\frac{s_2^{\,2}}{\sqrt{\cos\theta + s_2\sin\theta}} - \frac{s_1^{\,2}}{\sqrt{\cos\theta + s_1\sin\theta}}\right)\right\} + O(r^0)\end{aligned} \tag{A5}$$

$$\begin{aligned}\sigma_{yy} = {} & \frac{K_I}{\sqrt{2\pi r}}\mathrm{Re}\left\{\frac{1}{s_1 - s_2}\left(\frac{s_1}{\sqrt{\cos\theta + s_2\sin\theta}} - \frac{s_2}{\sqrt{\cos\theta + s_1\sin\theta}}\right)\right\} \\ & + \frac{K_{II}}{\sqrt{2\pi r}}\mathrm{Re}\left\{\frac{1}{s_1 - s_2}\left(\frac{1}{\sqrt{\cos\theta + s_2\sin\theta}} - \frac{1}{\sqrt{\cos\theta + s_1\sin\theta}}\right)\right\} + O(r^0)\end{aligned} \tag{A6}$$

$$\sigma_{xy} = \frac{K_I}{\sqrt{2\pi r}} \mathrm{Re}\left\{ \frac{s_1 s_2}{s_1 - s_2} \left(\frac{1}{\sqrt{\cos\theta + s_1 \sin\theta}} - \frac{1}{\sqrt{\cos\theta + s_2 \sin\theta}} \right) \right\} + \frac{K_{II}}{\sqrt{2\pi r}} \mathrm{Re}\left\{ \frac{1}{s_1 - s_2} \left(\frac{s_1}{\sqrt{\cos\theta + s_1 \sin\theta}} - \frac{s_2}{\sqrt{\cos\theta + s_2 \sin\theta}} \right) \right\} + O(r^0) \tag{A7}$$

Tangential component of the stress $\sigma_{\theta\theta}$ (hoop stress) can be obtained through the transformation law for stress component

$$\sigma_{\theta\theta} = \sigma_{xx} \sin^2\theta + \sigma_{yy} \cos^2\theta - 2\sigma_{xy} \sin\theta \cos\theta \tag{A8}$$

Substituting (A5), (A6) and (A7) into (A8),

$$\sigma_{\theta\theta} = \frac{K_I}{\sqrt{2\pi r}} \mathrm{Re}\left[\frac{s_1 s_2}{2(s_1 - s_2)} \left\{ \frac{1 + {s_2}^2 + (1 - {s_2}^2)\cos 2\theta + 2 s_2 \sin 2\theta}{s_2 \sqrt{\cos\theta + s_2 \sin\theta}} - \frac{1 + {s_1}^2 + (1 - {s_1}^2)\cos 2\theta + 2 s_1 \sin 2\theta}{s_1 \sqrt{\cos\theta + s_1 \sin\theta}} \right\} \right] + \frac{K_{II}}{\sqrt{2\pi r}} \mathrm{Re}\left[\frac{1}{s_1 - s_2} \left\{ (\cos\theta + s_2 \sin\theta)^{3/2} - (\cos\theta + s_1 \sin\theta)^{3/2} \right\} \right] + O(r^0). \tag{A9}$$

References

Budiansky, B., Hutchinson, J. W. and Evans, A. G., 1986, "Matrix fracture in fiber-reinforced ceramics," *J. Mech. Phys. Solids*, Vol. 34, pp. 167-189.

Budiansky, B. and Amazigo, J. C., 1989, "Toughening by aligned, frictionally constrained fibers," *J. Mech. Phys. Solids*, Vol. 37, pp. 93-109.

Budiansky, B. and Cui, Y. L., 1994, "On the tensile strength of a fiber-reinforced ceramic composite containing a crack-like flaw," *J. Mech. Phys. Solids*, Vol. 42, pp. 1-19.

Christensen, R. M., 1997, "Stress based yield/failure criteria for fiber composites," *Int. J. Solids Structures*, Vol. 34, pp. 529-543.

Echaabi, J., Trochu, F. and Gauvin, R., 1996, "Review of failure criteria of fibrous composite materials," *Polymer Composites*, Vol. 17, pp. 786-798.

Fleck, N. A., 1997, "Compressive failure of fiber reinforced composites," *Advances in Applied Mechanics*, Vol. 33, pp. 43-117.

Hashin, Z. and Rosen, B. W., 1964, "The elastic moduli of fiber-reinforced materials," *Journal of Applied Mechanics*, Vol. 31, pp. 223-232.

Hutchinson, J. W. and Suo, Z., 1992, "Mixed mode cracking in layered materials," *Advances in Applied Mechanics*, Vol. 29, pp. 63-191.

Lankford, J., 1997, "Shear versus dilatational damage mechanisms in the compressive failure of fibre-reinforced composites," *Composites*, Vol. 28A, pp. 215-222

Madhukar, M. S. and Drzal, L. T., 1992, "Fiber-matrix adhesion and its effect on composite mechanical properties. III. Longitudinal (0°) compressive properties of graphite/epoxy composites," *Journal of Composite Materials*, Vol. 26, pp. 310-333.

Marshall, D. B. and Cox, B. N., 1987, "Tensile fracture of brittle matrix composites:

influence of fiber strength," *Acta Metall.*, Vol. 35, pp. 2607-2619.

Oguni, K. and Ravichandran, G., 2000, "An energy-based model of longitudinal splitting in unidirectional fiber reinforced composites," to appear in *Journal of Applied Mechanics*.

Oguni, K., Tan, C. Y. and Ravichandran, G., 1999, "Failure mode transition in fiber reinforced composite under multiaxial compression," submitted to *Journal of Composite Materials*.

Parry, T. V. and Wronski, A. S., 1982, "Kinking and compressive failure in uniaxially aligned carbon fibre composite tested under superposed hydrostatic pressure," *Journal of Materials Science*, Vol. 17, pp. 893-900.

Rhee, K. Y. and Pae, K.D., 1995, "Effects of hydrostatic-pressure on the compressive properties of laminated, 0-degrees unidirectional, graphite fiber epoxy matrix thick-composite," *Journal of Composite Materials*, Vol. 29, pp. 1295-1307.

Schultheisz, C. R. and Waas, A. M., 1996, "Compressive failure of composites, Part I: Testing and micromechanical theories," *Progress in Aerospace Sciences*, Vol. 32, pp. 1-42.

Shuart, M. J., 1989, "Failure of compression-loaded multidirectional composite laminates," *AIAA Journal*, Vol. 27, pp. 1274-1279.

Sigley,R. H., Wronski, A. S. and Parry, T. V., 1992, "Axial compressive failure of glass-fibre polyester composites under superposed hydrostatic pressure: influence of fibre bundle size," *Composites Science and Technology*, Vol. 43, pp. 171-183.

Sih, G. C., Paris, P. C. and Irwin, G. R., 1965, "On cracks in rectilinearly anisotropic bodies," *International Journal of Fracture Mechanics*, Vol. 1, pp. 189-203.

Sih, G. C. and Chen, E. P., 1981, Cracks in Composite Materials, Martinus Nijhoff Publishers, The Hague.

Soden, P. D., Hinton, M. J. and Kaddour, A.S., 1998, "A comparison of the predictive capabilities of current failure theories for composite laminates," *Composites Science and Technology*, Vol. 58, pp. 1225-1254.

Soutis, C., 1991, "Measurement of the static compressive strength of carbon-fiber epoxy laminates," *Composites Science and Technology*, Vol. 42, pp. 373-392.

Sun, C. T. and Tao, J. X., 1998, "Prediction of failure envelopes and stress/strain behaviour of composite laminates," *Composites Science and Technology*, Vol. 58, pp. 1125-1136.

Tada, H., Paris, P. C. and Irwin, G. R., 1985, The Stress Analysis of Cracks Handbook. Del Research, St. Louis.

Tsai, S. W. and Wu, E. M., 1971, "A general theory of strength for anisotropic materials," *Journal of Composite Materials*, Vol. 5, pp. 58-80.

Waas, A. M. and Schultheisz, C. R., 1996, "Compressive failure of composites, Part II: Experimental studies," *Progress in Aerospace Science*, Vol. 32, pp. 43-78.

Waas, A. M., Takeda, N., Yuan, J. and Lee, S. H., 1997, "Static and dynamic compressive behaviour of glass fiber reinforced unidirectional composites," *Proceedings of the American Society for Composites, Twelfth Technical Conference*, pp. 552-561, Dearborn, Michigan.

Weaver, C. W., and Williams, J. G., 1975, "Deformation of a carbon-epoxy composite under hydrostatic pressure," *Journal of Materials Science*, Vol. 10, pp. 1323-1333.

List of tables

List of figures

interpolating function: $-\phi^2$, $K_{Ic}(0, \pm\pi)$ and $K_{Ic}(\pm\pi/2)$ computed by Eq. (8))

Figure 10 Effect of friction coefficient on crack surface on failure envelope (v_f = 60%, p = 1, interpolating function: $-\phi^2$, $K_{Ic}(0, \pm\pi)$ and $K_{Ic}(\pm\pi/2)$ computed by Eq. (8))

Figure 11 Comparison between the Tsai-Wu (1971) model and the present model predictions (Plane stress, v_f = 60%, p = 100, μ = 0.1, interpolating function: $-\phi^2$, $K_{Ic}(0, \pm\pi)$ and $K_{Ic}(\pm\pi/2)$ computed by Eq. (8))

Figure 12 Comparison between Christensen's model (Christensen, 1997) and the present model predictions (Plane strain, v_f = 60%, p = 100, μ = 0.1, interpolating function: $-\phi^2$, $K_{Ic}(0, \pm\pi)$ and $K_{Ic}(\pm\pi/2)$ computed by Eq. (8))

Table 1 Material constants of fiber, matrix and geometry of fiber

Fiber			Matrix	
E_f (GPa)	ν_f	d (μ m)	E_m (GPa)	ν_m
234[(a)]	0.2	3.4[(a)]	4.28[(a)]	0.34[(b)]

[(a)] Parry and Wronski (1982); [(b)] assumed

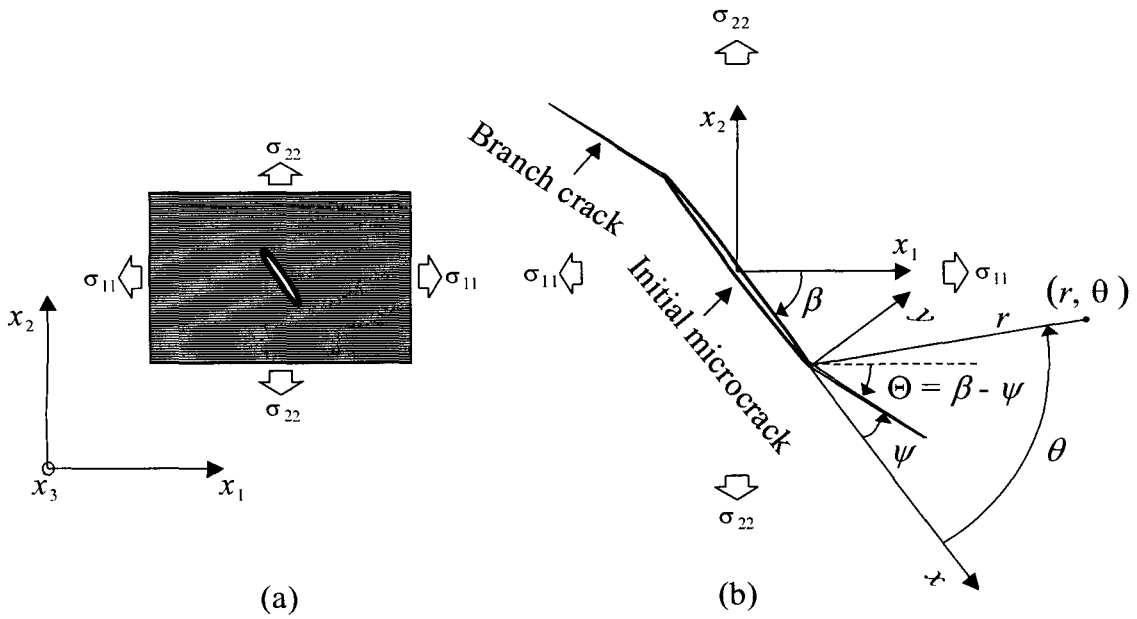

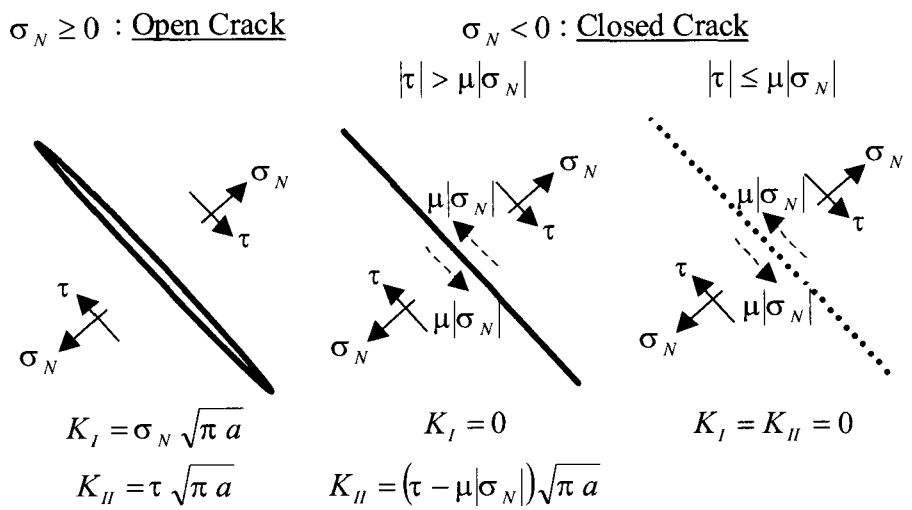

(c)

Figure 1 Schematics of a unidirectional fiber reinforced composite with a microcrack and coordinate systems for analysis

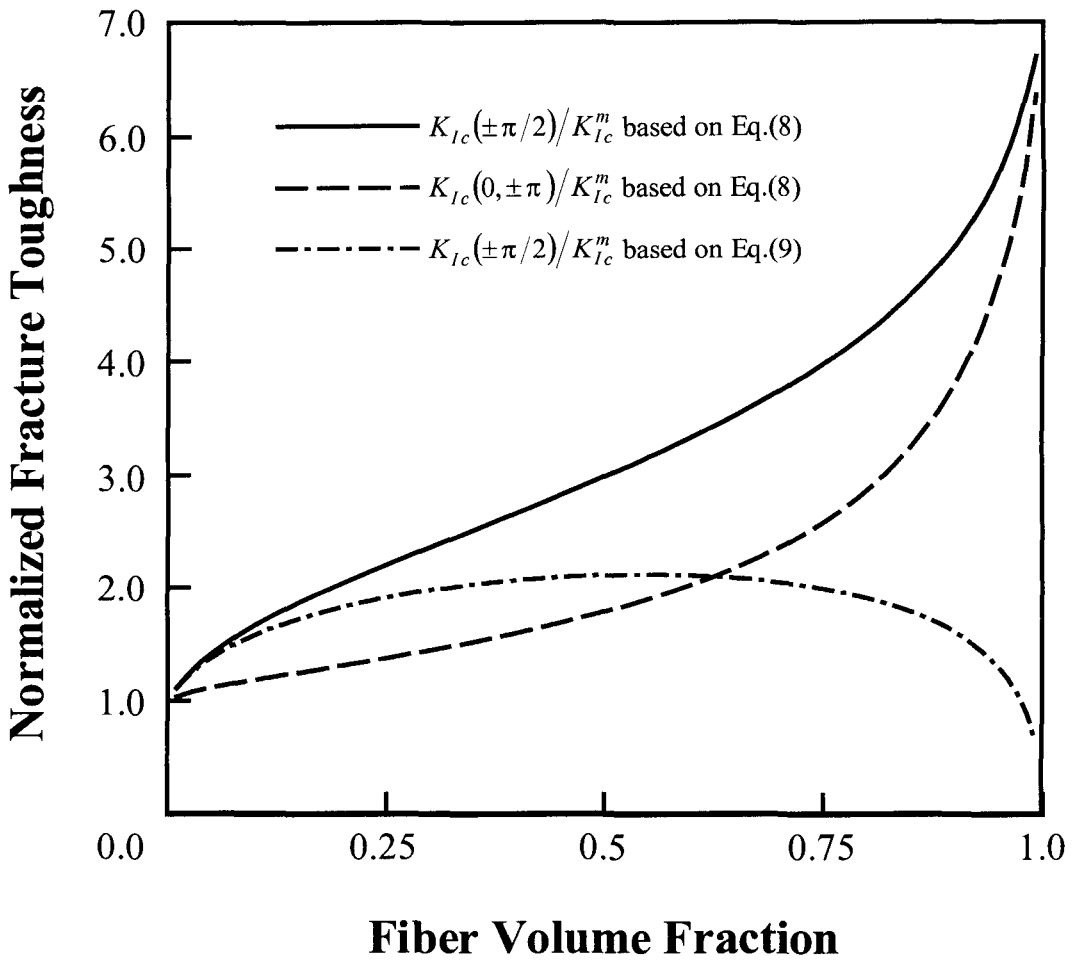

Figure 2 Normalized fracture toughness as a function of fiber volume fraction

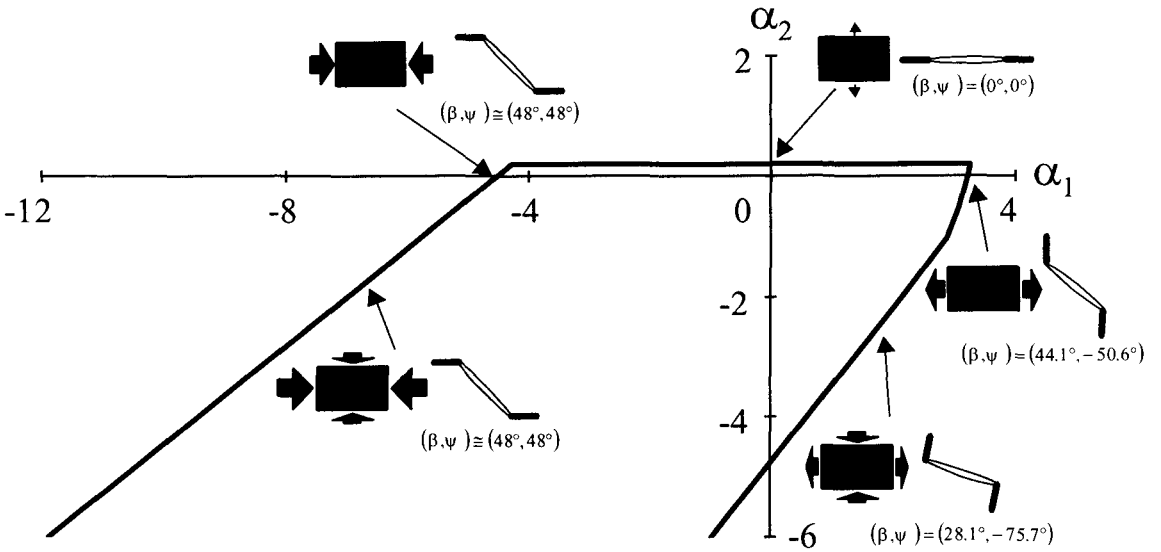

Figure 3 A typical failure envelope for a unidirectional fiber reinforced carbon/epoxy composite (v_f = 60%, p=100, μ =0.1, interpolating function: $-\phi^2$, $K_{Ic}(0, \pm\pi)$ and $K_{Ic}(\pm\pi/2)$ computed by Eq. (8))

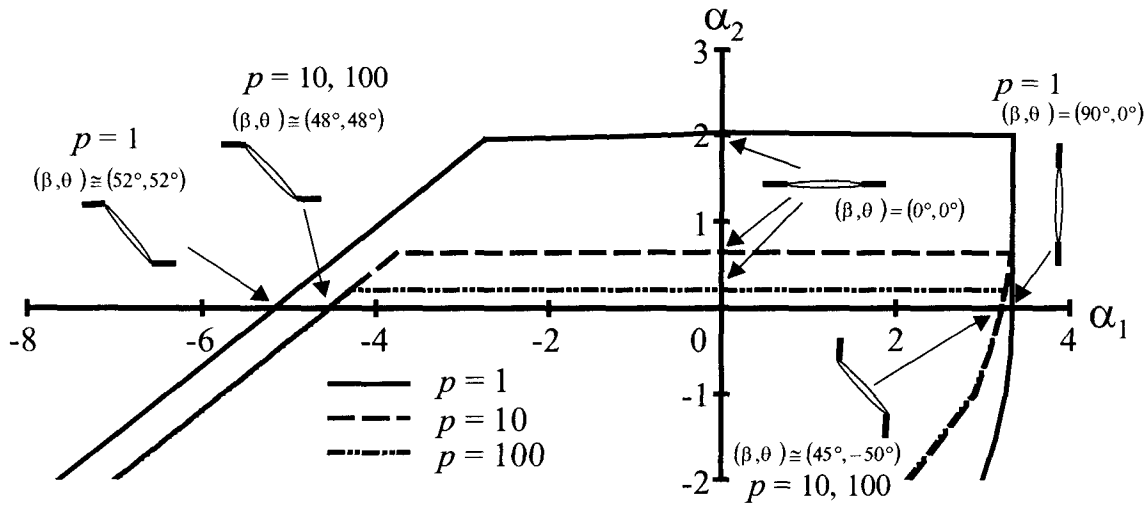

Figure 4 Effect of aspect ratio, p, on failure envelope (v_f = 60%, μ =0.1, interpolating function: $-\phi^2$, $K_{Ic}(0, \pm\pi)$ and $K_{Ic}(\pm\pi/2)$ computed by Eq. (8))

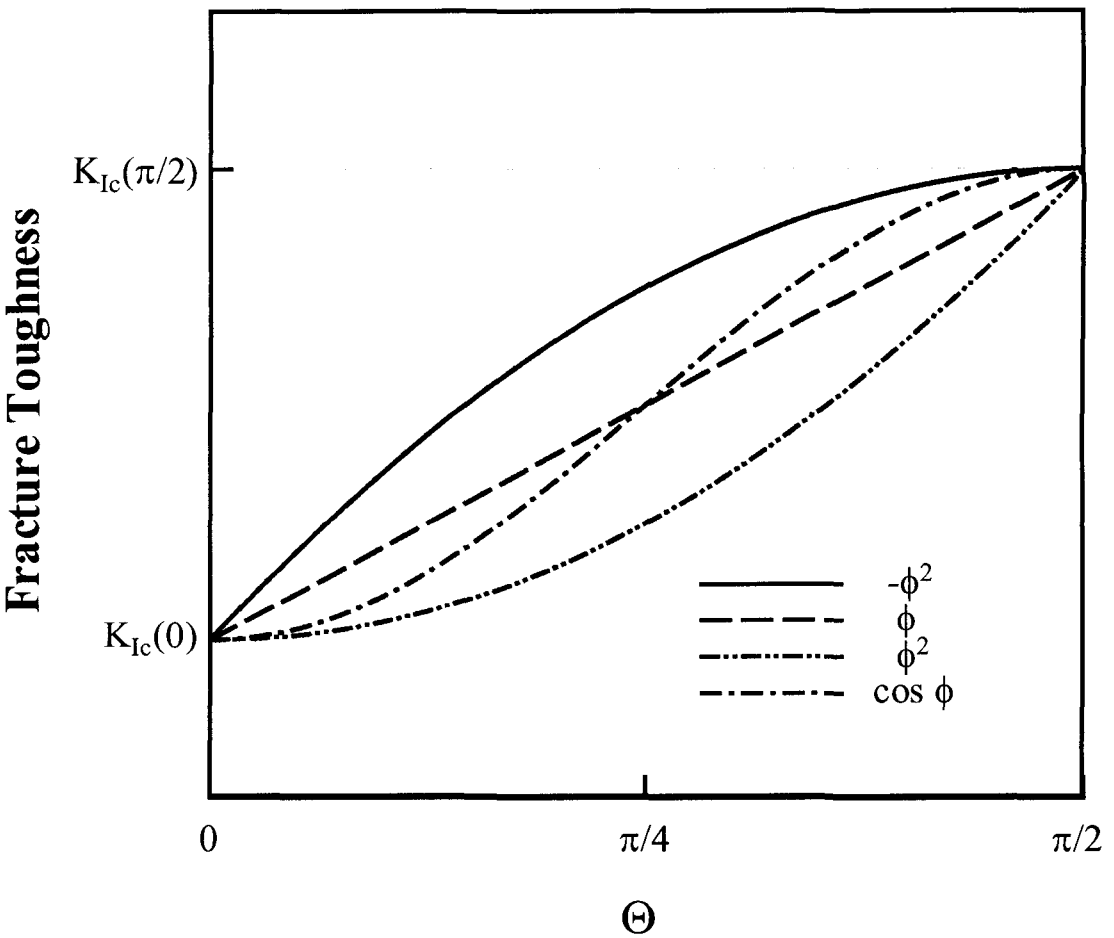

Figure 5 $K_{Ic}(\Theta)$ as a function of orientation of crack surface, Θ for different interpolating functions, $-\phi^2$, ϕ, ϕ^2 and $\cos\phi$ where $\phi=2\Theta/\pi$

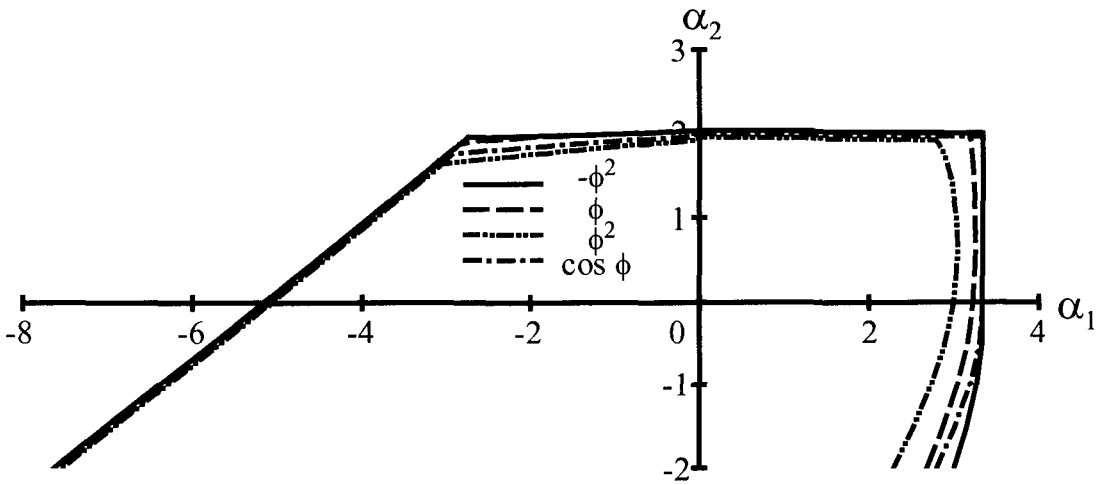

Figure 6 Effect of interpolating function on failure envelope (v_f = 60%, p = 1, μ = 0.1, $K_{Ic}(0, \pm\pi)$ and $K_{Ic}(\pm\pi/2)$ computed by Eq. (8))

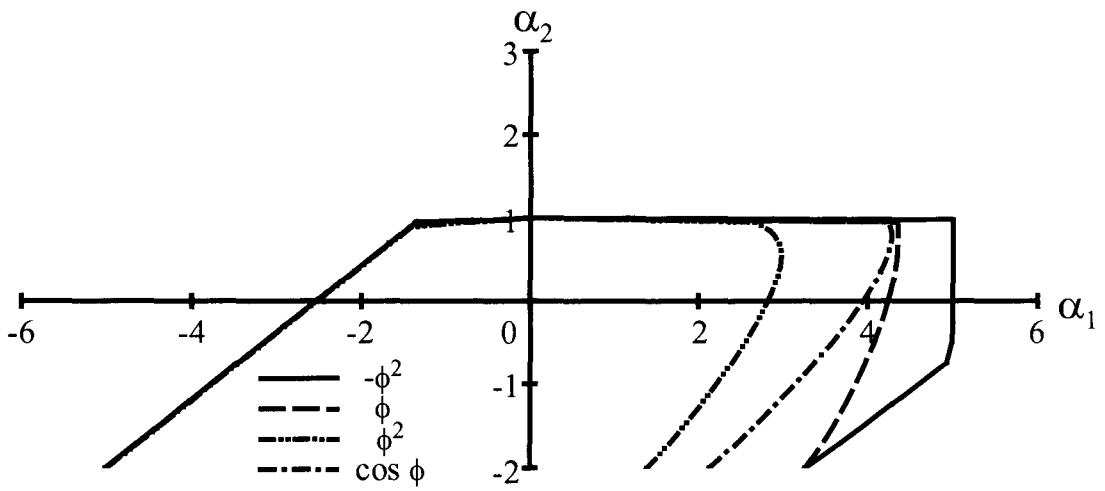

Figure 7 Effect of interpolating function on failure envelope (v_f = 60%, p = 1, μ = 0.1, $K_{Ic}(0, \pm\pi) = K_{Ic}^m$ and $K_{Ic}(\pm\pi/2) = 5K_{Ic}^m$)

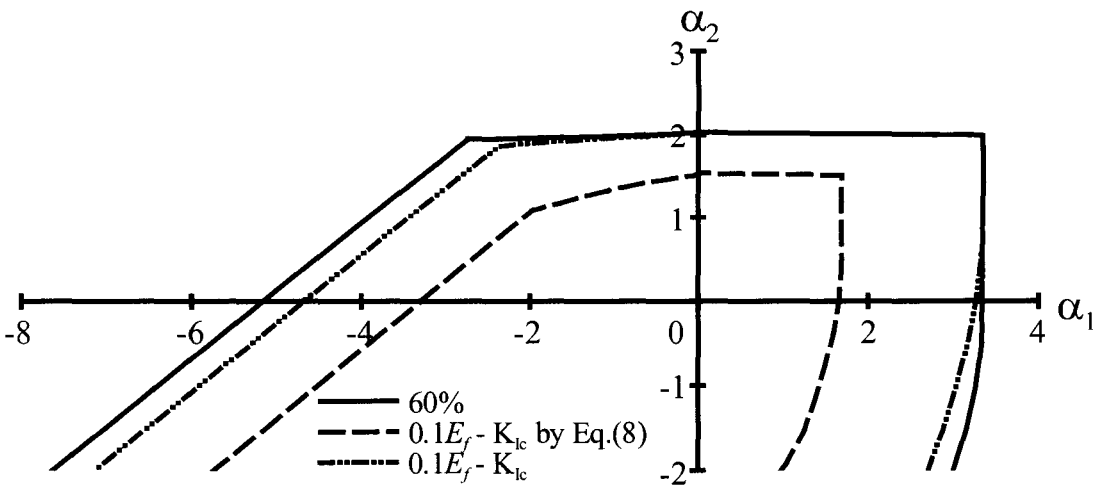

Figure 8 Effect of elastic material properties on failure envelope (v_f = 60%, p = 1, μ = 0.1, interpolating function: $-\phi^2$)

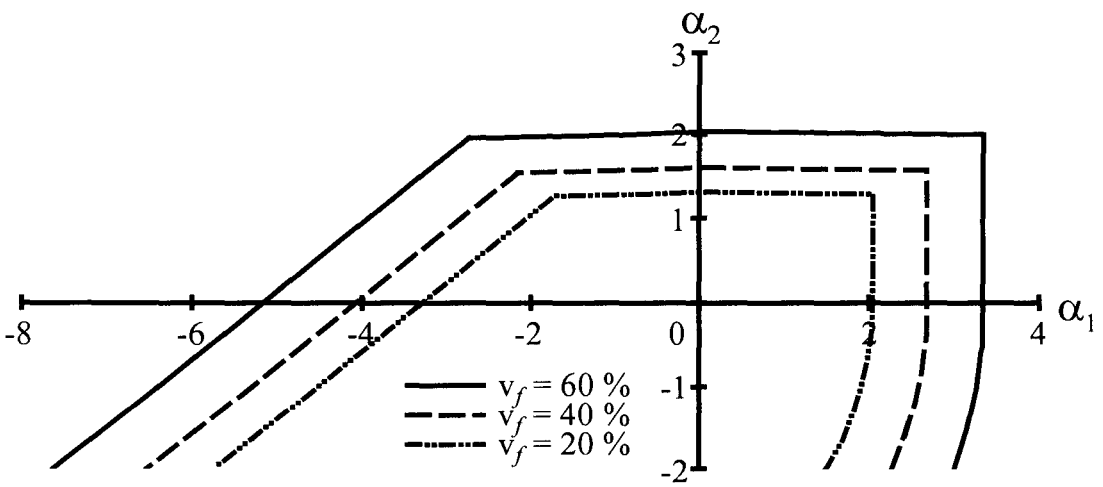

Figure 9 Effect of fiber volume fraction on failure envelope (p = 1, μ = 0.1, interpolating function: $-\phi^2$, $K_{Ic}(0, \pm\pi)$ and $K_{Ic}(\pm\pi/2)$ computed by Eq. (8))

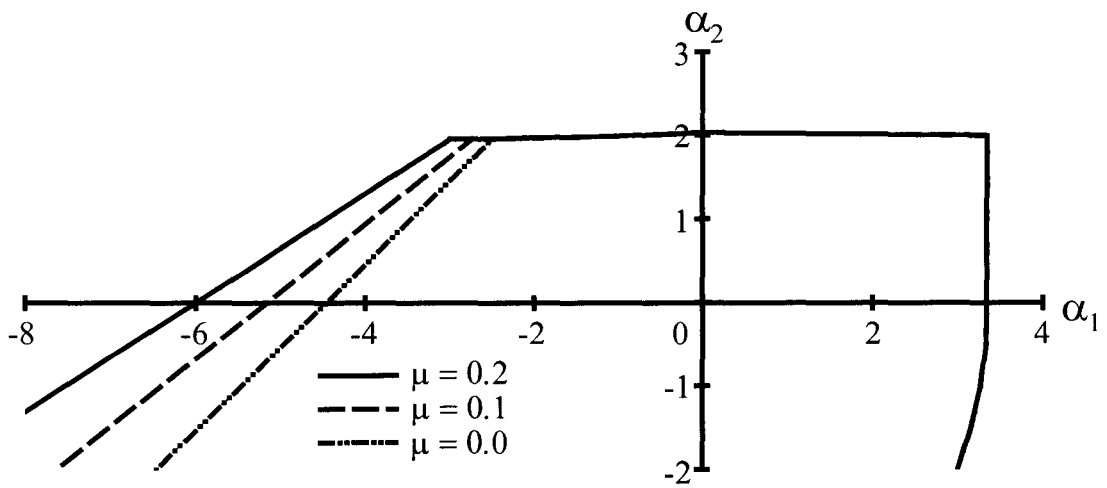

Figure 10 Effect of friction coefficient on crack surface on failure envelope (v_f = 60%, p = 1, interpolating function: $-\phi^2$, $K_{Ic}(0, \pm\pi)$ and $K_{Ic}(\pm\pi/2)$ computed by Eq. (8))

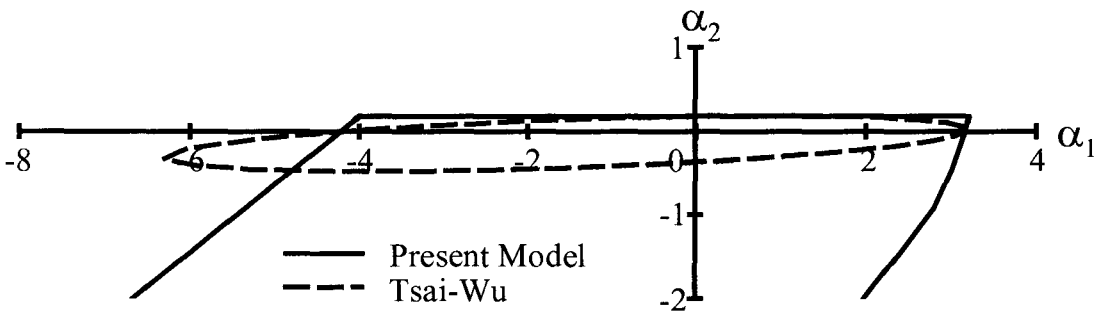

Figure 11 Comparison between the Tsai-Wu (1971) model and the present model predictions (Plane stress, v_f = 60%, p = 100, μ = 0.1, interpolating function: $-\phi^2$, $K_{Ic}(0, \pm\pi)$ and $K_{Ic}(\pm\pi/2)$ computed by Eq. (8))

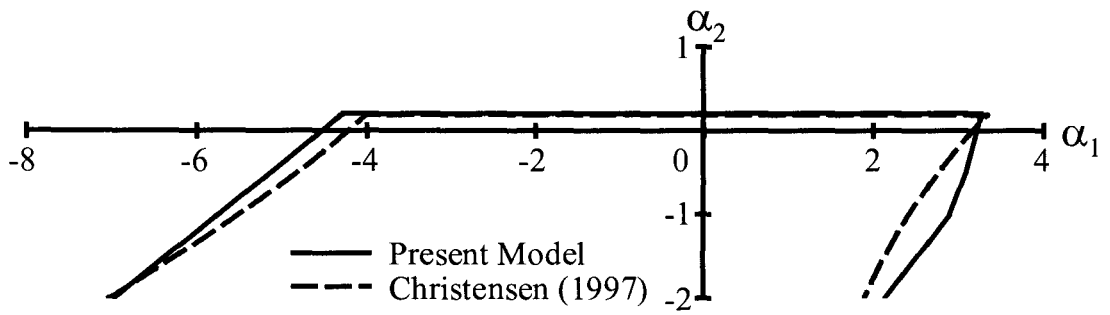

Figure 12 Comparison between Christensen's model (Christensen, 1997) and the present model predictions (Plane strain, $v_f = 60\%$, $p = 100$, $\mu = 0.1$, interpolating function: $-\phi^2$, $K_{Ic}(0, \pm\pi)$ and $K_{Ic}(\pm\pi/2)$ computed by Eq. (8))

Chapter IV Dynamic compressive behavior of unidirectional E-glass/vinylester composites

Abstract

Results from an experimental investigation on the mechanical behavior of unidirectional fiber reinforced polymer composites (E-glass/vinylester) with 30%, 50% fiber volume fraction under dynamic uniaxial compression are presented. Limited experimental results are presented for the 50% fiber volume fraction composite under proportional lateral confinement. Specimens are loaded in the fiber direction using a servo-hydraulic material testing system for low strain rates and a Kolsky (split Hopkinson) pressure bar for high strain rates, up to 3000/s. The results indicate that the compressive strength of the composite increases with increasing strain rate and increasing confinement. Post-test scanning electron microscopy is used to identify the failure modes. In uniaxial compression the specimens are split axially (followed by fiber kink band formation). Based on the experimental results and observations, an energy-based analytic model for studying axial splitting phenomenon in unidirectional fiber reinforced composites is extended to predict the compressive strength of these composites under dynamic uniaxial loading condition.

IV-1 Introduction

Deformation and fracture behavior of fiber reinforced composites have received considerable attention because of their importance in structural applications. Composites are also used in impact-related applications such as marine structures, turbine blades, automotive and others. Of particular interest for composite structures subjected to impact are their high-strain-rate mechanical properties, resistance to dynamic crack initiation and propagation as well as their strength and corresponding failure mechanisms under dynamic loading conditions. Specific instances where high strain rate properties of composites are needed for understanding of the phenomena include dynamic crack propagation (Coker et al., 1999), dynamic delamination (Lambros and Rosakis, 1997), perforation of panels by projectiles (Goldsmith et al., 1995) and drilling (Dharan and Won, 2000). Hence, investigation on the dynamic deformation behavior of fiber reinforced composites is needed in order to develop reliable constitutive models over a wide range of strain rates. However, relatively little is known concerning high-strain-rate behavior of fiber reinforced composites (e.g., Werner and Dharan, 1986; Lankford, 1997; Waas et al., 1997; Harding and Ruiz, 1998).

The limiting factor in the design of composite structures is their compressive strength and for unidirectional fiber reinforced composites, it is found to be roughly one-half of their tensile strength. Also, their compressive strength has been consistently and considerably lower than theoretical predictions. Extensive studies have been carried out on unidirectional fiber composites under static uniaxial compression; for an excellent review on this subject, see Waas and Schultheisz (1996).

In the present study, a modified Kolsky (split Hopkinson) pressure bar is used to study the high-strain-rate behavior of unidirectional E-glass/vinylester polymeric composites under compression in fiber direction. The deformation and failure responses of the composite over a range of strain rates and proportional confinement are presented and discussed. Examination of the failure surfaces of the recovered specimens from the experiments using a scanning electron microscope (SEM) revealed that failure mode of the composites under uniaxial compression is axial splitting followed by kink band formation. Motivated by these experimental observations, the energy-based model for splitting (Oguni and Ravichandran, 2000) is modified to study the high-strain-rate behavior of unidirectional composites. Under a wide range of strain rates, experimental results and model predictions of failure strength of composites are compared and show reasonable agreement.

In general, the loading in most applications such as aircraft structures, pressure vessels and submersibles is multiaxial. Even under uniaxial loading, due to shear coupling the stress state in a laminate is multi-dimensional. However, little is known concerning the multiaxial behavior of fiber reinforced composites (Weaver and Williams, 1975; Parry and Wronski, 1982; Lankford, 1997). The limited work concerning behavior of composites under multiaxial compression has been performed under hydrostatic pressure. In many applications involving composites, e.g., laminates, the loading path is proportional, i.e., stress components change in proportion to one another. A new experimental technique for studying the high-strain-rate behavior of unidirectional fiber reinforced composites under multiaxial compression using a modified Kolsky (split Hopkinson) pressure bar is presented. This modification of the current technique consists

of methods for generating proportional radial confinement, pulse shaping, specimen recovery and controlling specimen deformation. The deformation and failure response of a 50% fiber volume fraction E-glass/vinylester composite under multiaxial proportional compressive loading at high strain rates are presented and discussed.

IV-2 Experimental procedure

IV-2-1 Modified Kolsky (split Hopkinson) pressure bar

Kolsky (Split Hopkinson) pressure bar is a well-established apparatus commonly utilized in the high-strain-rate testing of ductile metals. Originally developed by Kolsky (1949), the concept has found widespread applications in testing ductile materials at strain rates up to 10^4/s. However, the application of this technique without adequate modifications for testing composite materials has serious limitations. As will be discussed below, modifications must be made to the conventional Kolsky (split Hopkinson) pressure bar to reliably obtain properties at small strains as well as to avoid repeated loading of the specimen. The modified Kolsky (Split Hopkinson) bar is shown in Fig. 1.

The conventional Kolsky pressure bar consists of a striker bar, an incident bar and a transmission bar. A specimen made of the material under investigation is placed between the incident bar and the transmission bar. When the striker bar impacts the incident bar, an elastic compressive stress pulse, referred to as the incident pulse, is generated and propagates along the incident bar towards the specimen. The pulse duration equals the round-trip time of a longitudinal elastic bar wave in the striker bar. When the incident pulse reaches the specimen, part of the pulse is reflected back in the incident bar due to impedance mismatch at the bar/specimen interface, and the remaining is transmitted

through the specimen into the transmission bar. The strain gages mounted on the bars provide time-resolved measures of the pulses in the incident and the transmission bars. For a specimen that is under mechanical equilibrium, Kolsky (1949) showed that the nominal strain rate $\dot{\varepsilon}$ (t) in the specimen could be calculated using the relation

$$\dot{\varepsilon}(t) = -\frac{2c_o}{l}\varepsilon_r(t) \qquad (1)$$

where l is the original length of the specimen, $\varepsilon_r(t)$ is the time-resolved reflected strain measured in the incident bar, and $c_0\left(=\sqrt{E/\rho}\right)$ is the longitudinal bar wave speed in the bar material for which E and ρ are the Young's modulus and the mass density respectively. Integration of (1) with respect to time gives the time-resolved axial strain of the specimen.

The nominal axial stress σ in the specimen is determined using the equation

$$\sigma(t) = E\frac{A_o}{A_s}\varepsilon_t(t) \qquad (2)$$

where A_s is the cross-sectional area of the specimen, and $\varepsilon_t(t)$ is the time-resolved strain in the transmission bar of area A_0. All the foregoing calculations are based on the assumption that the specimen undergoes homogeneous deformation. In the derivation of (1) and (2), the incident and transmission bars are assumed to be of the same material, remain elastic and of identical and uniform cross-sectional area.

When nominally brittle materials such as composites are tested in the conventional split Hopkinson pressure bar, the limitations of the technique must be recognized. In order to obtain reliable and consistent experimental data when testing these materials with the Kolsky pressure bar, appropriate modifications must be incorporated in both the experimental technique and the design of specimen geometry. For example, shaping of the loading pulse by a thin soft disc, called a pulse shaper, placed at the impact end of the incident bar has been used to prevent brittle high strength materials from failing before equilibrium is attained in the specimen. In addition to pulse shaping, reliable strain data at small strains (<1%) has been obtained during testing of brittle materials by mounting strain gages on the specimen surface (Chen and Ravichandran, 1997). The limiting strain rate below which reliable deformation and failure data for a brittle material can be obtained using the split Hopkinson pressure bar technique has been established (Ravichandran and Subhash, 1994). The stress in the specimen is computed from the transmitted pulse using (2) and for brittle materials; this has been shown to be in close agreement with the nominal stress in the specimen (Chen et al., 1994).

Using the conventional split Hopkinson pressure technique, it is possible for the specimen to be loaded multiple times due to subsequent wave reflections in the incident bar. In the investigation, the transmission bar was made to be shorter than the incident bar (Chen and Ravichandran, 1996) as shown in Fig. 1. With this modification, the shorter transmission bar will act as a momentum trap; thereby moving the transmission bar away from the specimen before a second compressive pulse due to reflected tensile pulse in the incident bar reloads the specimen. Thus, the specimen having been subjected to a single

known loading pulse can be recovered for microstructural characterization and unambiguous interpretation of failure modes.

IV-2-2 Proportional lateral confinement

A schematic for imposing proportional lateral confinement on a specimen that is axially loaded is shown in Figs. 2 a and b. The experimental set-up consists of a cylindrical specimen placed in a hollow cylinder with a sliding/running fit and is axially loaded using platens. The hollow cylinder and the loading platens are designed to remain elastic during the experiments. The confining cylinder and the platens are made of high strength alloys. Proportional loading is achieved by proper choice of the geometry (the inner and outer radii, a and b respectively) and the material properties for the hollow cylinder. The lateral confinement, σ_c, in the elastic regime is a function of the axial stress, σ, the cylinder geometry (Fig. 2 b) and the elastic properties of the composite specimen and the confining cylinder,

$$\sigma_c = \frac{\sigma}{\left[\frac{(1-\nu)E_{22}a^2}{\nu_{12}E(b^2-a^2)}\left\{1+\frac{(1+\nu)}{(1-\nu)}\frac{b^2}{a^2}\right\}+\frac{(1-\nu_{32})}{\nu_{12}}\right]} \qquad (3)$$

where E and ν are the Young's modulus and Poisson's ratio of the sleeve material and E_{22}, ν_{12} and ν_{32} are the elastic properties for the composite (Oguni et al., 1999).

With the guidance from (3) and proper material choice, desired lateral confinement can be attained using the hollow cylinder configuration in Fig. 2. A strain gage mounted on the external surface of the confining cylinder is used to measure the

circumferential or hoop strain (ε_c) and to ascertain the confining stress, $\sigma_c = E\varepsilon_c$. Such a configuration to apply proportional confinement loading can be used both under quasi-static and dynamic loading conditions.

IV-2-3 Experimental setup

The dimensions of the bars in the Kolsky pressure bar setup used in this study are 1220 and 580 mm in length for the incident and transmission bar respectively, with a common diameter of 12.7 mm. The striker bars are also of 12.7 mm diameter varied in their lengths from 50 to 100 mm to achieve the desired loading pulse duration. All the bars are made of high strength maraging steel (C-350, Rockwell hardness, Rc=60) with a yield strength of 2.7 GPa. A thin, half-hardened copper disc of 3 mm diameter and 0.85 mm in thickness is typically used as a pulse shaper. The material as well as the diameter and the thickness of the pulse shaper are varied to control the rise time of the incident pulse. The rise time and shape of the pulse are tailored to ensure stress equilibration within the specimen (Ravichandran and Subhash, 1994). High resistance (1000 Ω) strain gages (Micro-measurements WK-06-250BF-10C) with excitation voltage of 30 volts are used to measure the surface strain on the specimen as well as on the bars. Also, a strain gage (Micro-measurements EA-06-062AQ-350, resistance = 350 Ω) with excitation voltage of 10 volts is mounted on the surface of the specimen to directly measure the deformation of the specimen in fiber direction. Raw strain gage signals without any pre-amplifiers that may distort the signals are recorded using a high-speed 12-bit digital oscilloscope, Nicolet model 440. The loading faces were lubricated to avoid frictional

effects between the specimen and the bars during loading so that one-dimensional stress state in specimen can be achieved.

The confinement sleeve (Fig. 2a) is typically made of a 7075 aluminum alloy and the dimensions are chosen to provide the desired confinement level (3). The inner diameter is carefully machined to provide smooth sliding fit on the specimen as well as the hardened sleeves. The inner and outer diameters of a typical sleeve used in the experiments are 6.25 mm and 30 mm respectively. The loading platens are made of hard tool steel, Rockwell hardness Rc=60 and dimensions 6.25 mm in diameter and 2.5 mm in length. The lengths of the sleeve and the platens are chosen to provide a predetermined clearance (δ) used to control the extent of deformation imposed on the specimen.

IV-2-4 Materials

Unidirectional fiber reinforced composites (E-glass/vinylester) with 30% and 50% fiber volume fraction are investigated in the present study. This material is finding increasing applications in marine structures because of the relatively low cost in manufacturing using techniques such as resin transfer molding (RTM) and vacuum assisted RTM (VRTM). Continuous E-glass (Certainteed R099-625) fibers of 24.1 μm in diameter are aligned in a glass tube and are impregnated with vinylester resin (Dow Derakane 411-C50). Following curing, specimens of desired length (6.25 mm) are sectioned using a low speed diamond saw and are sized to desired diameter (6.25 mm) using low speed machining. The ends of the specimen are made parallel and polished using diamond paste. The details of the material and specimen preparation can be found elsewhere (Waas et al., 1997). Also, mechanical behavior of pure matrix material,

vinylester (Dow Derakane 411-C50), is investigated in this study. Vinylester resin is machined and polished using the same procedure as for the composites.

IV-3 Results

Experiments on the unidirectional fiber reinforced E-Glass/vinylester composite materials were performed at low stain rates (10^{-4}/s - 1/s) using a servo-hydraulic materials testing system (MTS) and at high strain rates (500/s - 3,000/s) using the modified Kolsky (split Hopkinson) pressure bar. Limited experiments under proportional confinement were conducted in the strain rate range of 10^{-3}/s to 3,000/s. Experiments were also performed on the pure matrix material, vinylester (Dow Derakane 411-C50).

IV-3-1 Stress-strain response

The typical stress-strain curves obtained from experiments for the composite specimens with 30% fiber volume fraction loaded in the fiber direction for nominal strain rates between 10^{-4}/s and 2,000/s are shown in Fig. 3. The stress-strain curves are essentially linear up to a maximum stress prior to catastrophic load drop. Young's modulus in fiber direction increased from 19.3 GPa at a strain rate of 10^{-4}/s to 30.6 GPa at a strain rate of 2,000/s. Similarly, the peak stress increased from 468 MPa at a strain rate of 10^{-4}/s to 596 MPa at a strain rate of 2,000/s. The failure strength versus strain rate for 30% fiber volume fraction composite from a total of 12 tests is plotted in Fig. 4. The failure strength shows scatter around 450 MPa at low strain rates (up to 800/s) and a rapid rise in strength is observed beyond a strain rate of 800/s. The failure strength has a rate

sensitivity exponent ($\partial log(\sigma)/\partial log(\dot{\varepsilon})$) of 0.193 at high strain rates. All the specimens in the above uniaxial compression experiments failed by axial (longitudinal) splitting.

Figure 5 shows the typical stress-strain curves obtained from experiments for the composite specimens with 50% fiber volume fraction loaded in the fiber direction with nominal axial strain rates between 10^{-4}/s and 3,000/s. The stress-strain curves are almost linear up to a maximum stress prior to catastrophic load drop. Young's modulus in fiber direction increased from 37.7 GPa at a strain rate of 10^{-4}/s to 52.7 GPa at a strain rate of 3,000/s. The peak stress increased from 591 MPa at a strain rate of 10^{-4}/s to 844 MPa at a strain rate of 3,000/s. Figure 6 shows the failure strength versus strain rate for 50% fiber volume fraction composite from a total of 24 tests. The failure strength is about 600 MPa at the lowest strain rate (10^{-4}/s) reported here. Subsequently, there is considerable scatter in the failure strength at intermediate strain rates (10^{-1} to 1/s). A rapid increasing trend in strength is observed beyond a strain rate of 800/s. The failure strength has a rate sensitivity exponent ($\partial log(\sigma)/\partial log(\dot{\varepsilon})$) of 0.177 at high strain rates. Specimens that were loaded at low strain rates (10^{-4}/s - 1/s) failed by axial splitting followed by formation of kink band. The scatter in failure strength at low strain rates can be attributed to the high degree of sensitivity of strength on failure mode, i.e., kink banding induced by splitting. At low strain rates, the failure is initiated by the formation of an axial split within the specimen. However, the size of the initial split may vary between specimens depending on many factors such as the variability in interfacial strength between fiber and matrix. It is then conceivable that the peak strength reported here is related to the onset of the kink band and could vary considerably depending on the size of

the split ("buckling length"). At high strain rates (500/s - 3,000/s), all the specimens failed by axial splitting.

The response of the matrix under uniaxial compression was highly non-linear for all strain rates as shown in Fig. 7. As a general trend, the flow stress increases with the increasing strain rate from 75 MPa at a strain rate of 10^{-4}/s to 223 MPa at a strain rate of 2,000/s. The flow strength at a strain rate of 3,000/s is 206 MPa and is lower than that for 2,000/s. This decreasing trend may be due to thermal softening or instabilities in matrix material. The Young's modulus (initial slope) of the stress-strain curve is plotted against strain rate in Fig. 8. At low strain rates (10^{-4}/s–1/s), the modulus increases slowly as the strain rate increases. Then, rapid increase in modulus is observed as the strain rate increases beyond a strain rate of 700/s.

The multiaxial compression experiments were designed for the stress ratio σ_c/σ of 0.3 using (3). The axial stress-strain curves for the multiaxial compression experiments loaded in the fiber direction and confined laterally (Fig. 2) are shown in Fig. 9 for the strain rates of 10^{-4}/s, 1,000/s and 2,000/s. Experiments were stopped at a strain of 0.05 by choosing a proper gap δ between the confining sleeve and the loading platen heads (Fig. 2a) to enable the failure mode characterization of the specimens. The maximum stress attained during the experiments on confined specimens increased with increasing strain rate from 600 MPa at 10^{-4}/s to 900 MPa at 2,000/s. At low strain rate (10^{-4}/s), the material exhibited a linear response up to 400 MPa followed by load drops and degradation of modulus. Extensive acoustic emission activity was observed during these load drops (Oguni et al., 1999). At a given strain rate, the maximum stress that the material appears to sustain under multiaxial compression is greater than its unconfined

strength. Also, at higher strains, the strength appears to be saturating for a given strain rate.

IV-3-2 Failure mode characterization

The longitudinal failure surfaces of the specimen from the experiments were coated with gold and examined using a scanning electron microscope (SEM). Figures 10 a and b show the failure surface of 30% fiber volume fraction composite specimen under quasi-static uniaxial compression in fiber direction. Higher magnification micrograph (Fig. 10 b) shows that the failure mode in this specimen is axial splitting in fiber direction. Under high strain rate loading condition, 30% fiber volume fraction composite specimens broke into numerous columns. Micrographs of a column recovered from dynamic compression test at a strain rate of 500/s are shown in Figs. 11 a and b. A high magnification micrograph of the surface of a column (Fig. 11 b) shows debonding between fibers and matrix as well as rupture of matrix material. Specimens under higher strain rates are broken into thinner columns, i.e., a few fibers and fragments of matrix. The failure mode in 30% fiber volume fraction composite under uniaxial compression in fiber direction is axial splitting for all the strain rates examined.

Failure surface of the 50% fiber volume fraction composite specimen under quasi-static uniaxial compression in fiber direction is shown in Figs. 12 a and b. Both axial splitting and kink banding are observed in the specimen. Since the crack due to the axial splitting (running from **A** to **B**) is bent by kink band at **C** and **D**, axial splitting had occurred before kink band formation. Therefore, the main failure mechanism in this specimen was axial splitting and the kink band was *induced* by axial splitting. The

specimen splitting appeared to have preceded by debonding of the fiber leading to local stiffness reduction. The local softening lead to lateral displacement causing the specimen to split. The splitting resulted in relaxation of the stress state in the surrounding matrix leading to microbuckling and kink band formation and subsequent fiber failure. The axial splitting is manifested as a catastrophic load drop and is seen in Fig. 5. On the other hand, 50% fiber volume fraction composite specimens broke into numerous columns and no kink band formation is observed under dynamic loading condition. SEM micrographs of the surface of a column recovered from dynamic compression test at a strain rate of 420/s are shown in Figs. 13 a and b. Cracks due to axial splitting are observed, but no kink band is evident. Specimens under higher strain rates are broken into thinner columns (i.e., a few fibers and fragments of matrix) with no fiber kinking. The dominant failure mechanism in 50% fiber volume fraction composite under uniaxial compression in fiber direction is axial splitting for all strain rates examined. Under quasi-static loading condition, kink band is formed *after* axial splitting. One possible explanation for the lack of kink band formation in the 50% volume fraction composite specimen under dynamic compressive loading is suggested here. Due to the high rate of deformation, the unidirectional composite specimen splits into columns by dynamic crack propagation and hence lacking the time required for a kink band to nucleate and broaden. Indeed, very high crack velocities in unidirectional fiber reinforced composites have been observed, up to 90% of the dilatational wave speed (Coker et al., 1999).

Figures 14 a and b are SEM micrographs of the longitudinal cross-section of the 50% fiber volume fraction E-glass/vinylester composite under proportional lateral confinement deformed at a strain rate of 2000/s showing multiple kink banding. Kink bands are

reflected at the lateral boundaries of the specimen. Distinct kink boundary can be observed in Fig. 14 b as broken fibers. Kink width, w, defined in Fig. 14 b is $400\,\mu\mathrm{m}$, which is approximately 20 times of the fiber diameter. Comparison between the longitudinal cross-section of the specimen from static experiment (Oguni et al., 1999) and that from the present dynamic experiment shows no significant difference in failure mode.

IV-4 Energy-based model of axial splitting

Motivated by the preceding experimental observations, an energy-based model (Oguni and Ravichandran, 2000) has been modified to investigate the failure mechanism for low level of lateral confinement, i.e., longitudinal or axial splitting in unidirectional composites. Due to the heterogeneity and anisotropy of the fiber reinforced composite, excessive elastic energy is stored in the composite under compression. Axial splitting can be regarded as a process in which the excessive elastic energy is released through the formation of new surfaces. Thus, the failure criterion is that when the reduction of the stored elastic energy by splitting compensates the surface energy, the specimen splits.

This energy-based failure criterion combined with the effective properties of the composite based on the elastic properties of the matrix and the fiber provides an analytical expression for the unconfined longitudinal compressive strength for the composite,

$$\sigma^* = 2\left(\frac{2\gamma \mathrm{v}_f}{a}\right)^{\frac{1}{2}}\left(\frac{\mathrm{v}_f}{E_f}+\frac{\left(1-\mathrm{v}_f\right)}{E_m}-\frac{1}{E_{11}}\right)^{-\frac{1}{2}}. \qquad (4)$$

This expression illustrates the effect of material properties and geometry on the critical axial compressive stress, σ^* for axial splitting. E_{11} is the effective longitudinal modulus of the composite in the fiber direction, E_f and E_m are the Young's modulus of fiber and matrix respectively, γ is the fracture (surface) energy, v_f is the fiber volume fraction and a is the fiber radius. In general, the rule of mixture's expression for E_{11}, $E_{11} = \mathrm{v}_f E_f + (1 - \mathrm{v}_f) E_m$, suffices for computing the compressive strength. More rigorous expressions for E_{11} can be found in Hashin and Rosen (1964). Equation (4) shows that the unconfined strength is proportional to the square root of surface energy and inversely proportional to the square root of fiber diameter as one would expect from the scaling considerations. This result indicates that for a given volume fraction, all other things remaining unchanged, composites with larger fiber diameter are more susceptible to axial splitting than smaller diameter fibers. Further details of the model and its implications can be found in Oguni and Ravichandran (2000).

IV-4-1 Extension of the model to dynamic loading

In the experiments presented above, although the loading condition ranges from quasi-static to dynamic, specimen is always in mechanical equilibrium. Therefore, principle of minimum potential energy still applies and thus, the energy-based model (Oguni and Ravichandran, 2000) is applicable in the entire range of strain rates examined in the experiments. In order to apply the present energy-based model to predict the

strength of unidirectional fiber reinforced composites under uniaxial dynamic loading, the following factors should be taken into account:

i) strain rate dependence of the Young's modulus of matrix material, E_m;

ii) loading rate dependence of the surface energy, γ.

The Young's modulus of the fiber is in general relatively independent of strain rate. As for the information needed in i), results from uniaxial compression on matrix material can be used. Figure 15 shows the dependence of the Young's modulus of the matrix material on strain rate obtained from experiments (Fig. 8) and the best fit curve for the experimental results based on least square method. From this curve fitting, the experimentally measured Young's modulus of the matrix can be expressed as a function of strain rate as follows,

$$E_m = E_0\left(1+\left(\frac{\dot{\varepsilon}}{\dot{\varepsilon}_0}\right)^n\right) \qquad (5)$$

where E_m is strain rate dependent Young's modulus of the matrix material, $E_0 = 3.84$ GPa, $\dot{\varepsilon}_0 = 2{,}060\,/\mathrm{s}$ and $n = 0.73$ are the quasi-static Young's modulus, the reference strain rate and the strain rate sensitivity exponent obtained from best curve fitting to the experimental data, respectively. Since (5) is based on the experimental data for $\dot{\varepsilon} \geq 10^{-5}$ /s, (5) is valid only for $\dot{\varepsilon} \geq 10^{-5}$ /s.

For the information required in ii), only limited experimental data is available (Lambros and Rosakis, 1997a). The surface energy γ can be interpreted in terms of the fracture energy or the energy release rate, $G_c=2\gamma$, in the sprit of Griffith. In the preceding

experimental observations, the matrix material is observed to be more brittle as the strain rate increases. All the specimens of the matrix material deformed under low strain rate deformation ($\dot{\varepsilon} \leq 1/\mathrm{s}$) remained intact following axisymmetric shortening during compression. On the other hand, dynamically compressed specimens showed brittle cracking and broke into fragments. The SEM micrographs from the failure surface of one of these fragments are shown in Figs. 16 a and b. The smooth mirror like fracture surface suggests the brittle nature of the material at high strain rates. These observations leads to the conclusion that as the strain rate increases, surface energy for the matrix material decreases which is consistent with the increase in flow stress (Fig. 7).

IV-4-2 Comparison with experiments

The input parameters required for predicting the unconfined compressive strength of unidirectional fiber reinforced composites using (4) are

i) elastic material properties (E_f, ν_f) and radius (a) of fibers;

ii) elastic material properties of matrix (E_m, ν_m);

iii) fiber volume fraction (v_f);

iv) surface energy (γ).

As for the parameters in i) constant values for $E_f = 72.4\,\mathrm{GPa}$, $\nu_f = 0.2$ and $a = 12.1\,\mu\mathrm{m}$ are used (Waas et al., 1997). The modulus of the fiber material, E-glass, is assumed to be rate independent since the glass transition temeprature ($\mathrm{T_g} = 846\,^{\circ}\mathrm{C}$) of the material is far above the room tmeperature at which the composite is deformed. The dependence of the modulus of the polymeric matrix, vinylester ($\mathrm{T_g} = 100\,^{\circ}\mathrm{C}$) is a direct

consequence of the viscoelastic (time-dependent) nature of the material. Experimentally observed strain rate dependence of Young's modulus of matrix material, E_m, is given by (12). The Poisson's ratio of the matrix is assumed to be constant, $\nu_m = 0.38$, obtained under quasi-static loading (Waas et al., 1997). Since the composite undergoes constant strain rate deformation in the fiber direction, using (4) to determine compressive strength can be viewed as the quasi-elastic approximation. Given the fiber volume fraction, v_f, the only parameter which remains to be specified is the surface (fracture) energy, γ.

In the present model, γ has been assumed to be the surface energy associated with longitudinal splitting consisting of the sum of energies for delamination between fiber and matrix and matrix failure. In the case of high v_f, surface energy associated with matrix failure is negligible since the average distance between fibers is small and the area of the surface created by matrix failure is much smaller than the one created by interface (fiber-matrix) debonding. On the other hand, for low v_f, the average distance between fibers increases and the surface energy associated with matrix failure becomes no longer negligible. As the strain rate increases, the matrix becomes more brittle and hence surface energy associated with its failure decreases and becomes negligible even in the case of low v_f. This results in the convergence of the surface energy for all fiber volume fraction at high strain rates. There have been recent experimental observations of the decrease in the dynamic energy release rate ($G_c=2\gamma$) for interface debonding (delamination failure) as a function of increasing crack velocity (e.g., Lambros and Rosakis, 1995). Under quasi-static loading conditions, the axial splitting proceeds at slow speeds and under high strain rate defromation of the composite, the splitting occurs

dynamically with crack speeds presumably in the subsonic regime. However, quantiative information concerning the splitting speeds as a function of strain rate are not currently avaiable.

Based on the discussion above, different surface energy values are assumed for low ($\dot{\varepsilon} \leq 1/\mathrm{s}$) and high ($\dot{\varepsilon} > 400/\mathrm{s}$) strain rate regions. Values of the surface energy used in the present analysis in low strain rate region are $\gamma = 180\ J/m^2$ for $\mathrm{v}_f = 30\%$ and $\gamma = 120\ J/m^2$ for $\mathrm{v}_f = 50\%$. The values for γ used in the model predictions are consitent with data available for similar compsoite materials (Daniel and Ishai, 1994) by assuming G_c=2γ. For both volume fractions, the surface energy is decreased to $\gamma = 100\ J/m^2$ in the high strain rate region to reflect the dependence of fracture energy on delamination veleocity and brittle nature of the matrix at high strain rates. Further work towards quantification of fracture energies in fiber reinforced composites as a function of volume fraction and laoding rate is needed.

Comparison between the model prediction (4) and experimental results for 30% fiber volume fraction E-glass/vinylester composite is shown in Fig. 17. The compressive strength is plotted as a function of strain rate. Figure 18 shows comparison between the model prediction and experimental results for 50% fiber volume fraction E-glass/vinylester composite. The model predicitons show reasonable agreement with the experimental results by taking into account the depenedence of the modulus of the matrix and the fracture energy on loading rate discussed above.

As one can deduce from (4) and (5), in the present model, the rate sensitivity of the strength of the composites at high strain rates is due to the rate sensitivity of the Young's modulus of the matrix material and the fracture energy. Therefore, from theoretical point

of view, 30% fiber volume fraction composite is expected to have higher rate sensitivity than 50% fiber volume fraction composite does. In fact, this tendency is observed in the experimental results (Figs. 17 and 18).

IV-5 Summary

A modified Kolsky (split Hopkinson) pressure bar has been used to investigate the response of unidirectional fiber reinforced composites at high strain rates. Methods for pulse shaping, specimen recovery and controlling specimen deformation have been outlined. Experiments on 30% and 50% by volume E-glass/vinylester composites at various strain rates of up to 3,000/s revealed an increase in compressive strength with increasing strain rate. The experimental data is currently being used to develop high-strain rate constitutive models for fiber reinforced composites as a function of stress state.

An energy-based model for axial splitting has been used for predicting the compressive strength of unidirectional fiber reinforced composites under dynamic uniaxial compression in fiber direction. The compressive strength can be computed as a function of the effective properties of the unsplit and the split composite as well as the rate dependent fracture energy. The results from the analysis indicate that the effect of strain rate is reflected on strength through the increase of modulus of the matrix material and the decrease of surface energy due to the increase of loading rate. The splitting analysis is able to capture the essential features of experimental data for unidirectional fiber reinforced composites under the wide range of strain rates. Insights gained from the modeling regarding the influence of various material parameters, length scales and strain

rate on the strength of composites are useful in designing marine and other structures with composites.

Acknowledgements

The research reported in this chapter is supported by the Office of Naval Research (Dr. Y. D. S. Rajapakse, Scientific Officer) through a grant to the California Institute of Technology and is gratefully acknowledged. We thank Professor A. M. Waas, University of Michigan, for providing the E-Glass/vinylester composite specimens used in this study.

References

Bhattacharya, K., Ortiz, M. and Ravichandran G., 1998, "Energy-based model of compressive splitting in heterogeneous brittle solids," *J. Mech. Phys. Solids*, Vol. 46, pp. 2171-2181.

Chen, W., Subhash, G. and Ravichandran, G., 1994, "Evaluation of Ceramic Specimen Geometries used in a Split Hopkinson Pressure Bar," *Dymat Journal*, Vol. 1, pp. 193-210.

Chen, W. and Ravichandran, G., 1996, "An Experimental Technique for Imposing Dynamic Multiaxial-Compression with Mechanical Confinement," *Experimental Mechanics,* Vol. 36, pp. 435-438.

Chen, W. and Ravichandran, G., 1997, "Dynamic Failure of a Glass Ceramic under Lateral Confinement," *J. Mech. Phys. Solids,* Vol. 45, pp. 1303-1328.

Coker, D., Rosakis, A. J. and Huang, Y. Y., 1999, "Subsonic and intersonic dynamic crack growth in unidirectional composites," *Thick composites for load bearing structures* (Eds. G. A. Kardomateas and Y. D. S. Rajapakse), AMD-Vol. 235, pp. 75-86.

Daniel, I.M. and Ishai, O., 1994, Engineering Mechanics of Composite Materials, Oxford University Press.

Dharan, C. K. H. and Won, M. S., 2000, "Machining parameters for an intelligent machining system for composite laminates," *International Journal of Machine Tools & Manufacture*, Vol. 40, pp. 415-426.

Goldsmith, W., Dharan, C. K. H. and Chang, H., 1995, "Quasi-static and ballistic perforation of carbon-fiber laminates," *Int. J. Solids Structures*, Vol. 32, pp. 89-103.

Harding, J. and Ruiz, C., 1998, "The mechanical behavior of composite materials under impact loading," *Impact Response and Dynamic Failure of Composites and Laminate Materials*, Vol. 141-1, pp. 403-425.

Hashin, Z. and Rosen, B. W., 1964, "The elastic moduli of fiber-reinforced materials," *Journal of Applied Mechanics*, Vol. 31, pp. 223-232.

Kolsky, H., 1949, "An investigation of the mechanical properties of materials at very high rates of loading," *Proceedings of Royal Society, London,* Vol. B62, pp. 676-700.

Lambros, J. and Rosakis, A. J., 1995, "Dynamic decohesion of bimaterials: Experimental observations and failure criteria," *Int. J. Solids Structures*, Vol. 32, pp. 2677-2702.

Lambros, J. and Rosakis, A. J., 1997, "An experimental study of dynamic delamination of thick fiber reinforced polymeric matrix composites," *Experimental Mechanics*, Vol. 37, pp. 360-366.

Lankford, J., 1997, "Shear Versus Dilatational Damage Mechanisms in the Compressive Failure of Fiber-Reinforced Composites," *Composites*, Vol. 28A, pp. 215-222.

Oguni, K. and Ravichandran, G., 2000, "An Energy-Based Model of Longitudinal Splitting In Unidirectional Fiber Reinforced Composites," to appear in *Journal of Applied Mechanics*.

Oguni, K., Tan, C. Y. and Ravichandran, G. 1999, "Failure mode transition in unidirectional E-glass/vinylester composites under multiaxial compression," submitted to *Journal of Composite Materials*.

Parry, T. V. and Wronski, A. S., 1982, "Kinking and Compressive Failure in Uniaxially Aligned Carbon Fiber Composite Tested Under Superposed Hydrostatic Pressure," *Journal of Materials Science*, Vol. 17, pp. 893-900.

Ravichandran, G. and Subhash, G., 1994, "Critical Appraisal of Limiting Strain Rates for Testing Ceramics in a Split Hopkinson Pressure Bar," *Journal of the American Ceramic Society*, Vol. 77, pp. 263-67.

Waas, A. M. and Schultheisz, C. R., 1996, "Compressive Failure of Composites, Part 2: Experimental Studies," *Progress in Aerospace Science,* Vol. 32, pp. 43-78.

Waas, A. M., Takeda, N., Yuan, J. and Lee, S. H., 1997, "Static and Dynamic Compressive Behavior of Glass Fiber Reinforced Unidirectional Composites," *Proceedings of the American Society for Composites, Twelfth Technical Conference*, Dearborn, Michigan, pp. 552-561.

Weaver, C. W. and Williams, J. G., 1975, "Deformation of a Carbon-Epoxy Composite Under Hydrostatic Pressure," *Journal of Materials Science,* Vol. 10, pp. 1323-1333.

Werner, S. M. and Dharan, C. K. H., 1986, "The dynamic-response of graphite fiber-epoxy laminates at high shear strain rates," *Journal of Composite Materials*, Vol. 20, pp. 365-374.

List of figures

Figure 18 Comparison between experimental results and model prediction for uniaxial compressive strength of 50% fiber volume fraction E-glass/vinylester composite

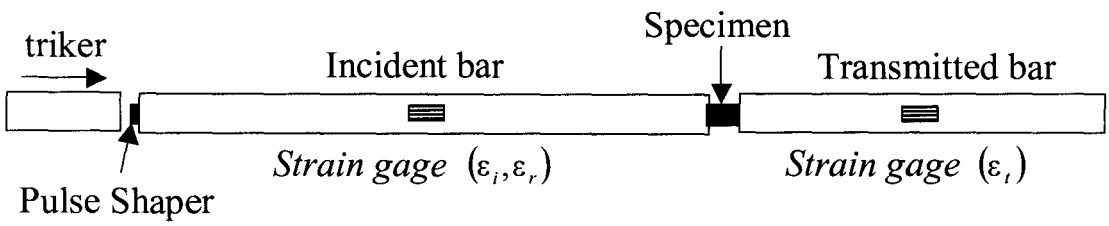

Figure 1 Schematic of a modified Kolsky (split Hopkinson) pressure bar for investigating compressive failure in fiber reinforced composites

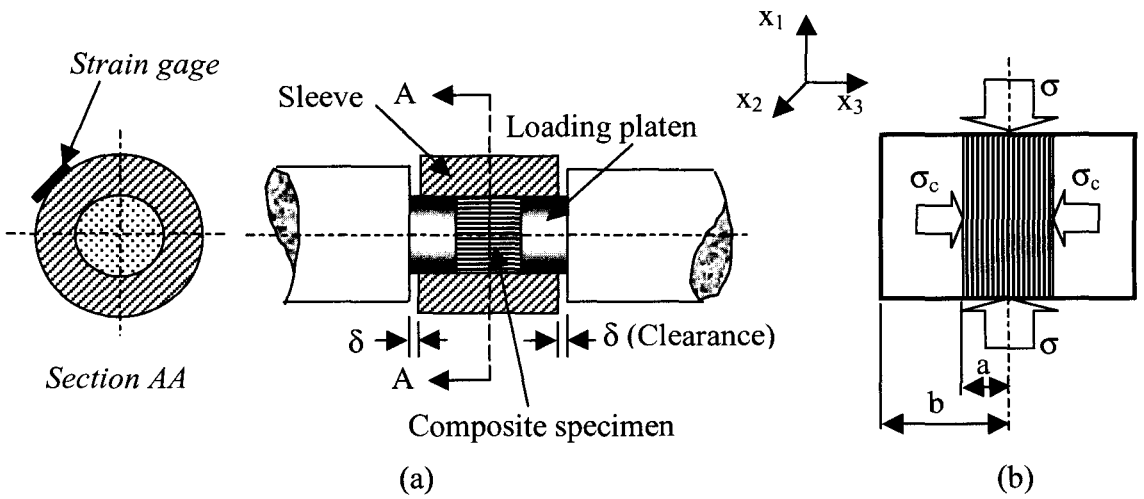

Figure 2 (a) Schematic of a composite specimen laterally confined by a metallic sleeve and axially loaded through hardened platens; (b) Geometry and stress state of an ideally confined composite specimen

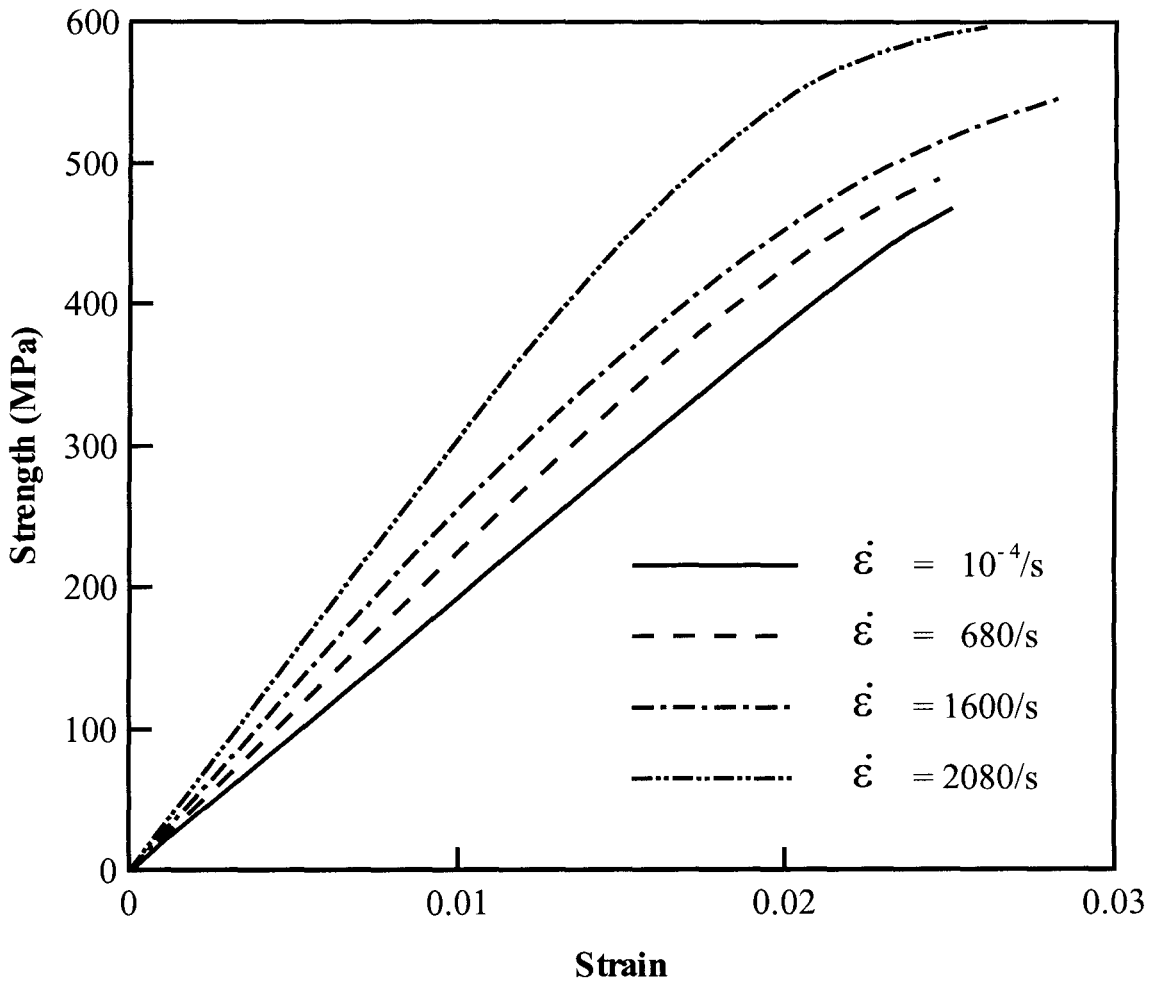

Figure 3 Stress-strain curves for 30% fiber volume fraction E-glass/vinylester composite at various strain rates under uniaxial compression

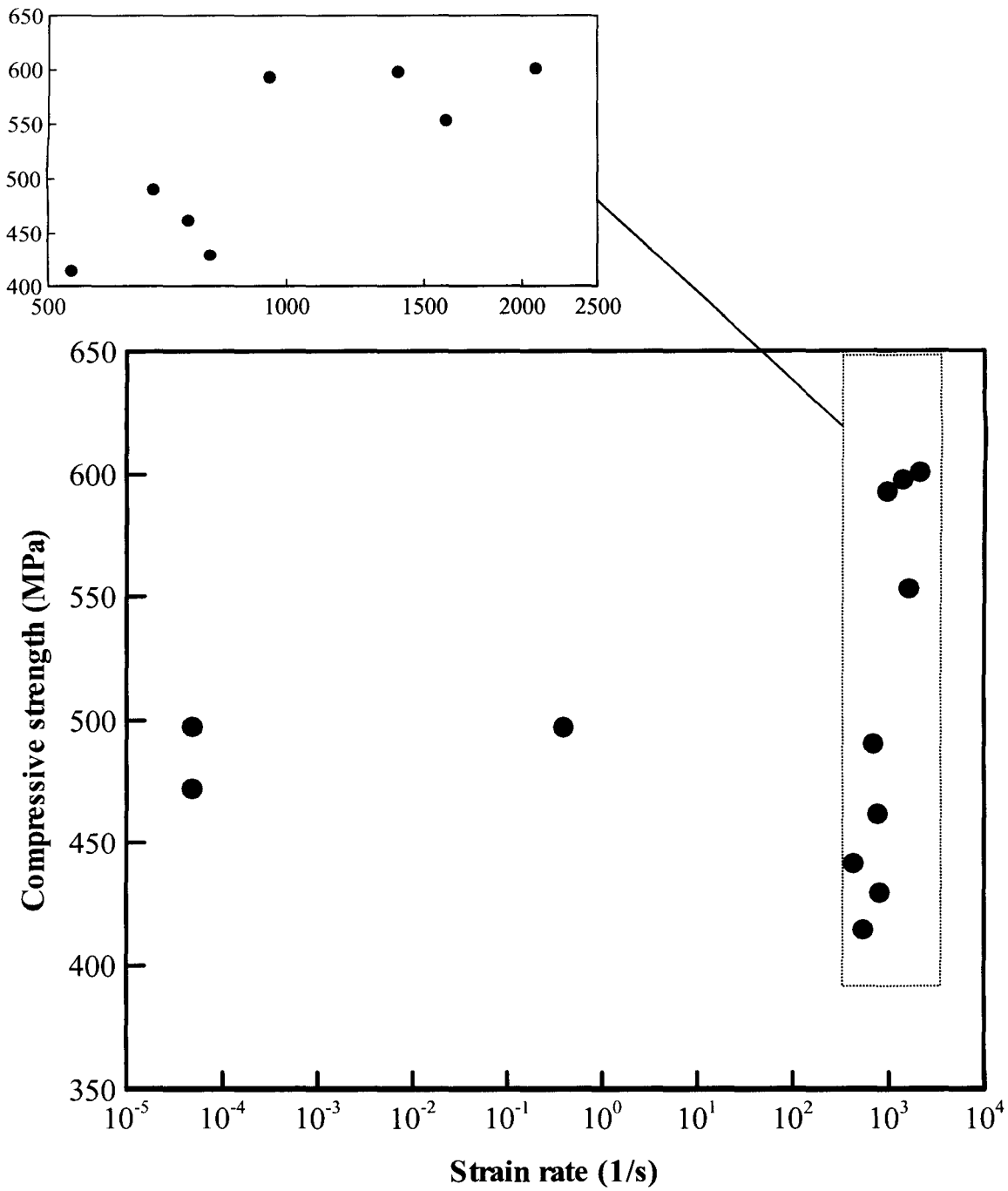

Figure 4 Plot of compressive strength versus strain rate for 30% fiber volume fraction E-glass/vinylester composite under uniaxial compression with magnified plot of high strain rate data

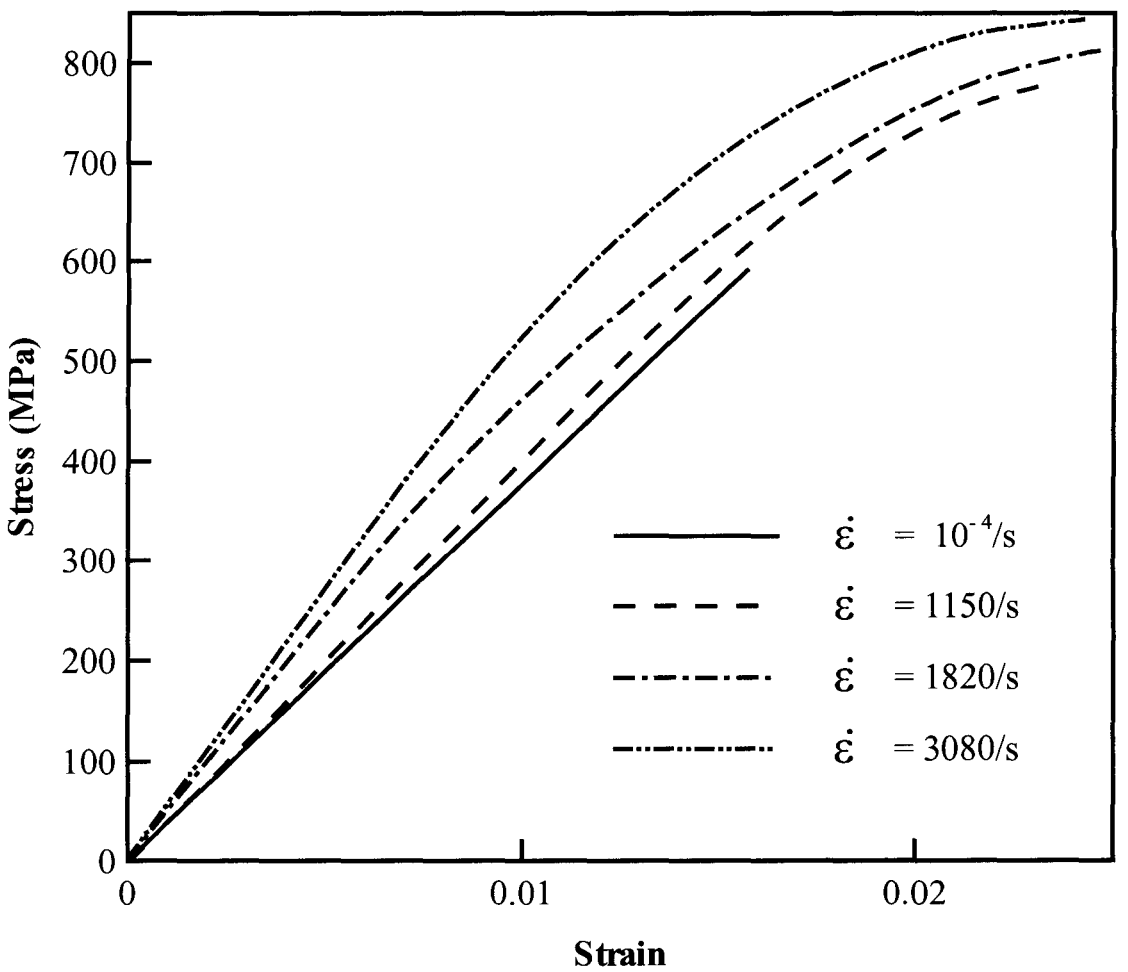

Figure 5 Stress-strain curves for 50% fiber volume fraction E-glass/vinylester composite at various strain rates under uniaxial compression

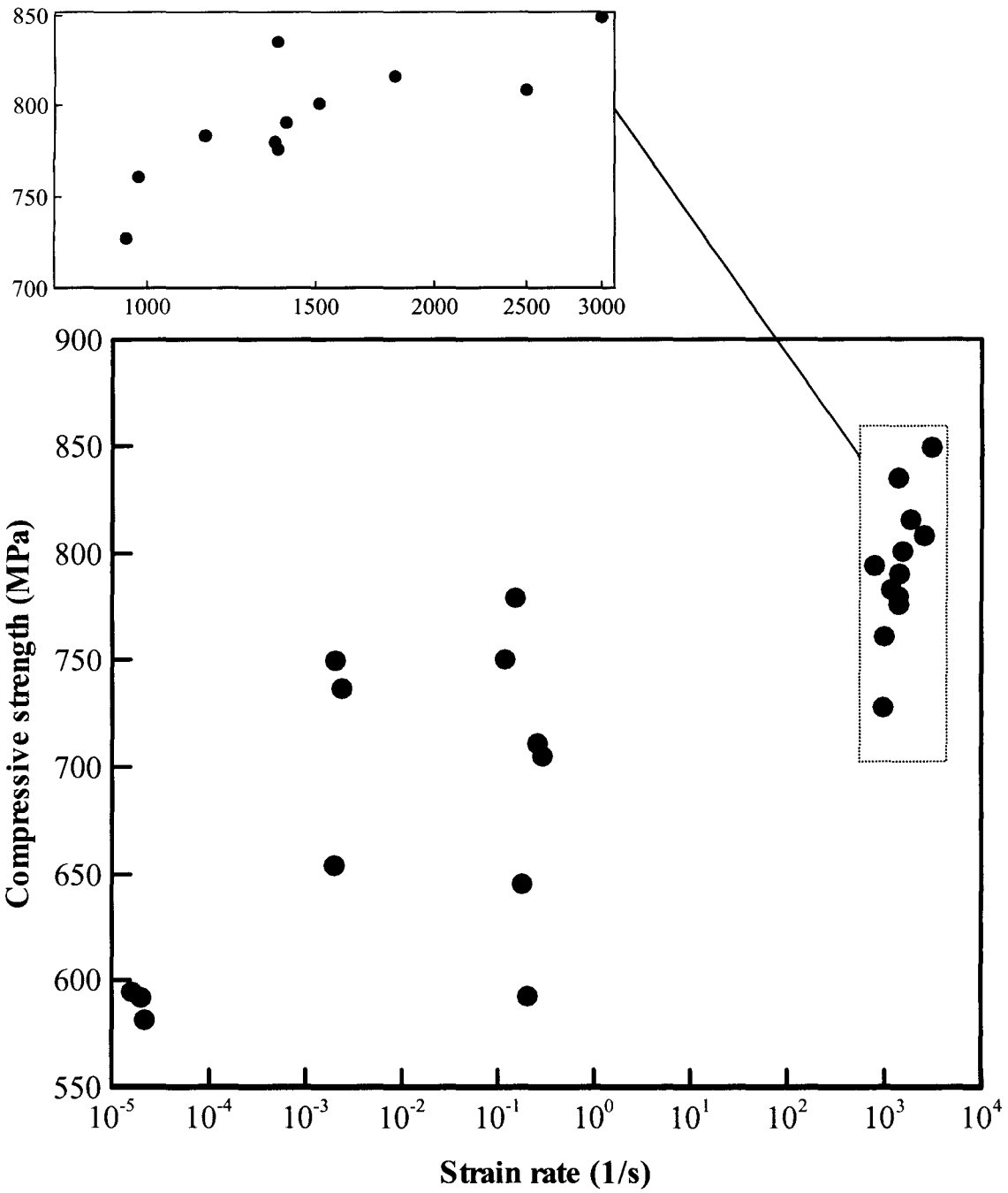

Figure 6 Plot of compressive strength versus strain rate for 50% fiber volume fraction E-glass/vinylester composite under uniaxial compression with magnified plot of high strain rate data

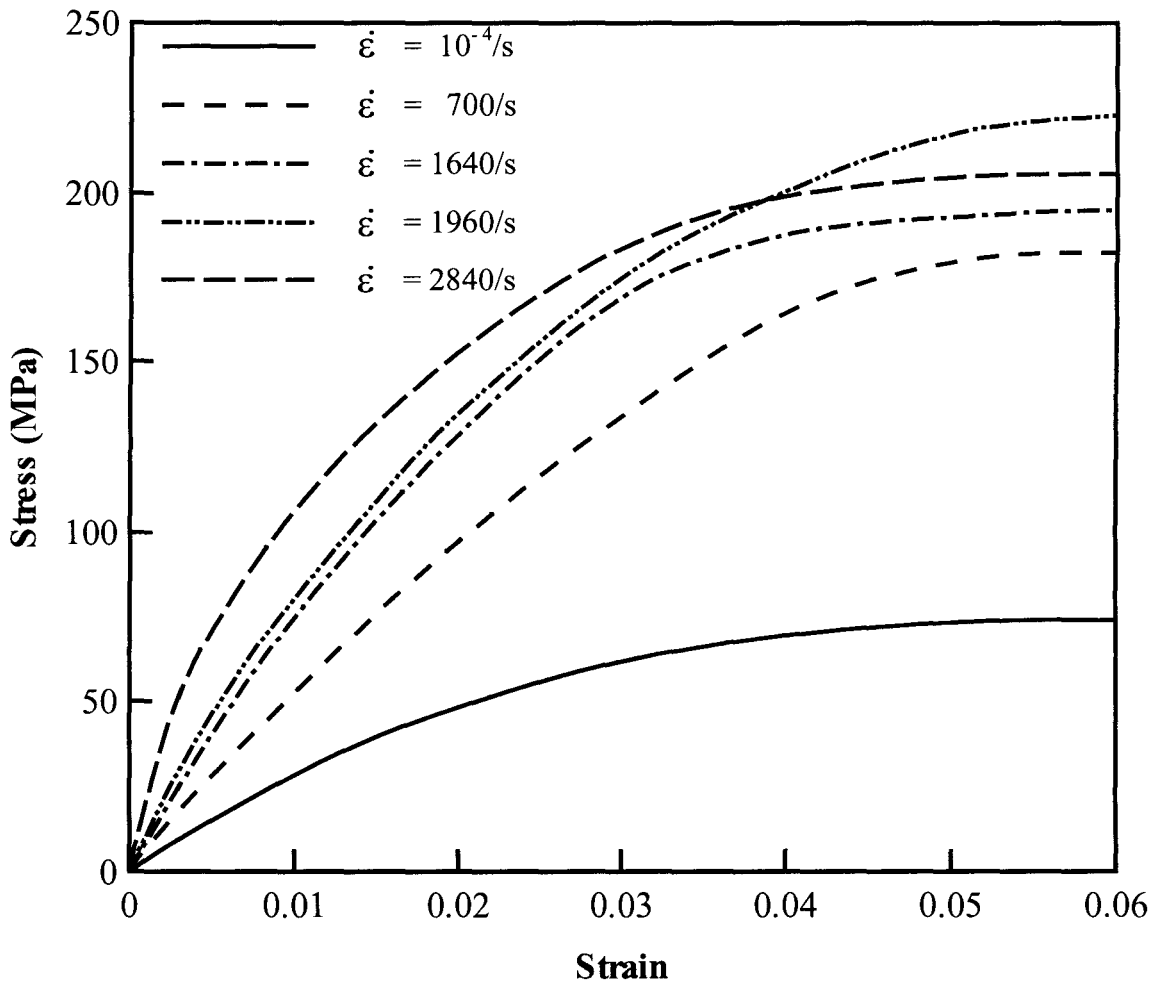

Figure 7 Stress-strain curves for pure vinylester matrix at various strain rates under uniaxial compression

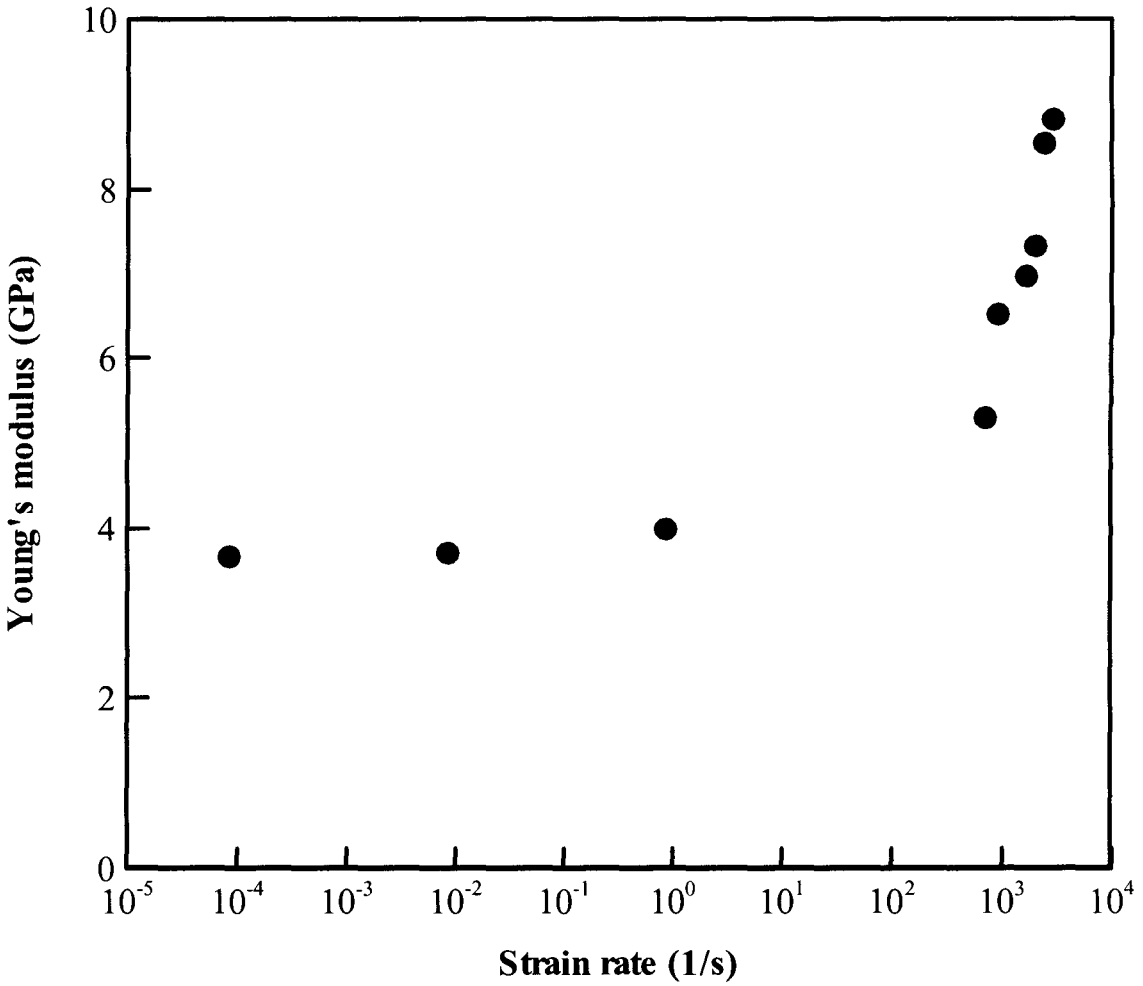

Figure 8 Plot of Young's modulus versus strain rate for pure matrix material (vinylester) under uniaxial compression

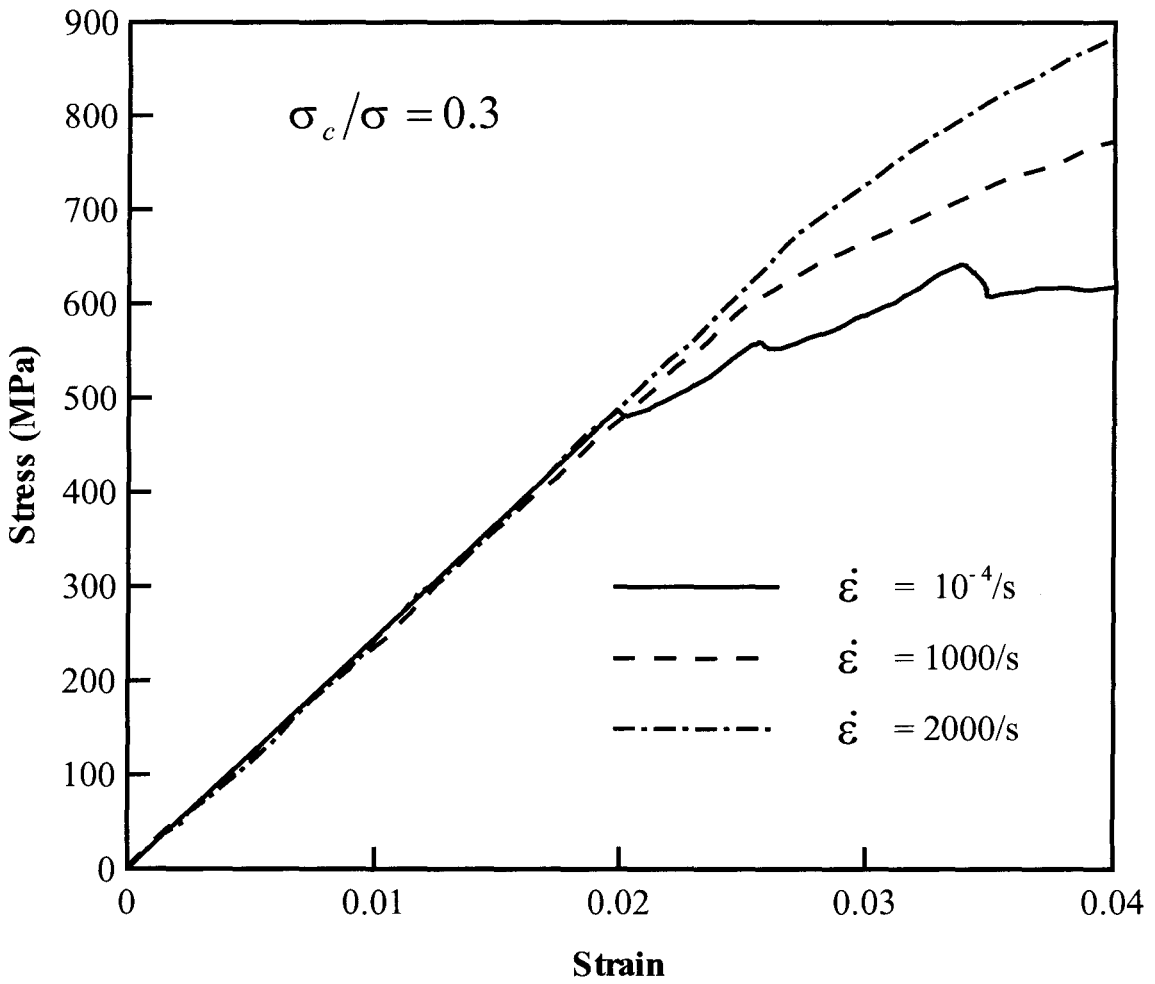

Figure 9 Axial stress-strain curves for laterally confined 50% fiber volume fraction E-glass/vinylester composite at various strain rates for a nominal lateral confinement ratio of $\sigma_c/\sigma = 0.3$

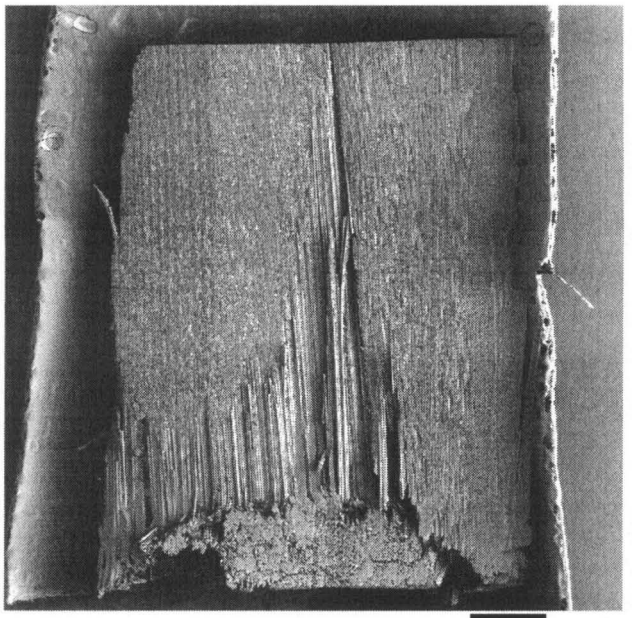

(a) 1mm

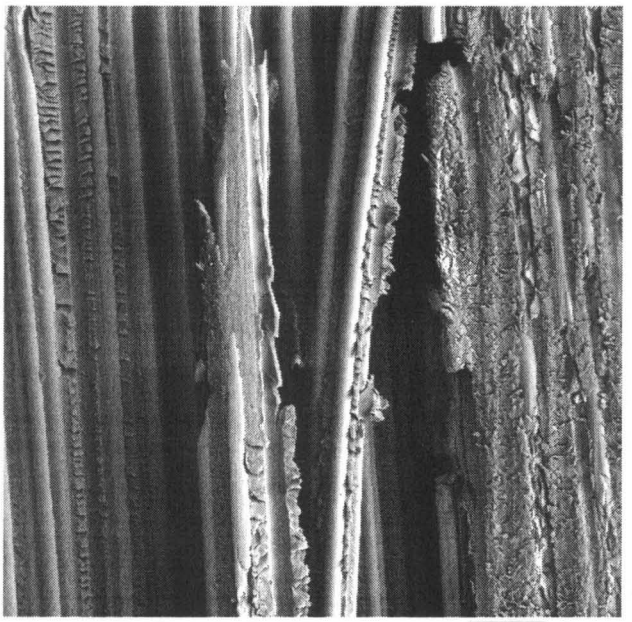

(b) 100μm

Figure 10 SEM micrographs of a failed 30% fiber volume fraction E-glass/vinylester composite under uniaxial quasi-static compression showing axial splitting

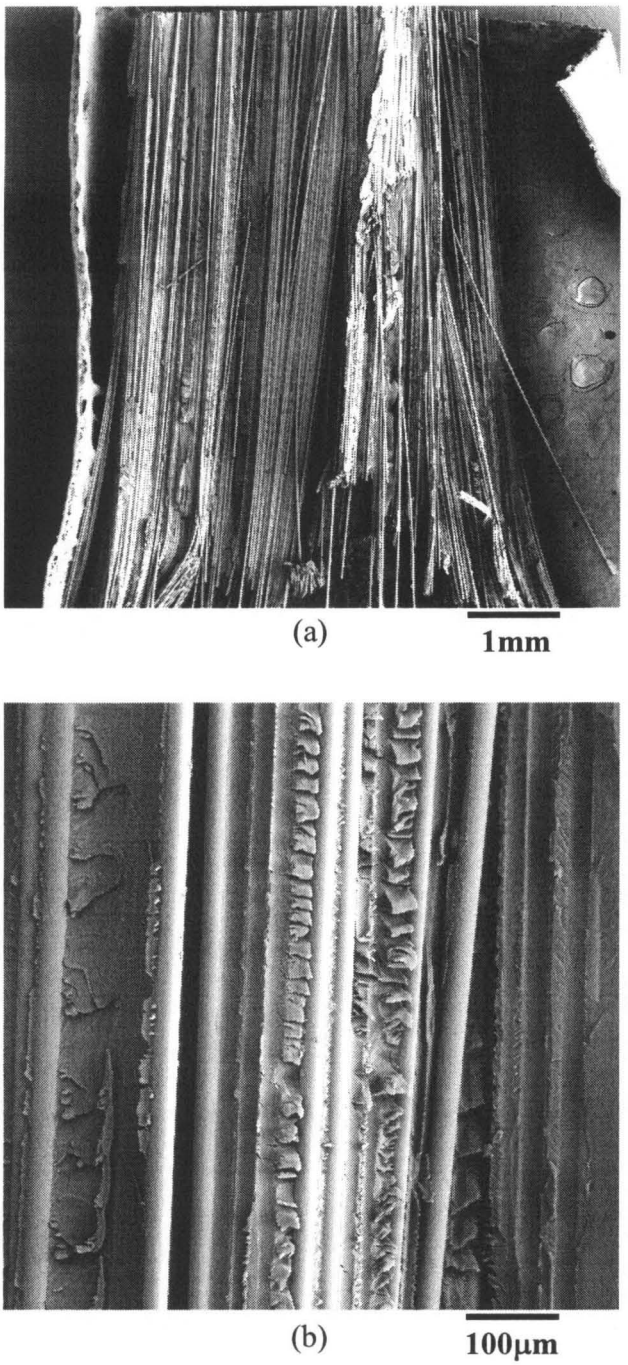

Figure 11 SEM micrographs of a failed 30% fiber volume fraction E-glass/vinylester composite under uniaxial compression at a strain rate of 500/s showing fiber-matrix debonding and matrix rupture

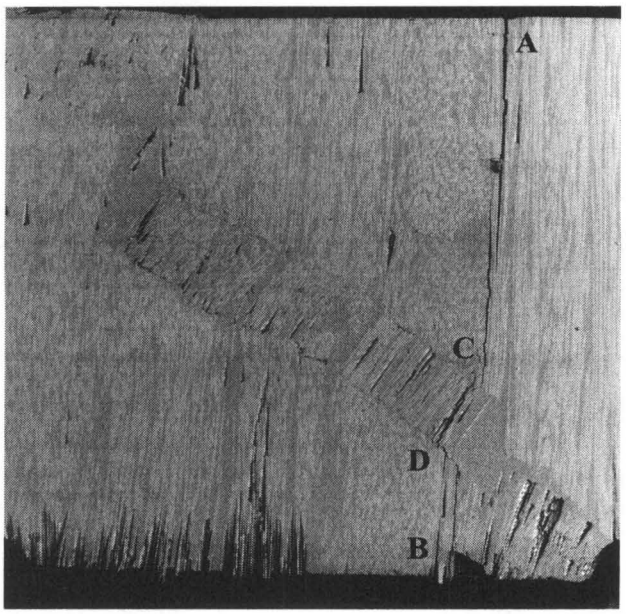

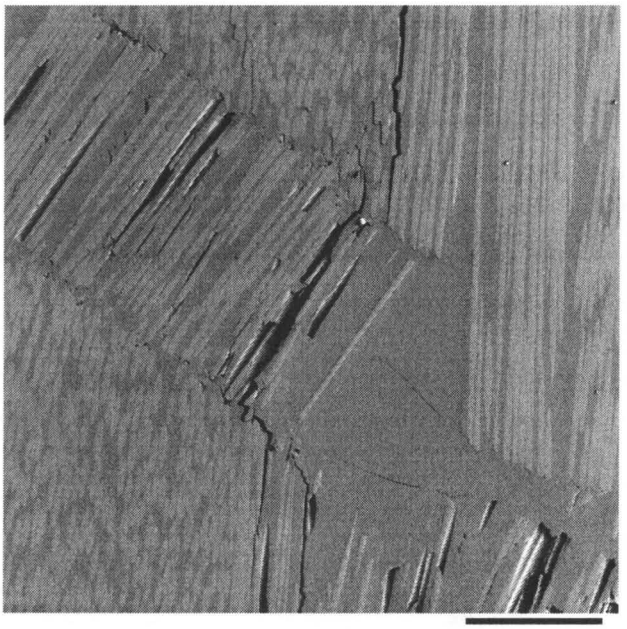

Figure 12 SEM micrographs of a failed 50% fiber volume fraction E-glass/vinylester composite under uniaxial quasi-static compression showing '*splitting induced*' kink band

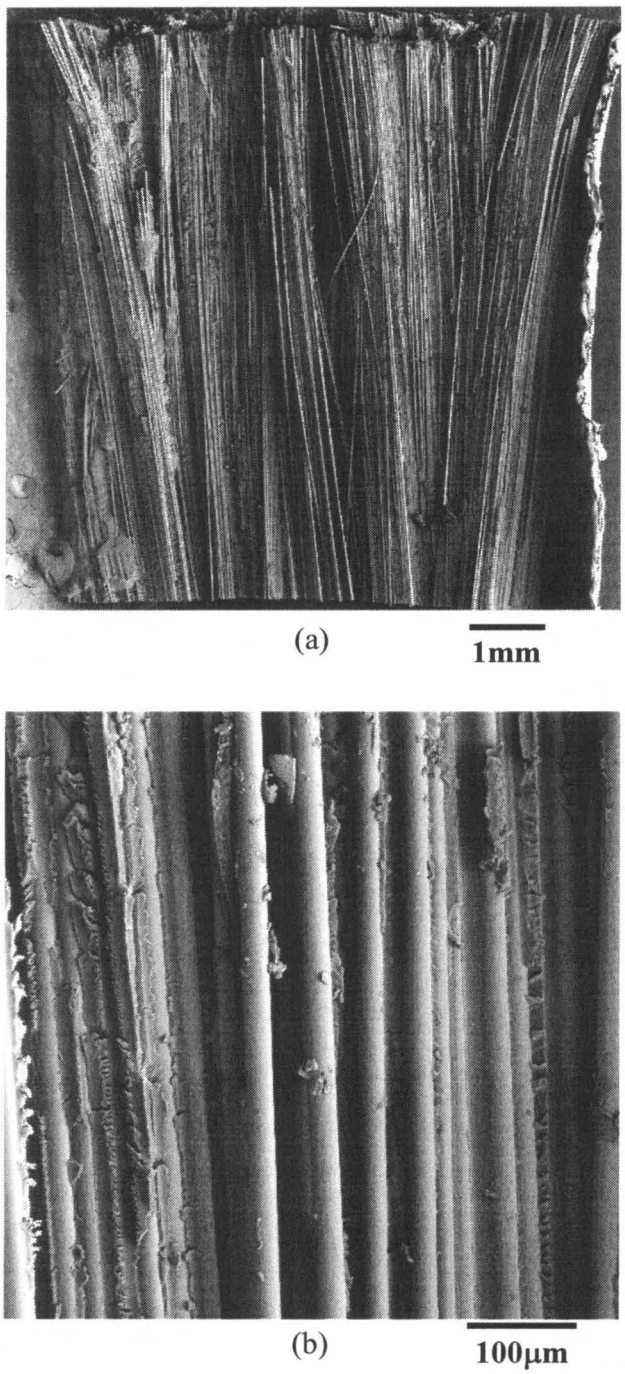

Figure 13 SEM micrographs of a failed 50% fiber volume fraction E-glass/vinylester composite under uniaxial compression at a strain rate of 420/s showing axial splitting

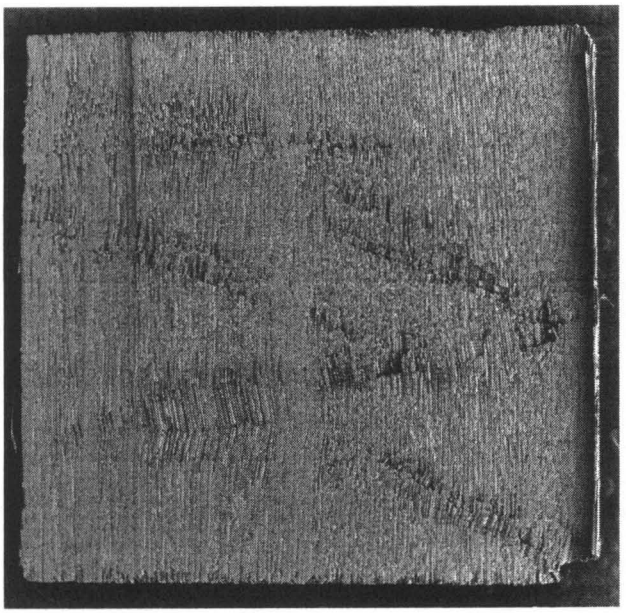

(a) 1mm

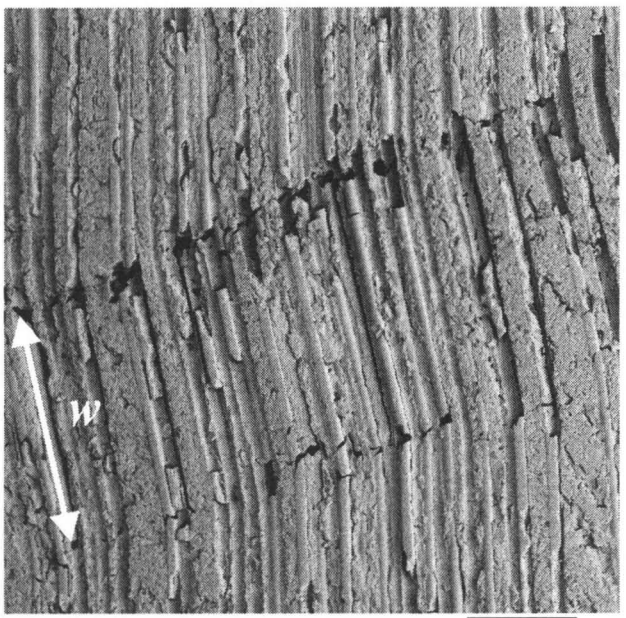

(b) 200μm

Figure 14 SEM micrographs of longitudinal cross-section of the 50% fiber volume fraction E-glass/vinylester composite under lateral confinement deformed at a strain rate of 2000/s showing multiple kink banding

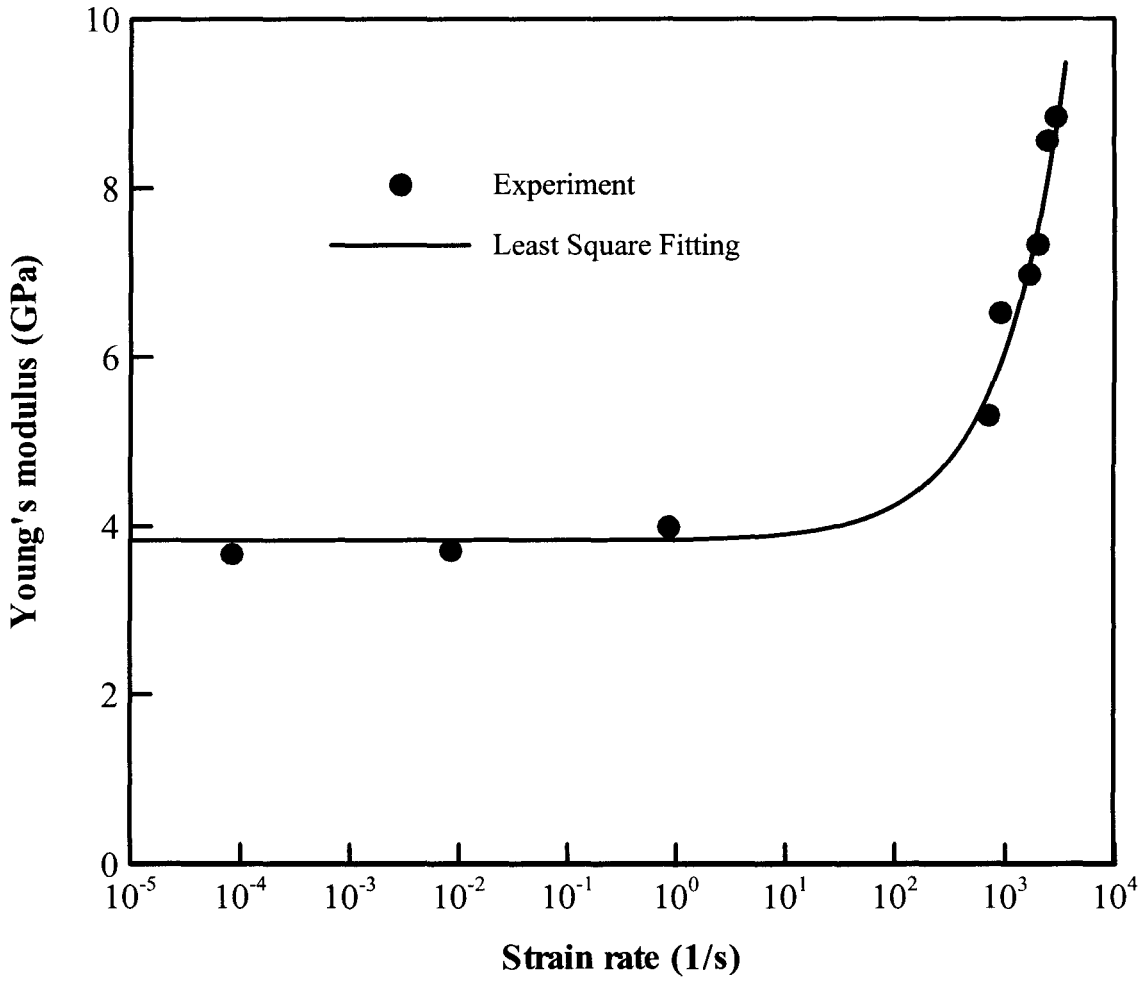

Figure 15 Plot of best fitting curve to experimentally measured Young's modulus of pure matrix material, vinylester, as a function of strain rate

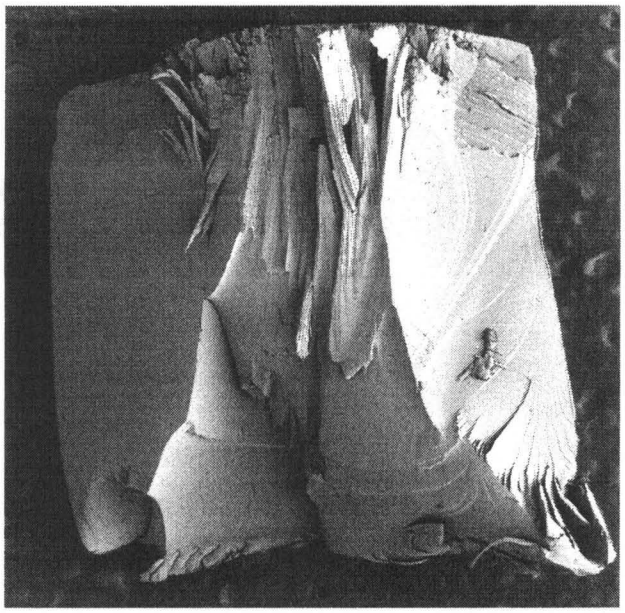

(a) 1mm

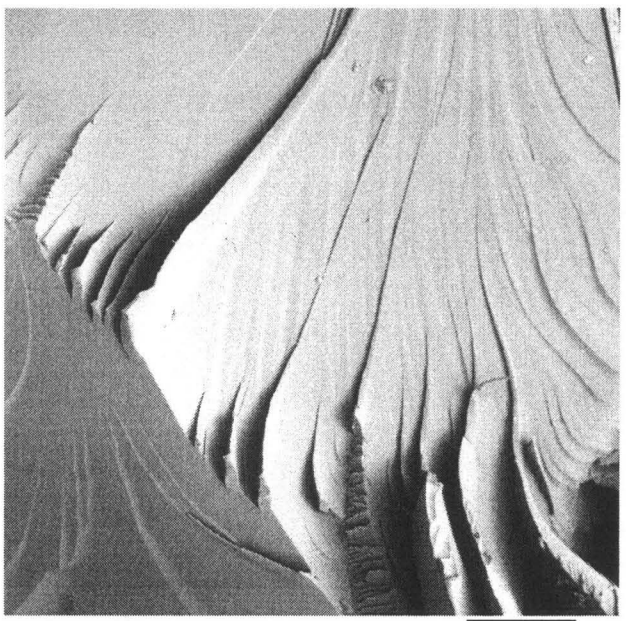

(b) 200μm

Figure 16 SEM micrographs of the surface of a fragment from a dynamically loaded pure matrix material, vinylester, showing brittle failure

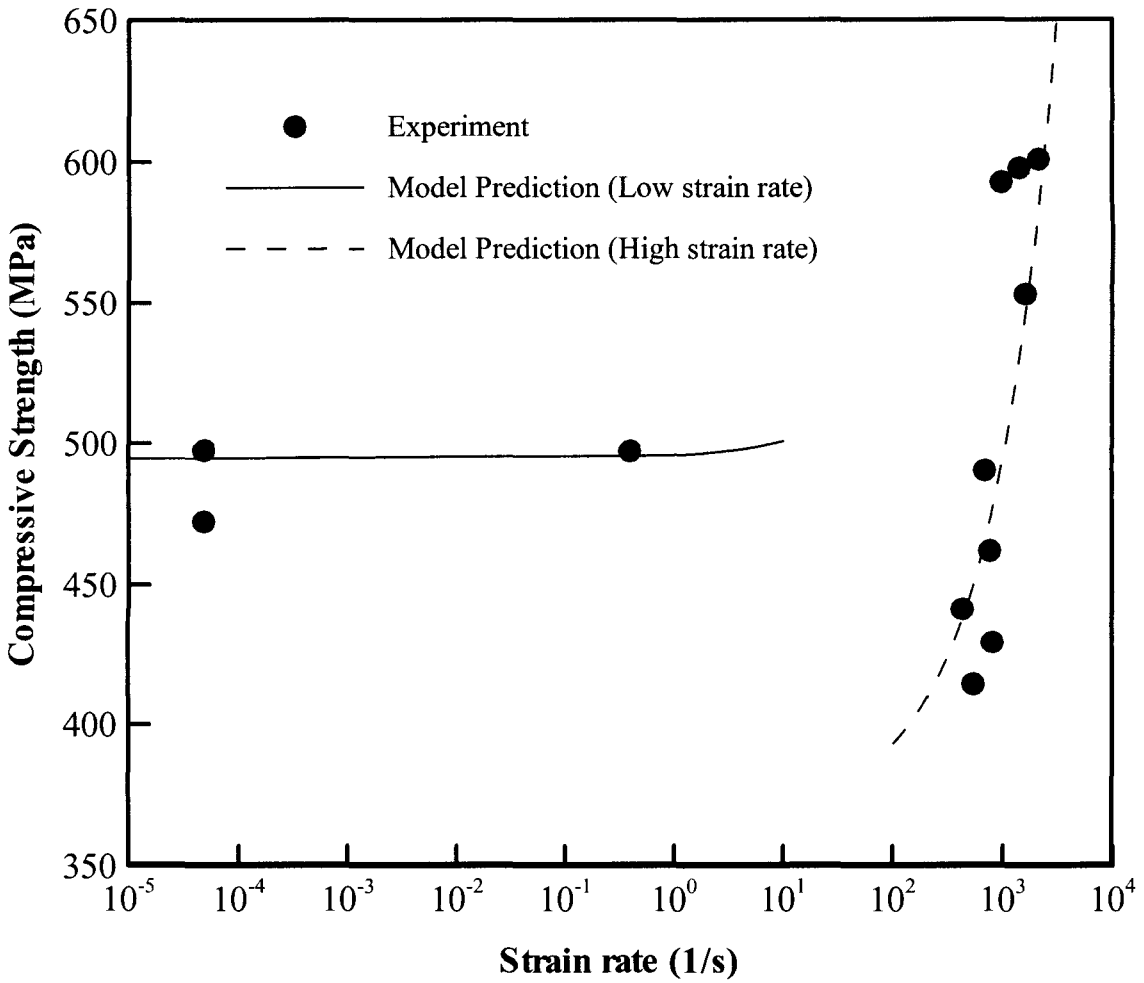

Figure 17 Comparison between experimental results and model prediction for uniaxial compressive strength of 30% fiber volume fraction E-glass/vinylester composite

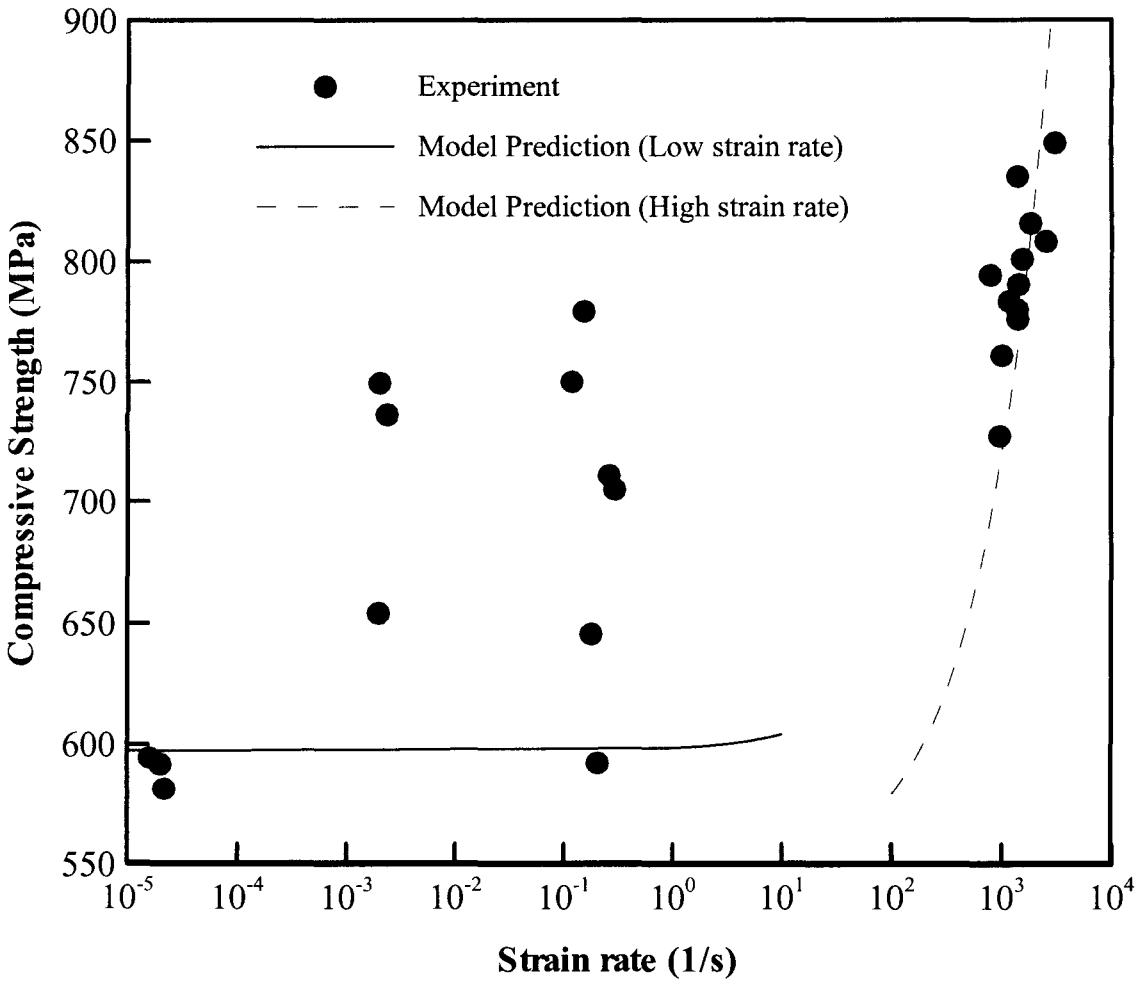

Figure 18 Comparison between experimental results and model prediction for uniaxial compressive strength of 50% fiber volume fraction E-glass/vinylester composite